

# HIGH-RESOLUTION, *H*-BAND SPECTROSCOPY OF BE STARS WITH SDSS-III/APOGEE: I. NEW BE STARS, LINE IDENTIFICATIONS, AND LINE PROFILES

S. DREW CHOJNOWSKI<sup>1,2</sup>

Department of Astronomy, University of Virginia, P.O. Box 400325, Charlottesville, VA 22904-4325, USA  
 drewski@virginia.edu

DAVID G. WHELAN<sup>3</sup>, JOHN P. WISNIEWSKI<sup>4</sup>, STEVEN R. MAJEWSKI<sup>1</sup>, MATTHEW HALL<sup>1</sup>,  
 MATTHEW SHETRONE<sup>5</sup>, RACHAEL BEATON<sup>1</sup>, ADAM BURTON<sup>1</sup>, GUILLERMO DAMKE<sup>1</sup>,  
 STEVE EIKENBERRY<sup>6</sup>, STEN HASSELQUIST<sup>2</sup>, JON A. HOLTZMAN<sup>2</sup>, SZABOLCS MÉSZÁROS<sup>7</sup>,  
 DAVID NIDEVER<sup>8</sup>, DONALD P. SCHNEIDER<sup>9,10</sup>, JOHN WILSON<sup>1</sup>, GAIL ZASOWSKI<sup>11</sup>,  
 DMITRY BIZYAEV<sup>2</sup>, HOWARD BREWINGTON<sup>2</sup>, J. BRINKMANN<sup>2</sup>, GARRETT EBELKE<sup>2</sup>,  
 PETER M. FRINCHABOY<sup>12</sup>, KAREN KINEMUCHI<sup>2</sup>, ELENA MALANUSHENKO<sup>2</sup>,  
 VIKTOR MALANUSHENKO<sup>2</sup>, MOSES MARCHANTE<sup>2</sup>, DANIEL ORAVETZ<sup>2</sup>, KAIKE PAN<sup>2</sup>,  
 AUDREY SIMMONS<sup>2</sup>  
*Draft version September 17, 2014*

## ABSTRACT

The Apache Point Galactic Evolution Experiment (APOGEE) has amassed the largest ever collection of multi-epoch, high-resolution ( $R \sim 22,500$ ), *H*-band spectra for B-type emission line (Be) stars. These stars were targeted by APOGEE as telluric standard stars and subsequently identified via visual inspection as Be stars based on H I Brackett series emission or shell absorption in addition to otherwise smooth continua and occasionally non-hydrogen emission features. The 128/238 APOGEE Be stars for which emission had never previously been reported serve to increase the total number of known Be stars by  $\sim 6\%$ . Because the *H*-band is relatively unexplored compared to other wavelength regimes, we focus here on identification of the *H*-band lines and analysis of the emission peak velocity separations ( $\Delta v_p$ ) and emission peak intensity ratios (V/R) of the usually double-peaked H I and non-hydrogen emission lines. H I Br11 emission is found to preferentially form in the circumstellar disks at an average distance of  $\sim 2.2$  stellar radii. Increasing  $\Delta v_p$  toward the weaker Br12–Br20 lines suggests these lines are formed interior to Br11. By contrast, the observed IR Fe II emission lines present evidence of having significantly larger formation radii; distinctive phase lags between IR Fe II and H I Brackett emission lines further supports that these species arise from different radii in Be disks. Several emission lines have been identified for the first time including C I 16895, a prominent feature in the spectra for almost a fifth of the sample and, as inferred from relatively large  $\Delta v_p$  compared to the Br11–Br20, a tracer of the inner regions of Be disks. Emission lines at 15760 Å and 16781 Å remain unidentified, but usually appear along with and always have similar line profile morphology to Fe II 16878. Unlike the typical metallic lines observed for Be stars in the optical, the *H*-band metallic lines, such as Fe II 16878, never exhibit any evidence of shell absorption, even when the H I lines are clearly shell-dominated. The first known example of a quasi-triple-peaked Br11 line profile is reported for HD 253659, one of several stars exhibiting intra- and/or extra-species V/R and radial velocity variation within individual spectra. Br11 profiles are presented for all discussed stars, as are full APOGEE spectra for a portion of the sample.

*Subject headings:* stars: emission-line, Be — infrared: stars — (stars:) circumstellar matter — stars: peculiar — stars: early-type — atlases — catalogs

## 1. INTRODUCTION

Since the first observational description (Struve 1931) of the characteristic double-peaked emission lines of classical

Be stars, a wealth of research has demonstrated that the emission lines are formed in geometrically-thin, equatorial circumstellar disks fed by gas ejected from the surfaces of rapidly rotating B stars (Porter & Rivinius 2003; Rivinius

<sup>1</sup> Department of Astronomy, University of Virginia, P.O. Box 400325, Charlottesville, VA 22904-4325, USA

<sup>2</sup> Apache Point Observatory and New Mexico State University, P.O. Box 59, Sunspot, NM, 88349-0059, USA

<sup>3</sup> Department of Physics, Austin College, 900 N. Grand Ave., Sherman, TX 75090, USA

<sup>4</sup> Department of Physics & Astronomy, The University of Oklahoma, 440 W. Brooks St. Norman, OK 73019, USA

<sup>5</sup> Department of Astronomy, The University of Texas at Austin, 2515 Speedway, Stop C1400 Austin, Texas 78712-1205, USA

<sup>6</sup> Department of Astronomy, University of Florida, 211 Bryant Space Science Center, Gainesville, FL 32611-2055, USA

<sup>7</sup> Department of Astronomy, Indiana University, Bloomington, IN 47405, USA

<sup>8</sup> Department of Astronomy, University of Michigan, 830 Dennison 500 Church St. Ann Arbor, MI 48109-1042, USA

<sup>9</sup> Department of Astronomy and Astrophysics, The Pennsylvania State University, University Park, PA 16802, USA

<sup>10</sup> Institute for Gravitation and the Cosmos, The Pennsylvania State University, University Park, PA 16802, USA

<sup>11</sup> Department of Physics & Astronomy, Johns Hopkins University, Bloomberg Center for Physics and Astronomy Room 366, 3400 N. Charles Street, Baltimore, MD 21218, USA

<sup>12</sup> Department of Physics and Astronomy, Texas Christian University, Box 298840, Fort Worth, TX 76129, USA

et al. 2013b). Rapid rotation is certainly involved in the formation of these disks, but a comprehensive model of Be disk formation has yet to be created and efforts toward one are complicated by factors including the lack of examples of critically-rotating Be stars, star-specific peculiarities, and the requirement of an ‘on/off’ switch to the Be phenomenon. For an uncertain but non-negligible fraction of Be stars the disks are transient, appearing in one epoch but not another (McSwain et al. 2009; Wisniewski et al. 2010). A variable rotation speed ( $v \sin i$ ) that occasionally reaches or exceeds the critical breakup limit is an attractive concept for such a phenomenon (Rivinius et al. 2013c) that needs to be explored for a sample of transient Be stars. Non-radial pulsation and turbulence due to small-scale magnetic fields remain the most likely mechanisms, along with rapid rotation, responsible for the creation of the disks (Rivinius et al. 2013b). When the disks are present, they appear to undergo Keplerian rotation (Meilland et al. 2007; Wheelwright et al. 2012), and many of the observational signatures are consistent with those predicted by the viscous decretion disk model (Lee et al. 1991; Carciofi et al. 2009; Carciofi 2011).

Multi-wavelength studies of Be disks are particularly valuable for diagnosing their structure because emission at different wavelengths originates from different physical locations within the disks (Carciofi 2011). However, unlike in the optical wavelength regime where they have been extensively studied at high spectral and temporal resolution, only a limited number of Be star surveys have been performed at near-infrared (NIR) wavelengths, and these have typically utilized low spectral resolution (Steele & Clark 2001) and small sample sizes (Murdoch et al. 1994; Clark & Steele 2000; Mennickent et al. 2009; Granada et al. 2010). Detailed NIR spectroscopic studies of individual Be stars are more common (e.g., Hony et al. 2000; Mathew et al. 2012) and have been used to better diagnose the gas distribution within Be disks, including the structure of one-armed density waves (Wisniewski et al. 2007; Štefl et al. 2009; Carciofi et al. 2009).

The Apache Point Observatory Galactic Evolution Experiment (APOGEE; Majewski 2012) is actively providing the first ever bulk view of the high-resolution  $H$ -band properties and variability of Be stars. APOGEE is one of four surveys comprising the Sloan Digital Sky Survey III (SDSS-III; Eisenstein et al. 2011). While the primary goal of the APOGEE survey is to measure the dynamical and chemical history of the Milky Way Galaxy using high-resolution  $H$ -band spectroscopic observations of  $10^5$  red giant branch (RGB) stars, APOGEE devotes 35 fibers per 300-fiber pointing to observe hot stars as telluric standards. This, in addition to the surveys large sky coverage and multi-epoch observing strategy, has made APOGEE ideal for serendipitous Be discoveries and high-resolution NIR time series data of Be stars.

Here, we present the first catalog APOGEE Be (ABE) stars. An overview of the APOGEE survey and APOGEE data is provided in Section 2, the Be sample is described in Section 3, and the identifications of observed metallic emission lines are discussed in Section 4. Sections 5 and 6 focus on quantitative and comparative analysis of emission double-peak separation ( $\Delta v_p$ ) and double-peak intensity ratios ( $V/R$ ). Commentary on the more unusual or ex-

ceptional Be stars within the ABE sample is interspersed throughout, and an atlas of Br11 profiles is provided in Section 7. The appendix includes supplemental figures displaying full APOGEE spectra for stars with strong emission features, as well as an expanded stellar data table. Future work will focus on the observed spectral variability of sources with multi-epoch APOGEE data as well as follow-up optical spectroscopy for a subset of the sample.

## 2. APOGEE OVERVIEW

### 2.1. APOGEE instrument and observations

The APOGEE instrument is a 300-fiber,  $R \sim 22,500$  spectrograph (Wilson et al. 2010) attached to the SDSS 2.5-meter telescope (Gunn et al. 2006) at Apache Point Observatory. APOGEE records a vacuum wavelength range of 15145–16955 Å via an arrangement of three Teledyne H2RG  $2048 \times 2048$  detectors. The detector layout consists of “blue”, “green”, and “red” detectors which cover 15145–15808 Å, 15858–16433 Å, and 16474–16955 Å respectively, resulting in coverage gaps between 15808–15858 Å and 16433–16474 Å. Dispersion varies with wavelength, but the central dispersions of the blue, green, and red detectors are  $0.326 \text{ Å pix}^{-1}$ ,  $0.283 \text{ Å pix}^{-1}$ , and  $0.236 \text{ Å pix}^{-1}$  respectively. As with the original SDSS spectrograph (Smee et al. 2013), APOGEE fibers are plugged into custom, pre-drilled aluminum plates which are loaded into the telescope’s focal plane and which can cover  $3^\circ$  diameter areas of sky. Each fiber has a  $2''$  field of view.

The APOGEE survey uses the Two Micron All Sky Survey (2MASS; Skrutskie et al. 2006) as a source catalog and focuses on observations of known or photometrically-likely RGB stars for its main science objective (230/300 fibers per plate). For calibration purposes, blank sky (35/300 fibers) and blue telluric standards (35/300 fibers) are also observed. Typical exposure times are 1-hr, and the number of repeat observations per field is approximately equal to the number of 1-hr observations needed to reach a combined signal-to-noise ratio per raw pixel (SNR) of 100 for stars at the field-specific  $H$  magnitude limit. The bright limit for science targets is always  $H = 7.0$ , while the faint limit is variable and can be  $H = 11.0$  (1-hr visit),  $H = 12.2$  (3 1-hr visits),  $H = 12.8$  (6 1-hr visits),  $H = 13.3$  (12 1-hr visits), or  $H = 13.8$  (24 1-hr visits). Cohorts of RGB targets with similar  $H$  magnitudes are exchanged in and out of the observing sequence as SNR  $\sim 100$  is reached.

### 2.2. APOGEE telluric standard stars

Hot O- and B-type (OB) stars are ideal candidates for telluric standard stars (TSS) in the  $H$ -band because the associated spectra are relatively featureless (Meyer et al. 1998; Steele & Clark 2001). Selection of the TSS for each APOGEE field is based on  $H$  magnitude and non-reddening-corrected color rather than on intrinsic spectral properties (Zasowski et al. 2013), such that the TSS for a given field are simply the apparent bluest available stars. Thus, APOGEE makes no distinction between “normal” and emission-line stars other than to prevent from selection as TSS any stars that are reddened with respect to other stars (e.g. dusty B[e] stars) in the  $3^\circ$  fields.

Unlike the RGB science targets, TSS are restricted to  $5.5 \leq H \leq 11.0$  and are therefore always expected to reach

SNR  $\geq 100$  in the typical hour exposures. In addition, the TSS for each APOGEE field are generally ‘locked-in,’ meaning that they are observed every time their respective fields are observed rather than being traded in and out of the sequence as are the RGB stars. A more comprehensive description of TSS selection is presented in Zasowski et al. (2013).

### 2.3. APOGEE spectra

There are several details worth noting about the APOGEE spectra. Vacuum wavelengths given in angstroms ( $\text{\AA}$ ) are used in APOGEE data and throughout this paper. Some of the spectra were recorded during APOGEE commissioning, prior to the instrument having achieved optimal focus. The resolution of red detector data in APOGEE spectra taken prior to MJD < 55804 (September 2011) is  $R \sim 16,000$ , while the resolution is  $R \sim 22,500$  for all blue and green detector data regardless of date and for all post-55804 red detector data. The raw data is processed by an automated reduction pipeline (Nidever, in preparation) that extracts the spectra, performs flat-field and wavelength calibration, and performs sky and telluric corrections. APOGEE’s reduction pipeline is designed to use sky and TSS exposures (see Section 2.2) to remove airglow and telluric absorption lines from the high-resolution spectra. Because the airglow removal process has not yet been perfected, residuals from partially subtracted airglow lines remain in the final reduced data products.

Since the APOGEE survey focuses on chemical abundance and radial velocity analysis, flux standard stars are not observed and therefore the spectra are not flux-calibrated. All spectra displayed in this paper were continuum normalized using the CONTINUUM task in IRAF by fitting low-order splines to sections of blank continuum adjacent to H I Brackett lines, separately for each detector. Quoted emission line intensities and V/R intensity ratios refer to intensity relative to normalized continuum level ( $F_\lambda/F_c$ ). Due to the proximity of the Br12 and Br14 lines to the coverage limits of the green detector (21 and 27  $\text{\AA}$  respectively), it was at times difficult to achieve a continuum fit that did not result in obviously incorrect intensity levels for those with respect to the other Brackett lines. The tendency of the full-width at continuum level for Brackett series emission lines to well exceed  $1000 \text{ km s}^{-1}$  was a further complication in salvaging the Br12 and Br14 lines, which are de-emphasized from analysis for these reasons.

Figure 1 displays examples of APOGEE spectra for two newly-discovered Be stars, demonstrating the three-detector arrangement and associated coverage gaps. The APOGEE Be star IDs and modified Julian dates (MJD) of observation are provided above or below ‘red detector’ continuum level, and commonly-observed emission lines (see Section 3.5) are labeled with blue text and arrows. Examples of airglow residuals are noted with red text and arrows. The right-hand panels show Br11 line profiles from the same spectra on a velocity scale, with the line profile features of interest labeled. In most cases, Br11 is the strongest hydrogen line covered as well as the hydrogen line least likely to be affected by airglow or telluric contaminants should those be a significant issue. In subsequent

figures, narrow contaminants (airglow and hot/cold/bad pixels) have been carefully trimmed from the spectra so as to avoid distraction from the features of astrophysical importance.

### 2.4. Public availability of the spectra

Both proprietary and publicly-available spectra are used and displayed in this paper. The publicly-available spectra were included in SDSS data release 10 (DR10: pertains to APOGEE data taken prior to MJD=56112), and the full data set will be made publicly-available in SDSS data release 12 (DR12: scheduled for December 2014). Shortly after DR12, we intend to convert the APOGEE Be star spectra to the format accepted by the Be Star Spectra Database (BeSS; Neiner et al. 2011) and deposit them there, ensuring convenient public access. More details on DR10-released APOGEE data can be found on the SDSS-III website (<https://www.sdss3.org/dr10/irspect/>).

## 3. THE ABE SAMPLE

### 3.1. Sample description

The sample at hand consists of 238 Be stars that have been observed by APOGEE a total of 1082 times. Of the 238 ABE stars, 202 were identified through periodic visual inspection of APOGEE spectra and 36 were targeted intentionally to expand the subset of previously-known Be stars.

We measured the velocity separations ( $\Delta v_p$ ) of the violet (V) and red (R) emission peaks of all lines with well-defined peaks in all spectra of sufficient quality (typically SNR  $> 50$ ; dependent on emission strength) using the SPLOT feature of IRAF. Measurements pertaining to emission peaks coincident in wavelength position with strong airglow lines or diffuse interstellar bands (see Section 4.1) were thrown out. No attempt was made to remove underlying photospheric absorption prior to  $\Delta v_p$  measurement.

Table 1 provides the ABE identifiers, star names, 2MASS  $H$  magnitude (Cutri et al. 2003), literature spectral types and references where available (see Section 3.2), and the mean  $\Delta v_p$  for the Br11 line from all APOGEE spectra for each source. Star names beginning with “J” are 2MASS designations, and newly-identified Be stars are indicated by bold font for the ABE ID. If a  $\Delta v_p$  measurement for the Br11 line could not be made in any of the available spectra despite evidence of Br11 emission or shell absorption, one of the following abbreviations is provided in place of a  $\Delta v_p$  value: “w” weak emission-peaks not discernible; “sp” single-peaked emission; “sh” shell absorption without resolved adjacent emission peaks; “as” severe asymmetry in emission peak heights such that only one peak is discernible (not the same as single-peaked); “bl” V peak of Br11 is severely blended with Fe II 16792 (ABE-013); “tc” spectra are heavily contaminated by telluric features (ABE-058).

The ABE identifiers were assigned to avoid the use of sometimes lengthy survey identifiers which are the only star names available. Three groups of ABE stars are distinguished from one another by ABE ID as follows:

- **ABE-001–ABE-202** refer to Be stars that were quasi-randomly targeted by APOGEE as TSS and



subsequently identified as Be stars through visual inspection of the wavelength region encompassing Br11 and Fe II 16878. To account for sources only producing emission lines in certain epochs, which was frequently the case, it was necessary to examine all  $>70,000$  individual spectra for all  $>17,000$  telluric stars.

- **ABE-A01–ABE-A36** refer to Be stars that we targeted intentionally via internal proposals for APOGEE observations of ancillary (hence the ‘A’ prefix of the ABE IDs) science targets falling within a subset of pre-planned APOGEE fields. Most of the intentionally-targeted Be stars are early-type (B3 and hotter) classical Be stars, showing stronger than average  $H$ -band emission in the APOGEE spectra, but two stars classified as B[e] in the literature were observed (ABE-A23 and ABE-A35) as was a reported Herbig Ae star (ABE-A33).
- **ABE-Q01–ABE-Q23** refer to stars which (a) had existing ‘emission line star’ classifications in the literature, (b) appeared to be hot OBA stars in the APOGEE spectra, but (c) did not produce any discernible emission in any of the associated APOGEE data (all have multi-epoch data), or in other words, were  $H$ -band quiescent (hence the ‘Q’ of the ABE IDs) during the observations.

### 3.2. Literature spectral types

The He I 17007 line, analogous to optical He I in terms of utility as an effective temperature ( $T_{\text{eff}}$ ) diagnostic for OB stars (Blum et al. 1997; Meyer et al. 1998) and the only non-hydrogen stellar absorption feature expected to be present for B-type stars (the earliest-O stars exhibit He II 15723, 16923 absorption), is not covered by APOGEE spectra. Therefore, detailed spectral classification of OB stars is not possible with these data and the literature was perused for the existing spectral classifications included in Table 1.

The Catalogue of Stellar Spectral Classification (CSSC; Skiff 2013) was the primary resource used for locating spectral type information, but some of the original sources of spectral types in the CSSC (primarily those pre-dating 1940) could not be tracked down. In those cases, the spectral types are enclosed in parentheses and the provided reference is “C.” Other second-hand spectral types, culled from modern compilations of historical data, are also enclosed in parentheses. The spectral types not enclosed in parentheses are therefore those that could be linked directly to the paper or catalog where the spectral type was determined or estimated.

### 3.3. New Be star discoveries

A total of 128 Be stars have been identified as Be stars for the first time via Brackett series emission in APOGEE spectra. According to the Be Star Spectra Database (BeSS; Neiner et al. 2011), which maintains a comprehensive database of classical Be and main sequence B[e] stars, 2070 Be stars are catalogued in the Milky Way and Magellanic clouds combined. The 128 new Be stars presented in this work therefore represent a  $\sim 6.2\%$  increase in the number of known Be stars.

The positions of all 238 ABE stars are shown in Figure 2, along with the Be star entries included in the BeSS database (Neiner et al. 2011). Although APOGEE observes a large number of fields in the Galactic Halo, the majority (90%) of Be stars observed during the survey reside along the plane of the Milky Way (at Galactic latitudes,  $|b| < 10$ ), similar to the trend seen in BeSS.

Stars included in the ABE sample were generally required to exhibit evidence of emission or shell absorption in at least the H I Br11 line. The exceptions to this rule are ABE-111, ABE-196, and ABE-A06; these stars appear clearly to have emission from Fe II 16878 (see Section 4.2) despite very weak or no emission in the Brackett lines. Figure 3 shows examples of new and previously-known Be stars representing the most borderline cases included in the ABE sample. For many of these stars, the Br11 emission is sufficiently weak that double-peaks are not discernible. Rather, the photospheric Br11 absorption wings appear filled in with emission, creating ‘shoulders’ on the line profiles (e.g. ABE-112) and making them easily distinguishable from purely photospheric lines profiles. Fe II emission is also apparent for a number of these stars, despite weakness of the H I emission.

The large number of new Be stars identified by APOGEE is due in large part to the high-resolution, high-SNR spectra which permit identification of very weak disk signatures (e.g. Figure 3) that might be overlooked in lower-resolution spectra or narrow-band photometry. Repeated observations of most of the stars ( $>1$  observation for 93% of sample) can provide confirmation of very weak disk signatures and also reveals transient Be disks, where Brackett series emission either fades away or appears unexpectedly from epoch to epoch (Wisniewski, in preparation). Among the reasons for 86/128 newly-identified ABE stars having been classified in the literature as normal O-, B-, or A-type stars is that the stars did not possess CS disks at the time the spectral types were determined or estimated.

### 3.4. ABE-144 and ABE-170: the brightest new Be stars

The brightest newly-identified Be star among the ABE sample is ABE-170, *a.k.a.* HR 2116 ( $V = 6.36$ ), and the second-brightest is ABE-144, *a.k.a.* HD 189847 ( $V = 6.92$ ). The lack of a prior indicator of emission lines for ABE-144 may be due to few or no historical spectroscopic observations of the star beyond Fehrenbach et al. (1962). It is unclear whether or not Balmer series emission would have been noticed in that study. ABE-170 has been observed spectroscopically in more recent studies including Abt et al. (2002) and Strom et al. (2005), but the spectra used in both of those papers were limited in wavelength coverage to the region encompassing He I 4471 and Mg II 4481, such that emission at H $\alpha$  or H $\beta$  would not have been recognized if present. Among the possible reasons for the Be nature of these stars not having been previously recognized is that ABE-144 and ABE-170 were normal B stars during past observations (similar to, e.g., Bjorkman & Miroshnichenko 2000).

### 3.5. Observed emission lines

The emission lines detected in APOGEE’s wavelength range are listed in Table 2. For each line, Table 2 pro-

vides the (1) line identification, (2) laboratory rest wavelength, (3) observed wavelength (see concluding paragraph of this section), (4) the difference between laboratory and observed wavelengths, (5) lower level energy  $E_i$ , (6) upper level energy  $E_k$ , (7) transition strength expressed as  $\log(g_i f_{ik})$ , (8) for metallic lines only, the number of confident and possible detections, (9) the number of stars for which  $\Delta v_p$  was measured, (10) the range of  $\Delta v_p$  measurements, (11) the average of all  $\Delta v_p$  measurements, (12) and other transitions possibly contributing to the observed emission line profiles.

Attempts to identify all non-hydrogen (metallic) lines, described in Section 4, made use primarily of Peter van Hoof’s Atomic Line List v2.05b16<sup>13</sup> (PLL from here on) and to a lesser extent the NIST Atomic Database (Kramida et al. 2013) and the Kurucz line list<sup>14</sup>. The identities of metallic emission lines at 15760 Å and 16781 Å remain ambiguous due to few transitions around the correct wavelengths having available transition probability data needed for confident identification. These lines, referred to as  $\lambda 15760$  and  $\lambda 16781$  throughout this paper, are discussed in more detail in Section 4.5. Since forbidden line emission was present for only one source, ABE-A23 *a.k.a.* MWC 922, the central star of the Red Square Nebula (Tuthill & Lloyd 2007), Table 2 is limited to the permitted (E1) transitions observed for Be stars. The  $H$ -band spectrum of MWC 922 is sufficiently different from the rest of the sample and sufficiently more complex that an in-depth analysis is currently being pursued separately (Whelan, in preparation).

The observed wavelengths as well as the differences between laboratory and observed wavelengths, provided in columns (4) and (5) of Table 2, pertain to the average position of double emission peaks for each line plus a correction factor based on the Doppler shift found for the Br11 line. Br11 is the strongest line covered for these stars and provides the most reliable peak position measurements, so correction to rest frame was done simply by adding to the observed wavelength of each line the difference between Br11 emission peak midpoint and Br11 rest wavelength.

#### 4. NON-HYDROGEN LINE IDENTIFICATION

##### 4.1. DIBs

The diffuse interstellar band (DIB) at 15271 Å, discovered by Geballe et al. (2011), is present in most of the ABE spectra and in numerous APOGEE spectra (Zasowski et al. 2014). Because DIB 15271 usually falls on or near the Br19 R emission peak, Br19 peak separation measurements are omitted from this paper. Examples of DIB 15271 absorption (marked with red dotted lines) in spectra for four active Be stars and two currently emission-less stars are displayed in Figure 4. Other DIBs (15615, 15651, 15671 Å) discussed in Geballe et al. (2011) are present for most objects with DIB 15271, as are other possible DIBs at  $\sim 15314$  Å and  $\sim 16154$  Å. Of the spectra shown in Figure 4, DIB 15314 appears most prominently in the spectrum for ABE-137.

##### 4.2. Fe II

The Fe II 16878 line appears in emission for between 32–46% (upper limit includes weak or ambiguous detections) of the 238 active Be stars discussed here, making it the most frequently-observed metallic feature in APOGEE’s coverage of the  $H$ -band. For stars with very strong Fe II 16878, the much weaker Fe II 16792 also appears in emission but is usually blended with Br11. As for Fe II 16878, proximity of the feature to C I 16895 often leads to a blend of the two lines, especially since C I emission is always broad compared to Fe II (see Section 5.2).

Examples of stars with emission from one or both  $H$ -band Fe II lines are presented in Figure 5. The left panel demonstrates the wide range of H I strength corresponding to Fe II detections. As is seen quite clearly for the lower-most stars (ABE-A06, ABE-111) in the left panel of Figure 5, Fe II emission may be present even when there is no perceptible emission from Brackett series lines, contrary to the finding of Steele & Clark (2001). ABE-A06 has been a Be-shell star at various epochs (see BeSS spectra), but in the APOGEE data exhibits only very weak filling of the Br11 photospheric absorption wings in addition to the weak Fe II 16878 emission that, for ABE-A06, persists in four spectra sparsely covering 0.77 years. Less evidence is available for H I emission in the case of ABE-111, despite the Fe II feature appearing in all six APOGEE covering 2.29 years. Though not shown in Figure 5, ABE-196 also lacks convincing evidence of H I emission and yet exhibits Fe II 16878 emission in all 13 APOGEE spectra covering 3.02 years. Line profile variability in the Brackett lines is observed for all three stars and is likely due to varying degrees of emission filling, but lack of knowledge of the true photospheric absorption profiles prevents us from confidently claiming H I emission is present.

The right panel of Figure 5 focuses on some of the more extreme Be stars in this sample, starting with the obvious outlier ABE-A23, an unclassified B[e] star (Lamers et al. 1998) for which the exceptionally strong Fe II and [Fe II] emission lines reported by Rudy et al. (1992) dominate the APOGEE spectra. In contrast to ABE-A23, where the emission lines all appear truly single-peaked, ABE-137 is likely a classical Be star viewed at an inclination,  $i$ , of nearly or exactly zero. The Brackett series lines for ABE-137 show some peak structure even though the peaks are not resolved. The Fe II 16878 line is very narrow and pointed but double peaks are resolved in the C I 16895 line, suggesting the presence of a circumstellar disk. ABE-A35 exhibits strong Fe II emission, and is the only source of the ABE sample for which the  $\Delta v_p$  of Fe II 16792 could be measured. The average Fe II peak separations from five spectra for ABE-A35 are in good agreement:  $\Delta v_p(\text{Fe II } 16878) = 52.6 \pm 2.53 \text{ km s}^{-1}$ ,  $\Delta v_p(\text{Fe II } 16792) = 48.3 \pm 4.01 \text{ km s}^{-1}$ . The lower resolution of red detector data from APOGEE commissioning data is likely a factor in the single-peaked appearance of the Fe II lines for ABE-015.

##### 4.3. Fe II profiles as a function of inclination

In past studies, optical Fe II lines have been used (Hanuschik 1996) to establish a strict definition of the shell, or edge-on, class of Be stars. Photospheric Fe II ab-

<sup>13</sup> <http://www.pa.uky.edu/~peter/newpage/>

<sup>14</sup> 1995 Atomic Line Data (R.L. Kurucz and B. Bell) Kurucz CD-ROM No. 23. Cambridge, Mass.: Smithsonian Astrophysical Observatory

sorption lines are usually observed at greatest strength for A-F supergiants (Gray & Corbally 2009), so if the central depression of an Fe II emission line for a Be star extends below undisturbed, adjacent continuum level, the implication is that the disk is viewed at sufficiently large inclination that our line of sight passes through an appreciable volume of cool gas in the inner, equatorial disk. It is a well-known fact that Fe II and Ti II shell lines are among the strongest metallic features present in the spectra of edge-on Be stars.

In contrast to the observed behavior of optical Fe II lines, stars with obvious shell absorption in the Brackett series lines exhibit no evidence of shell absorption in the  $H$ -band Fe II lines nor in any of the covered metallic lines, such that the Fe II line profile shapes for pole-on Be stars differ from those of edge-on Be stars only in line width. This fact is demonstrated in Figure 6, where the upper panel compares Br11 and Fe II profiles for five stars viewed over a range of inclination angles. As can be seen, the Fe II profiles are pure emission regardless of the what form the H I profiles take. The lower right panel of Figure 6 presents additional examples of H I-shell stars with Fe II emission, while the lower left panel (as well as the edge-on example in the upper panel) highlights ABE-035, the most extreme shell star within this sample in terms of Brackett series shell depth.

#### 4.4. C I and other neutral lines

An emission line at 16895 Å is identified for the first time as C I 16895.031 and is observed for between 18–26% of the 238 Be stars. Figure 5 displays 11 examples of stars with C I emission and the strongest detections will be discussed in Section 4.4.1. A C I 16895 absorption line is present in numerous APOGEE spectra of A-F stars, but the line is typically not present for OB stars unless in emission. Except in the case of very narrow-lined Be stars (e.g. ABE-015, ABE-040 in Figure 5), the R peak of the C I 16895 emission profile is frequently compromised by a strong airglow line around  $\sim 16904$  Å.

Prior mentions in the literature of NIR C I emission include Groh et al. (2007) and Štefl et al. (2009), where several C I emission lines were detected around 10700 Å in Be star spectra. Spectra showing C I 16895 emission have been included in a number of papers, but the line is usually either confused and/or blended with Fe II 16878, or not identified at all. Ashok & Banerjee (2000) noticed the C I 16895 line in a subset of low-resolution Be star spectra and realized that it was probably not Fe II 16878 due to the measured wavelength of the line ( $\sim 16893$  Å, or  $\sim 15$  Å from the Fe II wavelength). Kendall et al. (2003) presented medium resolution  $H$ -band spectra of three young stellar object (YSO) candidates, one of which, IRAS 17441-2910, was found to be a very strong emission line source. A plot of the spectrum shows single-peaked Br11 and Fe II 16878 emission and strong double-peaked C I 16895 emission, but the authors did not comment on the latter.

NIR emission from C I is not limited to classical Be stars. C I 16895 emission was present in a high-resolution spectrum shown by Kraus et al. (2012) for the Herbig B[e] star V921 Scorpii, and the C I emission line is also present in APOGEE spectra for both B[e] stars observed by APOGEE to date (see right-hand panel of Figure 5).

Even luminous blue variable (LBV) stars display evidence of C I emission lines (Groh et al. 2007), suggesting that NIR C I emission is ubiquitous across a wide range of evolutionary states.

##### 4.4.1. C I-strong Be stars

Abnormally strong C I 16895 emission is accompanied by weaker, similarly-profiled emission lines from neutral and singly-ionized species in the spectra for at least five ABE stars. Figure 7 displays full APOGEE spectra for ABE-A15, ABE-188, and ABE-084, ABE-031, and ABE-004, the best examples of this marked deviation from the typical  $H$ -band emission line content for Be stars. The C I 16895 emission is blended with Fe II 16878 for ABE-A15 and possibly also for ABE-188. Two other C I lines at 16009.27 Å and 16026.08 Å are blended in emission for these stars, leading us to refer to the group as ‘C I-strong’ Be stars.

Most of the metallic emission features for the C I-strong Be stars correspond to strong absorption lines for late-A and cooler stars. An APOGEE spectrum for HD 163271, which is either a single metallic-line A star (A2/A3m) or the superposition (A2/A3+F0) of an A star with an F star (Houk & Smith-Moore 1988; Renson et al. 1991), is provided in Figure 7 to demonstrate the typical line content for A-F stars. Small blue line segments indicate the numerous strong Fe I lines covered, with Fe I 15299 being the strongest and appearing in emission for the Be stars. It is likely that emission from other Fe I lines is involved in much of the blending in the C I-strong Be star spectra.

Detections of resolved emission peaks for the S I lines labeled in Figure 7 are unavailable, but the lines may contribute to the weak bumps and blending around Br17. The transition probability measures for these S I lines suggests S I 15426 should be the strongest of them and the A star spectrum appears to confirm this. Since the Br17 profiles for the C I-strong Be stars do not appear distorted by significant underlying emission from other lines however, it is unclear whether the S I lines are actually observed as emission features.

The strong emission lines redward of Br15 are due partly to several Mg I lines, with the strongest contributions being Mg I 15753.291 and Mg I 15770.149. The Mg I lines are also seen weakly in emission and unblended for ABE-149; all of the emission lines are single-peaked for that source, including H I, Fe II 16878, C I 16895, and the Mg I lines (see Appendix A). Above the ABE-A15 spectrum in Figure 7 is a small panel that zooms in on the Mg I blend for ABE-A15, demonstrating that emission from  $\lambda 15760$  is also a major contributing factor in the blend. Black arrows in the small panel point out the sharp  $\lambda 15760$  peaks that mimic the sharp  $\lambda 16781$  peaks. ABE-004 similarly has the  $\lambda 15760$  and  $\lambda 16781$  lines clearly in emission.

As for the line around 15964 Å, PLL suggests two possible identities: Cl I 15964.11 and Si I 15964.4218. Since other covered Cl I lines are expected to be stronger than Cl I 15964.11 are covered but do not appear in emission (e.g. Cl I 15524.70), Si I seems the more likely to cause the 15964 Å emission. The line blended with Br14 (most noticeable for ABE-084 and ABE-031) is suspected to be Si I 15892.7713, the next strongest Si I line covered after Si I 15964.4218.



The weak double-peaked line around  $\sim 16565$  Å is possibly Ca II 16565.59, but the ambiguous detection of Ca II 16654.43 calls the Ca II identification into question since the latter line should be stronger. On the other hand, the position of Ca II 16654.43 corresponds to a strong telluric band which is poorly-corrected and may cause the ambiguity. Emission from the Ca II triplet (8498, 8542, 8662 Å) is observed for some Be stars (Hiltner 1947; Polidan & Peters 1976), so *H*-band Ca II emission would not be terribly unexpected. A C I line at 16564.13 Å probably does not contribute since similar C I lines, covered and expected to be stronger than C I 16564, fail to appear.

The cause of the strong C I 16895 in addition to other weaker emission lines for the C I-strong Be stars remains unknown. Based on the available examples however, such as ABE-031 where the weak emission features persist in 12 spectra covering 1.2 years, the phenomenon appears to be permanent rather than a particular stage of short- or medium-term intrinsic variability.

#### 4.5. $\lambda 15760$ and $\lambda 16781$

The  $\lambda 15760$  and  $\lambda 16781$  emission lines discussed by Steele & Clark (2001) are present for between 15–21%. As is demonstrated in Figure 8, these lines always appear together with matching intensity and V/R orientation. In the available examples where peak separations were measurable for  $\lambda 15760$  and  $\lambda 16781$ , those values are nearly identical as well (see Section 5.2). Fe II 16878 is usually detected in unison with  $\lambda 15760$  and  $\lambda 16781$ , but this is not a strict rule. Non-detection of Fe II 16878 is accompanied by detections  $\lambda 15760$  and  $\lambda 16781$  for ABE-180, ABE-A05, and ABE-005, the three lower-most stars represented in Figure 8.

The  $\lambda 15760$  line has been identified as Fe II in several past papers (Steele & Clark 2001; Smith 2001; Kraus et al. 2012). In a study of  $\eta$  Carinae, Hamann et al. (1994) was apparently the first to note proximity of  $\lambda 15760$  to an Fe II transition. The authors of that paper appended a question mark to the Fe II identification listed in an emission line table, but it seems that over the years the question mark was forgotten. PLL lists an Fe II line at 15761.78 Å, but no indication of expected transition strength is available. NIST provides wavelength for different Fe II transitions, at 15759.720 Å and 15760.563 Å, with the lower energy levels again more than doubling those of Fe II 16878 (5.5 eV versus 13.4 eV) and again lacking transition strength indication. A firm identification for this emission line remains elusive.

Whereas Steele & Clark (2001) restricted the possible identifications for  $\lambda 16781$  to [Fe II] 16773 and Fe II 16792, the much higher-resolution APOGEE spectra rule out both of those lines as possibilities (see ABE-A23 spectrum in Figure 5). PLL includes several He I lines around 16780 Å, but considering that an absorption line is never seen at this wavelength for normal OB stars,  $\lambda 16781$  is probably not He I. Also listed in PLL is an O I multiplet at 16781.7 Å, lacking transition probability data and being quickly ruled out by non-detection of other O I lines covered and expected to be stronger. Through similar argument, other lines listed in PLL and NIST around  $\lambda 16781$  are readily ruled out as possibilities.

Whatever the identities of  $\lambda 15760$  and  $\lambda 16781$ , the fea-

tures behave similarly to Fe II in being present as emission lines or not present at all: no corresponding absorption for features are seen for APOGEE-observed stars of any type. Reliable spectral types have been reported for 24 ABE stars with  $\lambda 15760$  and  $\lambda 16781$  detections and 20/24 are B3 or hotter, so it is possible that  $\lambda 15760$  and  $\lambda 16781$  are relatively high-ionization lines. One possible example of  $\lambda 16781$  being detected despite absence of  $\lambda 15760$  is ABE-A36, a peculiar star discussed in Section 6.1. However, the bump in the V wing of Br11 for ABE-A36 is not sufficiently convincing to cause us to doubt that  $\lambda 15760$  and  $\lambda 16781$  should always be expected to appear simultaneously.

#### 4.6. N I

The expected strongest and second strongest N I lines covered are seen in emission for ABE-A35. Figure 9 shows a portion of a spectrum for ABE-A35 encompassing the N I 15586.545 and N I 15687.160 lines as well as Br16, Br15 and  $\lambda 15760$ . Neither of the N I lines are detected for any other objects beyond ABE-A35, but they are present in all five APOGEE spectra for ABE-A35. Although [Fe II] 15586.550 is coincident in position with the stronger N I line, it is far from the strongest [Fe II] feature covered. The lack of detection in the ABE-A35 spectra of the stronger [Fe II] lines rules those lines out as possibilities. Forbidden line emission in the optical was noted as early as 1976 for ABE-A35 (Allen & Swings 1976), but in the *H*-band the only clues suggesting the B[e] nature of this object are the abnormally strong H I, Fe II, and Fe II-like emission lines.

#### 4.7. Mg II and Si II

The lowest-energy Mg II and Si II lines covered in APOGEE data appear clearly in emission for ABE-A26 and are not confidently detected for any of the other stars. ABE-004, ABE-A05, and ABE-A29 possibly show exceedingly weak contributions from these lines, but blending renders the situation ambiguous in all cases aside from ABE-A26.

Figure 10 displays a spectrum for ABE-A26 over differing wavelength ranges: the upper panel shows the full spectrum, while the middle and lower panels focus on the weak emission lines around Br11. Identification of the line blueward of  $\lambda 16781$  as Mg II 16764.80 requires that the stronger of three lines comprising this Mg II multiplet also be detected, and indeed the lower panel of Figure 10 shows that Mg II 16804.52 is visible in the V wing of Br11 at apparently the correct intensity relative to Mg II 16764.80. Based on the intensities of these lines, the third Mg II line of the multiplet (16803.67 Å) is not expected to appear and would overlap with Mg II 16804 anyway. The weak emission line redward of Fe II 16878 in the middle panel of Figure 10 is identified as Si II 16911.430, the strongest Si II line covered and a line with very similar energy levels to the Mg II lines (see Table 2).

In addition to detection of the relatively high-ionization Mg II and Si II lines, the combination of single-peaked Brackett series lines and double-peaked metallic lines is unique to ABE-A26 among this sample. The double-peaked lines indicate that at least some of the circumstellar gas is organized in a disk. It is possible that ABE-A26

was observed by APOGEE during of after an outburst such that substantial Brackett series emitting gas is in the polar regions, leading to the single-peaked Brackett lines.

## 5. PEAK SEPARATIONS

### 5.1. Stars with abnormally large $\Delta v_p$

Optical spectroscopy revealed that two stars, ABE-050 (HD 345439) and ABE-075 (HD 23478), with extremely large Brackett emission widths and double-peak separations are not classical Be stars (Eikenberry et al. 2014). Rather, these stars are analogues to the prototype magnetic emission B star  $\sigma$  Orionis E first described as ‘Helium-rich’ by Greenstein & Wallerstein (1958) and subsequently providing the first application (Townsend et al. 2005) of the Rigidly Rotating Magnetosphere model of Townsend & Owocki (2005). Large  $\Delta v_p$  for the Brackett series emission was a clue suggestive of a non-classical nature for these stars, but confirmation lay in the fact that both stars exhibit H I emission well beyond the projected  $v \sin i$  values (in these cases, a factor of two or more beyond the projected  $v \sin i$ ). For classical Be stars with Keplerian disks, the velocity separations of emission peaks do not exceed  $2v \sin i$  (Dachs et al. 1992).

Figure 11 compares the Br11 profiles of ABE-050 and ABE-075 to the stars with the next largest peak separations. Arrows indicate the measured peak separations and for ABE-050 and ABE-075, the inner sets of arrows indicate the  $v \sin i$  values from Eikenberry et al. (2014). As there are only a handful of magnetic B emission stars known to exist, it seems more likely that the ABE-155, ABE-168, ABE-124, and ABE-099 are weak-disked, edge-on classical Be stars rather than additional  $\sigma$  Orionis E types. Either way, optical follow-up spectroscopy is required for proper diagnosis.

### 5.2. Line-by-line $\Delta v_p$ comparison

Figure 12 plots the peak separations for Br11 versus the peak separations for Br12–Br18, Br20,  $\lambda 16781$ ,  $\lambda 15760$ , Fe II 16878, Fe II 16792, C I 16895, Si I 15964, and Mg I 15770. Each point represents the average peak separation for a line, from all spectra for a given star in which the Br11  $\Delta v_p$  was measured in addition to the  $\Delta v_p$  of the line represented on the y-axis. In the upper nine panels, plus signs (red) correspond to stars for which the Br20 peak separation was measured and therefore to stars with strong or particularly sharp-peaked emission. The gaps between  $\sim 400$ – $500 \text{ km s}^{-1}$  in the Br11 vs. Br18 and Br11 vs. Br17 panels are due to strong airglow lines impacting the emission peaks at large line width. High velocity gaps in the Br11 vs. Br12 and Br11 vs. Br14 panels are caused by either the Br12 V peak or the Br14 R peak falling too close to gaps between detectors. For Br13 and Br15, telluric absorption contamination is more likely for large line width. Grey lines indicate 1-to-1 relationships between the lines plotted in each panel.

The effect of increasing  $\Delta v_p$  toward weaker H I lines is well-known for the Balmer (Hanuschik et al. 1988) and Paschen (Andrillat et al. 1990) lines, and the Brackett series lines are not an exception. Some stars (primarily the narrow-lined variety with Br11  $\Delta v_p < 200 \text{ km s}^{-1}$ ) show very little or no variation among Brackett series

$\Delta v_p$  but no convincing examples are found of decreasing  $\Delta v_p$  from Br11 toward Br20. We interpret the increasing peak separations toward weaker lines as kinematic in nature, such that the weaker Brackett lines (Br12–20) are simply formed closer to the rapidly-rotating central stars than e.g. Br11. The Br11–20 lines never take the form of winebottle-type profiles frequently observed in the optically-thick H $\alpha$  line, where the effect of non-coherent scattering can produce inflections in the emission profile and effectively reduce the observed peak separation (Hummel & Dachs 1992). Section 4 of Hanuschik et al. (1996) provides a summary of the line broadening factors that contribute to Be star emission line profile shapes.

Based on the lower three panels of Figure 12, when the  $\Delta v_p$  of  $\lambda 15760$  and  $\lambda 16781$  are measured simultaneously, very similar values are found. The  $\Delta v_p$  for these lines are usually slightly smaller than the Br11  $\Delta v_p$  but can be slightly larger as well. Excluding ABE-A26, for which Br11 is single-peaked, Fe II 16878 is a strictly small- $\Delta v_p$  line relative to Br11 with all  $\Delta v_p$  measurements less than  $140 \text{ km s}^{-1}$ . The C I 16895 Si I 15964, and Mg I 15770 lines share nearly identical  $\Delta v_p$  in the available examples (ABE-084, ABE-188, ABE-A15; see Figure 7), and all of the  $\Delta v_p$  measurements for C I 16895 exceed the Br11  $\Delta v_p$ .

### 5.3. Line-emitting disk radii

For Keplerian rotation in a gaseous disk, the orbital velocity decreases according to  $r^{-1/2}$ , where  $r$  is the radial distance from star to disk. Given knowledge of the stellar rotational velocity,  $v \sin i$ , the peak separation of an emission line can be used to calculate the approximate outer radius in the disk,  $r_d$ , at which that line is preferentially formed (Smak 1969; Huang 1972; Smak 1981; Horne & Marsh 1986). Many authors (e.g., Hanuschik 1987; Hanuschik et al. 1988; Dachs et al. 1992; Andrillat et al. 1990; Slettebak et al. 1992) have used this relation (Huang’s law) to study the geometry of Be disks by estimating the individual line-emitting radii for H I and metallic lines in the optical region. In units of stellar radii,  $R_*$ ,  $r_d$  is calculated via Huang’s Law (Huang 1972) as

$$r_d = \left( \frac{2 \times v \sin i}{\Delta v_p} \right)^2 \quad (1)$$

where the equation is squared due to the assumption of a circular orbit. The resulting outer disk radii measurements for the subset of stars with available  $v \sin i$  from the literature and Br11 or metallic line  $\Delta v_p$  measurements are listed in Table 3. In estimating  $r_d$ , the average  $\Delta v_p$  measured from all spectra for each star (the number of spectra used for each star is indicated in the ‘# Obs’ column) have been used. The relation in equation 1 may not necessarily hold for cases of emission lines with asymmetric peak intensities or for shell profiles so these instances have been noted in Table 3. In particular, large  $r_d$  estimates ( $r_d > 5r_*$ ) correspond to asymmetric and shell profiles.

Taking the average of the Br11  $r_d$  estimates for the 19 non-shell stars with roughly symmetric emission peaks, we find an average Br11 formation outer radius and associated standard deviation of

$$r_d (\text{Br11}) = 2.21 \pm 0.73 R_* \quad (2)$$



Hanuschik et al. (1988) found an average  $H\alpha$ -emitting radius of  $\sim 20 R_*$ , while Slettebak et al. (1992) found an average of  $\sim 19 R_*$ . It is important to note, however, that results from interferometry confirm that application of Huang’s law to the double peaks of winebottle-type profiles (appearing for optically-thick lines like  $H\alpha$ ) leads to artificially-large disc radii estimates (Hummel & Dachs 1992). Interferometric studies typically produce radii estimates of less than  $10 R_*$  over the optical and  $JHK$  bands (see disk radius measurements and papers referenced in Table 2 of Rivinius et al. 2013b), more similar to what is found here from the Brackett lines.

For  $H\gamma$  and  $\text{Fe II } 6516 \text{ \AA}$ , Slettebak et al. (1992) found emitting radii of  $\sim 7.4 R_*$  and  $\sim 3.9 R_*$  respectively. In a study of optical  $\text{Fe II}$  emission lines for Be stars, Arias et al. (2006) found that, on average, the optical  $\text{Fe II}$  lines are formed at an outer disk radius of 2.0 stellar radii. Therefore, the Br11-emitting outer radius is roughly coincident with the optical  $\text{Fe II}$ -emitting outer radius and well inside the  $H\alpha$ -emitting radius.

Given the sparsity and potential wide-range of quality of  $v \sin i$  information for our sample, disk radii are only estimated for the Br11 and metallic lines. However, it follows from Figure 12 that the Br12–Br20 formation outer radii are interior to that of Br11. Andrillat et al. (1990) and Slettebak et al. (1992) found a correlation between formation location of individual optical lines and the upper energy levels ( $E_k$ ) of the lines. Weaker lines with higher  $E_k$  were generally found to have larger  $\Delta v_p$  and hence smaller  $r_d$ . This is also the case for the Brackett series lines, where  $E_k$  increases slightly from Br11 to Br20.

A trend toward large  $r_d$  is evident for the  $\text{Fe II } 16878$  line with respect to Br11. The average of the five available  $r_d$  estimates for  $\text{Fe II}$  is  $\sim 19 R_*$ , almost ten times the disk radius where Br11 is preferentially formed. A consequence of the widely-varying formation radii between Br11 and  $\text{Fe II } 16878$  is discussed in the following section.

## 6. SINGLE-EPOCH VARIATION IN V/R AND RV

As outlined in Okazaki (1991), long-term V/R variability for Be stars often entails shifts in radial velocity (RV) of entire emission line profiles toward whichever peak is stronger at the time and differences in V/R orientation between lines with different formation loci, such that V/R is necessarily constant from atomic species to atomic species or from line to line. These effects are believed to be caused by perturbations with the disks that give rise to one-armed global density waves that slowly precess through the disk with periods averaging 7 years (Rivinius et al. 2013b).

Recent papers discussing the well known Be-shell star  $\zeta$  Tau provided an example of V/R phase lags between Balmer and Brackett series lines and also between individual Brackett series lines. Wisniewski et al. (2007) hypothesized that the optical/NIR phase lag in V/R could be understood in terms of differing preferential formation radii and of the global density perturbation within the disk taking the form of a spiral arm. Štefl et al. (2009) and Carciofi et al. (2009) subsequently showed this to be the case.

### 6.1. $H\text{ I}$ vs. $H\text{ I}$ V/R phase lags

Evidence of V/R phase lags within the Brackett series lines is present in the spectra for the ABE stars represented in Figure 13. Each Brackett line is displayed individually on a velocity scale in Figure 13 and, with the exception of ABE-A36 (discussed below), the V/R of Br11 for each spectrum is printed in left-most Br11 panels while the differences between the V/R of Br11 and the V/R of Br12–Br20 are printed in the Br12–Br20 panels. For ABE-A29, the V/R orientations progress from  $V < R$  at Br11 to  $V \simeq R$  at Br17. The Br19 profile is contaminated by DIB 15271 absorption, but the Br18 and Br20 profiles have  $V \simeq R$  similar to Br17. For ABE-A31 and ABE-181 the opposite progression takes place as the R peak increases in dominance from Br11 to Br20. Although the Br11 profiles for ABE-A36, ABE-A31, and ABE-181 are contaminated by underlying metallic emission ( $\lambda 16781$  and/or  $\text{Fe II } 16878$ ), the V/R phase lag is nonetheless plainly visible from comparison of the Br12 or Br13 profiles to Br20.

Of the 238 stars comprising the ABE sample, ABE-A36 is the only available example of quasi-triple-peaked (*qtp*) Brackett series lines (see upper row of Figure 13), where the “quasi” implies ambiguity as to whether there is actually a true third emission peak or whether instead the central absorption is split into multiple components. The V emission peak of Br11 for ABE-A36 is slightly higher than the R peak due to possible blending with  $\lambda 16781$ , and the possible third peak appears between the dominant outer emission peaks with lesser intensity than those peaks. Br12 is similar in profile to Br11, but from Br12–Br17 the profiles gradually assume a ‘flat-topped’ morphology with the apparent blue central absorption still weakly visible in contrast to the apparent red central absorption having all but disappeared. At Br18, evidence of the third (middle) emission peak emerges again, this time as the dominant peak since the outer V and R peaks have all but disappeared. Br19 is directly impacted by DIB 15271 but otherwise appears similar to Br18. Finally, the Br20 profile is smooth and rounded with only subtle traces of the blue central absorption and middle ‘emission peak’ (the outer emission peaks are no longer visible).

Štefl et al. (2009) pointed out that although *qtp*  $H\alpha$  profiles occur at certain times during the V/R cycle of  $\zeta$  Tau, optically thin lines like  $\text{O I } 8446$  and the Brackett series never exhibited any evidence of *qtp*. It is therefore unusual that *qtp* profiles are observed in the Brackett lines for ABE-A36. We can report no additional examples.

### 6.2. $H\text{ I}$ vs. metallic V/R and RV phase lags

The five examples shown in Figure 14 represent the first known examples of disagreement between the V/R orientations of Brackett series versus metallic lines ( $\text{Fe II } 16878$ ,  $\lambda 15760$ , and  $\lambda 16781$ ). ABE-097, ABE-181, and ABE-002 have  $V < R$  for  $H\text{ I}$  and  $V > R$  for metallic lines, while ABE-016 and ABE-013 have  $V > R$  for  $H\text{ I}$  and  $V < R$  for metallic lines. Due to the contaminated Br11 profiles for ABE-013, ABE-002, and ABE-181, where the V peak height has been increased by underlying  $\text{Fe II } 16792$  emission, the left-hand panels of Figure 14 are extended to encompass not only  $\lambda 15760$ , but also Br15–Br17 to show the typical  $H\text{ I}$  V/R orientation for each star.

Although the lack of available stellar absorption lines means that precise stellar RV determination is not pos-

sible, the spectrum for ABE-013 in Figure 14 has been corrected to rest frame based on the average positions of the deep absorptions in the Br12–Br20 lines, while the other spectra lack the deep H I absorptions and therefore were corrected for Doppler shift based on average emission peak shift for the Brackett lines. The result that emerges for ABE-013 is that the Brackett series absorptions do not coincide in RV not with the central depressions in the metallic emission lines as is normally true (see Figure 8), but instead the Brackett series absorptions coincide in RV with the R emission peaks of the metallic lines. More specifically, the Fe II 16878,  $\lambda$ 15760, and  $\lambda$ 16781 profiles are shifted in RV with respect to H I absorption by  $\sim 50 \text{ km s}^{-1}$  in the direction of stronger H I peaks as expected from Okazaki (1991).

ABE-002 and ABE-181 exhibit clear evidence of V/R-related RV shifts in the emission profiles, though of a slightly different variety from that of ABE-013. Metallic and H I emission wings for both stars are conspicuously enhanced on the side of the line profiles opposite the stronger emission peak for ABE-002 and ABE-181, with the H I wings being enhanced on the blue side and the metallic wings enhanced on the red side. The enhanced blue wings suggest that significantly more emission is being formed in the inner regions of the approaching side of the disk, and the steep declines in intensity, from stronger emission peak to narrower emission base (R side of H I for ABE-002 and ABE-181), imply cavities in the inner regions of the receding sides of the disks and relatively increased emission coming from the outer regions of the disks. We interpret these line profiles to suggest more tightly wound spiral patterns to the density oscillation in the disks of these stars versus  $\zeta$  Tau.

### 7. BR11 LINE PROFILES

Br11 line profiles from the highest-quality-available spectrum of each ABE star are displayed in Figures 15–20. In Figures 15–18, the Br11 profiles of 165 ABE stars are qualitatively sorted by profile type, going from single-peaked and narrow double-peaked profiles to deep shell profiles. According to the models of Hummel & Dachs (1992) and Hummel & Vrancken (2000), the major line profile shape differences for Be stars are an effect of the inclination angles ( $i$ ) at which the circumstellar disks are observed. Hanuschik et al. (1996) used high-resolution H $\alpha$  and optical Fe II profiles to devise a Be sub-classification scheme based on the notion of  $i$  dictating to a large extent line profile morphology. Silaj et al. (2010) later showed that line shape in an optically-thick line like H $\alpha$  is not dictated solely by  $i$  and that very different profile shapes may be observed at fixed  $i$ , but no such investigations of the Brackett series lines have been done.

In sorting the Br11 profiles of the ABE stars according to expected  $i$ , we relied largely on the models of optically thin lines from Hummel & Dachs (1992). The most readily classified Br11 profiles correspond to  $i \sim 0^\circ$  (pole-on), where single-peaked or narrow double-peaked emission is expected, and  $i \sim 90^\circ$  (edge-on), where deep shell absorption with a sharp core (with or without adjacent emission) is expected. The situation is far more ambiguous for profiles corresponding to intermediate  $i$ , but a general trend of

increasing central depression depth and overall line width with increasing  $i$  is apparent. Line profiles that could not be satisfactorily sorted by  $i$ , due to weakness or ambiguity of the disk features, are shown in Figures 19 and 20. Figure 19 profiles are sorted by Br11 peak separation, and Figure 20 profiles are sorted by ABE identifier.

### 8. CONCLUSIONS

SDSS-III/APOGEE has serendipitously provided the first high-resolution view of the  $H$ -band properties of a large number of Be stars, the majority of which are targeted quasi-randomly by the survey as telluric calibrators. Although significant progress has been made toward understanding Be stars over the past few decades via high-resolution optical, interferometric, and spectropolarimetric studies (Rivinius et al. 2013b), any fully explanatory model of the classical Be phenomenon will need to account for the multi-wavelength properties of these stars. Multi-wavelength studies of statistically-significant samples of Be stars are critical yet have historically been few and far between, though the limited exceptions (Clark & Steele 2000; Steele & Clark 2001) have been highly valuable. Due to simultaneous coverage in the  $H$ -band of numerous H I lines that are minimally affected by underlying photospheric absorption in comparison to the Balmer series lines, the  $H$ -band is particularly promising in terms of utility toward V/R variability and general Be disk studies. Despite the  $H$ -band covering only a limited number of metallic emission lines, we have shown that the Fe II and Fe II-like ( $\lambda$ 15760 and  $\lambda$ 16781) lines are highly interesting in the context of V/R variability and phase lags between various atomic species.

In the first of a series of papers exploring the  $H$ -band properties of Be stars, we have identified the non-hydrogen emission line content of the APOGEE Be star spectra, analyzed the kinematic properties of the metallic and H I features, and discussed the more exceptional Be stars within the sample as well as those deviating from the typical emission line content. Further investigation of the identities of emission lines at 15760 Å and 16781 Å is needed, but may require updated atomic line lists. Since little is known about most of the ABE stars themselves, including spectral type and rotation speed, optical follow-up study of these stars is also needed in order to develop a better understanding of  $H$ -band properties as they relate to known stellar parameters.

*Acknowledgements.* Funding for SDSS-III has been provided by the Alfred P. Sloan Foundation, the Participating Institutions, the National Science Foundation, and the U.S. Department of Energy Office of Science. The SDSS-III web site is <http://www.sdss3.org/>.

SDSS-III is managed by the Astrophysical Research Consortium for the Participating Institutions of the SDSS-III Collaboration including the University of Arizona, the Brazilian Participation Group, Brookhaven National Laboratory, Carnegie Mellon University, University of Florida, the French Participation Group, the German Participation Group, Harvard University, the Instituto de Astrofísica de Canarias, the Michigan State/Notre Dame/JINA Participation Group, Johns Hopkins University, Lawrence Berkeley National Laboratory, Max Planck Institute for Astrophysics, Max Planck Institute for Extraterrestrial Physics, New Mexico State University, New York University, Ohio State University, Pennsylvania State University, University of Portsmouth, Princeton University, the Spanish Participation Group, University of Tokyo, University of Utah, Vanderbilt University, University of Virginia, University of Washington, and Yale University.

We thank the anonymous referee, and Kevin Covey, both of whom provided feedback which substantially improved the paper. The first author additionally thanks his mother for proofreading drafts of the paper.

## REFERENCES

- Abt, H. A., Levato, H., & Grosso, M. 2002, *ApJ*, 573, 359
- Abt, H. A., & Morrell, N. I. 1995, *ApJS*, 99, 135
- Alknis, A. 1958, *Trudy Astrofiz. Lab. Riga*, 7, 33
- Allen, D. A., & Swings, J. P. 1976, *A&A*, 47, 293
- Andrillat, A., Jaschek, M., & Jaschek, C. 1990, *A&AS*, 84, 11
- Arias, M. L., Zorec, J., Cidale, L., et al. 2006, *A&A*, 460, 821
- Ashok, N. M., & Banerjee, D. P. K. 2000, *IAU Colloq. 175: The Be Phenomenon in Early-Type Stars*, 214, 468
- Bartaya, R. A. 1979, *Abastumanskaia Astrofizicheskaiia Observatoriia Byulleten*, 51, 1
- Bjorkman, K. S., & Miroshnichenko, A. S. 2000, *Bulletin of the American Astronomical Society*, 32, 1480
- Bhavya, B., Mathew, B., & Subramaniam, A. 2007, *Bulletin of the Astronomical Society of India*, 35, 383
- Bidelman, W. P. 1988, *PASP*, 100, 1084
- Blum, R. D., Ramond, T. M., Conti, P. S., Figer, D. F., & Sellgren, K. 1997, *AJ*, 113, 1855
- Bopp, B. W. 1988, *AJ*, 95, 1543
- Bouigue, R., Boulon, J., & Pedoussaut, A. 1961, *Annales de l'Observatoire Astron. et Meteo. de Toulouse*, 28, 33
- Cannon, A. J., & Mayall, M. W. 1949, *Annals of Harvard College Observatory*, 112, 1
- Carciofi, A. C., Okazaki, A. T., Le Bouquin, J.-B., et al. 2009, *A&A*, 504, 915
- Carciofi, A. C. 2011, *IAUS*, 272, 325
- Chargeishvili, K. B., Bartaya, R. A., & Kharadze, E. K. 2013, *VizieR Online Data Catalog*, 3271, 0
- Chauville, J., Zorec, J., Ballereau, D., et al. 2001, *A&A*, 378, 861
- Christy, J. W. 1977, *ApJ*, 217, 127
- Clark, J. S., & Steele, I. A. 2000, *A&A*, 141, 65
- Clausen, J. V., & Jensen, K. S. 1979, *IAU Colloq. 47: Spectral Classification of the Future*, 9, 479
- Covey, K. R., Cottaar, M., Foster, J. B., et al. 2014, *American Astronomical Society Meeting Abstracts*, 223, #442.10
- Cowley, A. 1972, *AJ*, 77, 750
- Cutri, R. M., Skrutskie, M. F., van Dyk, S., et al. 2003, *VizieR Online Data Catalog*, 2246, 0
- Dachs, J., Hummel, W., & Hanuschik, R. W. 1992, *A&AS*, 95, 437
- Davis, R. J. 1977, *ApJ*, 213, 105
- Dommanget, J., & Nys, O. 2002, *VizieR Online Data Catalog*, 1274, 0
- Duflot, M., Fehrenbach, C., Duflot, A., Rouviere, E., & Schneider, D. 1958, *Journal des Observateurs*, 41, 43
- Eikenberry, S. S., Chojnowski, S. D., Wisniewski, J., et al. 2014, *arXiv:1403.3239*
- Eisenstein, D. J., Weinberg, D. H., Agol, E., et al. 2011, *AJ*, 142, 72
- Esteban, C., & Fernandez, M. 1998, *MNRAS*, 298, 185
- Fabircius, C., Makarov, V. V., Knude, J., & Wycoff, G. L. 2002, *A&A*, 386, 709
- Feast, M. W., & Thackeray, A. D. 1963, *MmRAS*, 68, 173
- Fehrenbach, C., Rebeiro, E., Petit, M., Peyrin, Y., & Monvoisin, C. 1962, *Journal des Observateurs*, 45, 349
- Frémat, Y., Zorec, J., Hubert, A.-M., & Floquet, M. 2005, *A&A*, 440, 305
- Frémat, Y., Neiner, C., Hubert, A.-M., et al. 2006, *A&A*, 451, 1053
- Garrison, R. F., & Gray, R. O. 1994, *AJ*, 107, 1556
- Geballe, T. R., Najarro, F., Figer, D. F., Schlegelmilch, B. W., & de La Fuente, D. 2011, *Nature*, 479, 200
- Granada, A., Arias, M. L., & Cidale, L. S. 2010, *AJ*, 139, 1983
- Gray, R. O., & Corbally, C. J. 2009, *Stellar Spectral Classification by Richard O. Gray and Christopher J. Corbally*. Princeton University Press, 2009. ISBN: 978-0-691-12511-4,
- Greenstein, J. L., & Wallerstein, G. 1958, *ApJ*, 127, 237
- Grenier, S., Baylac, M.-O., Rolland, L., et al. 1999, *A&AS*, 137, 451
- Grillo, F., Sciortino, S., Micela, G., Vaiana, G. S., & Harnden, F. R., Jr. 1992, *ApJS*, 81, 795
- Groh, J. H., Daminieli, A., & Jablonski, F. 2007, *A&A*, 465, 993
- Guetter, H. H. 1968, *PASP*, 80, 197
- Gunn, J. E., Siegmund, W. A., Mannery, E. J., et al. 2006, *AJ*, 131, 2332
- Halbedel, E. M. 1996, *PASP*, 108, 833
- Hamann, F., Depoy, D. L., Johansson, S., & Elias, J. 1994, *ApJ*, 422, 626
- Hanuschik, R. W. 1987, *A&A*, 173, 299
- Hanuschik, R. W. 1988, *A&A*, 190, 187
- Hanuschik, R. W., Kozok, J. R., & Kaiser, D. 1988, *A&A*, 189, 147
- Hanuschik, R. W., Hummel, W., Sutorius, E., Dietle, O., & Thimm, G. 1996, *A&AS*, 116, 309
- Hanuschik, R. W. 1996, *A&A*, 308, 170
- Hardorp, J., Rohlf, K., Slettebak, A., & Stock, J. 1959, *Hamburger Sternw. Warner & Swasey Obs.*, 0
- Heckmann, O., Dieckvoss, W., & Kox, H. 1956, *Astronomische Nachrichten*, 283, 109
- Heintz, W. D. 1998, *ApJS*, 117, 587
- Henize, K. G. 1976, *ApJS*, 30, 491
- Hernández, J., Calvet, N., Briceño, C., Hartmann, L., & Berlind, P. 2004, *AJ*, 127, 1682
- Hill, P. W., & Lynas-Gray, A. E. 1977, *MNRAS*, 180, 691
- Hiltner, W. A. 1947, *ApJ*, 105, 212
- Hiltner, W. A. 1956, *ApJS*, 2, 389
- Hony, S., Waters, L. B. F. M., Zaai, P. A., de Koter, A., Marlborough, J. M., Millar, C. E., Trams, N. R., Morris, P. W., & de Graauw, Th. 2000, *A&A*, 355, 187
- Horne, K., & Marsh, T. R. 1986, *MNRAS*, 218, 761
- Houk, N., & Smith-Moore, M. 1988, *Michigan Catalogue of Two-dimensional Spectral Types for the HD Stars. Volume 4, Declinations -26 to -12.*. N. Houk, M. Smith-Moore. Department of Astronomy, University of Michigan, Ann Arbor, MI 48109-1090, USA. 14+505 pp. Price US 25.00 (USA, Canada), US 28.00 (Foreign) (1988).
- Houk, N., & Swift, C. 1999, "Michigan catalogue of two-dimensional spectral types for the HD Stars ; vol. 5. By Nancy Houk and Carrie Swift. Ann Arbor, Michigan : Department of Astronomy, University of Michigan, 1999. ("This is the fifth of a projected seven volumes in a program of systematic reclassification of the Henry Draper stars on the MK system..." (preface).)",
- Houk, N. 1982, *Michigan Catalogue of Two-dimensional Spectral Types for the HD stars. Volume.3. Declinations -40 to -26.*, by Houk, N.. Ann Arbor, MI(USA): Department of Astronomy, University of Michigan, 12 + 390 p.,
- Huang, S.-S. 1972, *ApJ*, 171, 549.
- Huang, W., Gies, D. R., & McSwain, M. V. 2010, *ApJ*, 722, 605
- Huang, W., & Gies, D. R. 2006, *ApJ*, 648, 580
- Hummel, W., & Dachs, J. 1992, *A&A*, 262, L17
- Hummel, W., & Vrancken, M. 2000, *A&A*, 359, 1075
- Jaschek, C., & Jaschek, M. 1993, *A&AS*, 97, 807
- Kendall, T. R., de Wit, W. J., & Yun, J. L. 2003, *A&A*, 408, 313
- Kharchenko, N. V. 2001, *Kinematika i Fizika Nebesnykh Tel*, 17, 409
- Kohoutek, L., & Wehmeyer, R. 1997, *Astronomische Abhandlungen der Hamburger Sternwarte*, 11,
- Kramida, A., Ralchenko, Yu., Reader, J., & NIST ASD Team 2013, *NIST Atomic Spectra Database (version 5.1)*, [Online]. Available: <http://physics.nist.gov/asd> [Thursday, 26-Dec-2013 13:32:45 EST]. National Institute of Standards and Technology, Gaithersburg, MD.
- Kraus, S., Calvet, N., Hartmann, L., et al. 2012, *ApJ*, 752, 11
- Lamers, H. J. G. L. M., Zickgraf, F.-J., de Winter, D., Houziaux, L., & Zorec, J. 1998, *A&A*, 340, 117
- Lee, U., Osaki, Y., & Saio, H. 1991, *MNRAS*, 250, 432
- Lesh, J. R., & Aizenman, M. L. 1973, *A&A*, 22, 229
- Lesh, J. R. 1968, *ApJS*, 17, 371
- Levenhagen, R. S., & Leister, N. V. 2006, *MNRAS*, 371, 252
- Majewski, S. R. 2012, *American Astronomical Society Meeting Abstracts #219, 219, #205.06*
- Mathew, B., & Subramaniam, A. 2011, *Bulletin of the Astronomical Society of India*, 39, 517
- Mathew, B., Banerjee, D. P. K., Naik, S., & Ashok, N. M. 2012, *MNRAS*, 423, 2486
- McCuskey, S. W. 1959, *ApJS*, 4, 1
- McCuskey, S. W. 1967, *AJ*, 72, 1199
- McSwain, M. V., Huang, W., & Gies, D. R. 2009, *ApJ*, 700, 1216
- Meillard, A., Stee, P., Vannier, M., et al. 2007, *A&A*, 464, 59
- Mennickent, R. E., Sabogal, B., Granada, A., & Cidale, L. 2009, *PASP*, 121, 125
- Merrill, P. W., & Burwell, C. G. 1949, *ApJ*, 110, 387
- Merrill, P. W., Burwell, C. G., & Miller, W. C. 1942, *ApJ*, 96, 15
- Meyer, M. R., Edwards, S., Hinkle, K. H., & Strom, S. E. 1998, *ApJ*, 508, 397
- Miller, W. C., & Merrill, P. W. 1951, *ApJ*, 113, 624
- Miroshnichenko, A. S., Kusakin, A. V., Bjorkman, K. S., et al. 2003, *A&A*, 412, 219
- Morgan, W. W., Whitford, A. E., & Code, A. D. 1953, *ApJ*, 118, 318
- Morgan, W. W., Code, A. D., & Whitford, A. E. 1955, *ApJS*, 2, 41
- Murdoch, K. A., Drew, J. E., & Anderson, L. S. 1994, *A&A*, 284, 27
- Nassau, J. J., & Harris, D., III 1952, *ApJ*, 115, 459
- Negueruela, I. 2004, *Astronomische Nachrichten*, 325, 380
- Negueruela, I., Steele, I. A., & Bernabeu, G. 2004, *Astronomische Nachrichten*, 325, 749
- Neiner, C., de Batz, B., Cochard, F., et al. 2011, *AJ*, 142, 149
- Nesterov, V. V., Kuzmin, A. V., Ashimbaeva, N. T., et al. 1995, *A&AS*, 110, 367
- Ochsenbein, F. 1980, *Bulletin d'Information du Centre de Données Stellaires*, 19, 74
- Okazaki, A. T. 1991, *PASJ*, 43, 75
- Oksala, M. E., Kraus, M., Cidale, L. S., Muratore, M. F., & Borges Fernandes, M. 2013, *A&A*, 558, A17



- Polidan, R. S., & Peters, G. J. 1976, *Be and Shell Stars*, 70, 59
- Popper, D. M. 1950, *ApJ*, 111, 495
- Porter, J. M., & Rivinius, T. 2003, *PASP*, 115, 1153
- Racine, R. 1968, *AJ*, 73, 233
- Radoslavova, T. 1989, *Astronomische Nachrichten*, 310, 223
- Reig, P., Zezas, A., & Gkouvelis, L. 2010, *A&A*, 522, A107
- Renson, P., Gerbaldi, M., & Catalano, F. A. 1991, *A&AS*, 89, 429
- Rivinius, T., Štefl, S., & Baade, D. 2006, *A&A*, 459, 137
- Rivinius, T. 2013, *Stellar Pulsations: Impact of New Instrumentation and New Insights*, 31, 253
- Rivinius, T., Carciofi, A. C., & Martayan, C. 2013, *arXiv:1310.3962*
- Rivinius, T., Baade, D., Townsend, R. H. D., Carciofi, A. C., & Štefl, S. 2013, *A&A*, 559, L4
- Roman, N. G. 1978, *AJ*, 83, 172
- Roslund, C. 1963, *Arkiv for Astronomi*, 3, 97
- Rudy, R. J., Erwin, P., Rossano, G. S., & Puetter, R. C. 1992, *ApJ*, 398, 278
- Sato, K., & Kuji, S. 1990, *A&AS*, 85, 1069
- Schmidt-Kaler, T. 1967, *PASP*, 79, 181
- Sebastian, D., Guenther, E. W., Schaffenroth, V., et al. 2012, *A&A*, 541, A34
- Silaj, J., Jones, C. E., Tycner, C., Sigut, T. A. A., & Smith, A. D. 2010, *ApJS*, 187, 228
- Skiff, B. A. 2013, *VizieR Online Data Catalog*, 1, 2023
- Skrutskie, M. F., Cutri, R. M., Stiening, R., et al. 2006, *AJ*, 131, 1163
- Slettebak, A., Collins, G. W., II, & Truax, R. 1992, *ApJS*, 81, 335
- Smak, J. 1969, *ACA*, 19, 155
- Smak, J. 1981, *ACA*, 31, 395
- Smee, S. A., Gunn, J. E., Uomoto, A., et al. 2013, *AJ*, 146, 32
- Smith, N. 2001, *Eta Carinae and Other Mysterious Stars: The Hidden Opportunities of Emission Spectroscopy*, 242, 81
- Sota, A., Maiz Appelániz, J., Walborn, N. R., Alfaro, E. J., Barb'a, R. H., Morrell, N. I., Gamén, R. C., & Arias, J. L. 2011, *ApJS*, 193, 24
- Steele, I. A., Negueruela, I., & Clark, J. S. 1999, *A&AS*, 137, 147
- Steele, I. A., & Clark, J. S. 2001, *A&A*, 371, 643
- Štefl, S., Rivinius, T., Carciofi, A. C., et al. 2009, *A&A*, 504, 929
- Stephenson, C. B., & Sanduleak, N. 1977, *Publications of the Warner & Swasey Observatory*, 2, 71
- Stephenson, C. B., & Sanduleak, N. 1977, *ApJS*, 33, 459
- Strom, S. E., Wolff, S. C., & Dror, D. H. A. 2005, *AJ*, 129, 809
- Struve, O. 1931, *ApJ*, 74, 225
- Townsend, R. H. D., & Owocki, S. P. 2005, *MNRAS*, 357, 251
- Townsend, R. H. D., Owocki, S. P., & Groote, D. 2005, *ApJ*, 630, L81
- Turner, D. G., Forbes, D., & Pedreros, M. 1992, *AJ*, 104, 1132
- Turner, D. G. 1976, *ApJ*, 210, 65
- Turner, D. G. 1993, *A&AS*, 97, 755
- Tuthill, P. G., & Lloyd, J. P. 2007, *Science*, 316, 247
- Uesugi, A., & Fukuda, I. 1970, *Contributions from the Institute of Astrophysics and Kwasan Observatory, University of Kyoto*, Kyoto: University, Kwasan Observatory, Institute of Astrophysics, 1970,
- Uesugi, A., & Fukuda, I. 1982, *Kyoto: University of Kyoto, Departement of Astronomy*, 1982, Rev.ed.,
- Uzpen, B., Kobulnicky, H. A., Monson, A. J., et al. 2007, *ApJ*, 658, 1264
- Voroshilov, V. I., Guseva, N. G., Kalandadze, N. B., et al. 1976, *Kiev Izdatel Naukova Dumka*,
- Voroshilov, V. I., Guseva, N. G., Kalandadze, N. B., et al. 1985, *Kiev, Izdatel'stvo Naukova Dumka*, 1985, 140 p. In Russian.,
- Wackerling, L. R. 1970, *MmRAS*, 73, 153
- Walborn, N. R., Howarth, I. D., Evans, C. J., et al. 2010, *AJ*, 139, 1283
- Walborn, N. R. 1971, *ApJS*, 23, 257
- Wheelwright, H. E., Bjorkman, J. E., Oudmaijer, R. D., et al. 2012, *MNRAS*, 423, L11
- Whelan, D. G., Chojnowski, S. D., Wisniewski, J. P., Zasowski, G., Majewski, S., Nidever, D., et al. 2014, *ApJ*
- Wilson, J. C., Hearty, F., Skrutskie, M. F., et al. 2010, *Proc. SPIE*, 7735,
- Wisniewski, J. P., Kowalski, A. F., Bjorkman, K. S., Bjorkman, J. E., & Carciofi, A. C. 2007, *ApJ*, 656, 21
- Wisniewski, J. P., Draper, Z. H., Bjorkman, K. S., et al. 2010, *ApJ*, 709, 1306
- Yudin, R. V. 2001, *A&A*, 368, 912
- Zasowski, G., Johnson, J. A., Frinchaboy, P. M., et al. 2013, *AJ*, 146, 81
- Zasowski, G., Ménard, B., Bizyaev, D., et al. 2014, *arXiv:1406.1195*

Table 1: List of ABE stars

ABe ID	Star Name	2MASS mag	Lit. Spec. Type	Ref.	$\Delta v_{\text{pBr11}}$ $\text{km s}^{-1}$
001	VES 203	9.108	B0.5Ve	74	208
002	HD 228576	9.888	Ae	29	152
003	HR 7757	6.548	B6IIIe	22	305
004	HD 229221	6.734	B0.2IIIe	66	115
005	Hen 3-1876	9.699	OB	6	271
006	HD 179405	8.084	B2Ve	68	294
007	HD 178920	9.236	B8II/III	58	181
008	J18000176-2323071	10.699	...	...	233
009	TYC 3586-282-1	9.192	(B8)	C	175
010	BD+50 3188	9.311	(B)	C	138
011	TYC 3583-670-1	9.698	...	...	252
012	J20554731+5040274	10.766	...	...	115
013	EM* CDS 1038	10.428	OB	24	bl
014	HD 204860	6.931	B5.5Ve	60	326
015	HD 166629	9.155	B5nnne	41	70
016	HD 168135	7.406	B8Ve	59	238
017	BD-15 4863	9.695	Be	24	376
018	J18194798-1724130	10.976	...	...	sp
019	HD 223924	8.177	B1.5:III:n	25	296
020	SS 412	10.528	OB:e	33	217
021	HD 232940	8.625	(B9)	C	291
022	TYC 3727-1849-1	9.438	...	...	495
023	BD+44 709s	10.546	OB	14	386
024	TYC 1846-17-1	9.596	(A3)	C	158
025	HD 247042	9.165	O9.5:	15	346
026	HD 38708	8.015	B3:e:psh	8	324
027	TYC 2405-1358-1	9.825	...	...	489
028	HD 42529	8.090	B9V	57	297
029	HD 254168	9.169	...	...	301
030	HD 43681	8.806	(A2)	39	333
031	HD 257473	9.378	B5e	5	133
032	SS 453	10.200	Be:	33	508
033	HD 240249	9.250	(B8)	C	205
034	MWC 1085	8.787	(B3Ve)	54	551
035	Hen 3-14	9.650	B	24	241
036	HR 2364	6.113	B3Ve	69	456
037	HD 40254	9.210	(B8)	39	234
038	HD 345589	10.595	(A3)	52	224
039	SS 338	9.647	B8e:	33	259
040	HD 159845	6.773	B3IIIe	45	99
041	J18382765-1014211	10.640	...	...	141
042	BD-10 4799	10.094	(B)	C	181
043	HD 161004	7.880	B9IVe	41	290
044	HD 316179	7.673	Be:	35	247
045	TYC 3692-1234-1	10.321	...	...	344
046	HD 13544	9.055	B0.5III:n	27	294
047	HD 37266	7.309	B8V	57	250
048	BD+42 4162	8.916	(A0)	39	333
049	HR 8107	6.360	B6IV	22	197
050	HD 345439	10.629	B2Vpe	77	1153
051	HD 345339	9.869	(A0)	52	373
052	TYC 6854-2016-1	10.009	(B8)	61	405
053	HD 317026	9.467	(B9)	52	216
054	HD 32811	6.523	B8.5V	57	315
055	HD 51893	9.077	B9V	58	344
056	HIP 2382	9.710	B6III	48	as(sh)
057	TYC 4056-415-1	9.293	(B5)	61	sh
058	HD 165517	6.967	B0Iae	45	tc

Table 1: continued.

Abe ID	Star Name	2MASS mag	Lit. Spec. Type	Ref.	$\Delta v_{\text{pBr11}}$ km s <sup>-1</sup>
059	HD 167113	9.030	(B9IV:)	61	415
060	HD 55200	8.297	(A0)	39	sh
061	HD 28942	8.159	Ash	44	sh
062	TYC 4060-96-1	8.398	...	...	456
063	HD 260153	9.417	B8III	42	w
064	TYC 5126-2325-1	10.733	...	...	291
065	HD 173075	9.358	B9IV	58	235
066	TYC 5121-940-1	10.299	...	...	187
067	HR 1047	5.902	B7Vne	51	133
068	HD 157174	8.488	A0IV	45	208
069	J18274975-1104312	10.165	...	...	238
070	BD-09 4724	9.550	(A0IV)	C	w
071	TYC 5696-503-1	10.454	Be	33	138
072	HD 165174	6.224	B0IIIIn	22	w
073	BD+54 2887	9.538	(A0)	61	193
074	HD 182550	8.818	B8V	47	66
075	HD 23478	6.486	B3IVe	10	913
076	VES 828	10.896	...	...	301
077	J04423114+3830469	10.455	...	...	162
078	TYC 3975-1585-1	10.101	B8	12	400
079	HD 54551	8.775	B1.5II	45	524
080	BD+44 3475	9.451	...	...	sh
081	HD 628	7.521	(B9)	39	205
082	BD+12 938	10.172	...	...	250
083	HD 247299	9.987	(A0)	62	119
084	HD 236611	8.978	(A)	C	265
085	HD 236689	8.853	B1.5V:epsh	8	321
086	TYC 3683-1262-1	9.840	...	...	209
087	HD 60260	9.232	B3Ve	58	129
088	HD 6343	6.843	B5Vn:e	20	115
089	TYC 4029-428-1	9.595	...	...	342
090	BD+66 64	8.588	(B9)	C	sh
091	HD 39984	9.140	(A2)	39	115
092	TYC 3320-1906-1	9.425	B7	9	417
093	TYC 4306-1125-1	9.115	B8V	37	337
094	HD 232214	8.855	(B8)	C	92
095	HD 45396	8.907	(A2)	39	w
096	HD 45828	8.506	(B8?)	C	w
097	HD 34193	8.498	(A0e)	39	203
098	HD 219523	7.218	B5V	36	301
099	HD 41639	8.599	B6Vne:	38	578
100	HD 36467	8.167	B9III	37	300
101	BD+47 1108	9.581	(A0)	39	326
102	TYC 2400-1784-1	10.396	...	...	273
103	J17494627-2249517	10.473	...	...	<61
104	BD-02 4698	8.853	(B)	C	sh?
105	HD 235350	8.652	B0.5IV	8	502
106	TYC 3690-1236-1	10.581	...	...	480
107	TYC 3617-2074-1	10.112	...	...	233
108	HD 254842	8.631	...	...	185
109	HD 256137	9.734	(A2)	39	106
110	HD 29035	7.930	B9.5Ve	64	w
111	AS 332	9.639	Be	43	w
112	HD 28543	7.725	(A0)	39	w
113	HD 29096	7.323	B8IV	57	333
114	TYC 3347-1615-1	10.713	...	...	sh?
115	J20185676+3745319	11.326	...	...	139
116	HD 159032	8.725	B9IV	45	387
117	HD 162345	8.291	(B8)	39	128



Table 1: continued.

ABe ID	Star Name	2MASS mag	Lit. Spec. Type	Ref.	$\Delta v_{\text{pBr11}}$ km s <sup>-1</sup>
118	HD 316573	9.850	(B9)	52	115
119	AS 251	9.961	B	24	259
120	HD 316475	9.225	(B9)	39	282
121	TYC 6262-3203-1	9.292	...	...	166
122	TYC 5681-507-1	10.027	(A5)	62	179
123	TYC 5681-151-1	10.614	...	...	177
124	HD 167401	9.322	B4II/III	41	627
125	TYC 5689-54-1	10.273	...	...	<60
126	HD 169418	8.995	B9.5III	45	326
127	HD 168566	8.710	B9III	45	114
128	HIP 91591	8.825	B8Ve	49	276
129	GSC 05692-00540	10.451	B7	17	267
130	GSC 05692-00399	10.508	B7	17	423
131	BD-07 4647	9.642	B5	17	143
132	BD-07 4630	8.963	B9	17	w
133	88 Her	6.913	B6IIInpsh	53	285
134	J18295996-0908375	10.761	...	...	198
135	HD 173010	7.179	O9.7Ia	73	sh?
136	HD 165365	7.024	B7.5III	41	232
137	NGC 6531 F195	11.130	...	...	<25
138	HD 180126	7.565	B2IV	68	365
139	HD 180587	7.578	ApsH	18	sh
140	HR 7807	6.228	B2Vne	63	382
141	HD 201036	8.996	B6/8Vn	38	247
142	HD 183035	7.844	A0V	70	320
143	HD 333378	10.150	(A0)	52	313
144	HD 189847	7.122	B7V	16	260
145	TYC 6262-1413-1	9.926	...	...	sh?
146	HD 41600	7.132	B9IV	57	w
147	HD 186485	8.484	B9V	34	123
148	HD 345506	9.683	(B8)	52	sh?
149	IRAS F03406+3133	10.780	...	...	sp
150	J18412551-0534033	10.902	...	...	388
151	TYC 5692-1370-1	10.799	B7	17	137
152	SS 120	10.733	B8e:	35	461
153	J17221970-2833450	10.940	...	...	sh
154	TYC 1310-2084-1	9.969	(B8)	61	360
155	TYC 3692-1671-1	10.611	...	...	819
156	HD 222185	8.343	(A2)	39	w
157	HD 186637	7.937	(B9e)	39	359
158	AS 478	9.792	...	...	87
159	MWC 1062	8.804	B5:e	3	265
160	HD 206135	7.811	B3V	21	316
161	TYC 3968-1354-1	10.574	OB-	14	422
162	BD+27 981	9.960	(B8)	62	219
163	HD 215837	8.104	(A0)	39	357
164	HD 212044	7.702	B1:V:nneP	8	191
165	HD 212666	8.681	B5.5e	59	397
166	TYC 4812-2496-1	9.971	...	...	308
167	HD 49787	7.836	B1Ve	68	300
168	HD 51477	8.223	B3Ve	58	628
169	HD 40897	8.000	(B9)	39	255
170	HR 2116	6.400	B8V	26	153
171	TYC 1326-1188-1	10.257	(A2)	62	362
172	HD 34906	8.641	(B9V)	61	142
173	TYC 1283-1360-1	10.617	...	...	sh
174	HD 35269	7.552	A0V	76	448
175	TYC 1300-652-1	10.731	...	...	w
176	HD 33656	9.215	B5	2	551

Table 1: continued.

Abe ID	Star Name	2MASS mag	Lit. Spec. Type	Ref.	$\Delta v_{\text{pBr11}}$ km s <sup>-1</sup>
<b>177</b>	HD 280849	9.654	(B3)	52	522
<b>178</b>	CoRoT 102762536	11.651	B1V	75	sp
179	EM* RJHA 51	10.563	B5Ib	75	243
180	EM* RJHA 40	10.613	B3Ib	75	183
181	HD 37115	7.204	B7.5V	58	238
<b>182</b>	TYC 2934-118-1	10.240	...	...	376
<b>183</b>	HD 60993	9.131	B2II	45	348
<b>184</b>	HD 245174	9.790	(B3)	62	268
<b>185</b>	HD 40132	7.564	B9	19	85
<b>186</b>	HD 54167	9.672	B5/7Ib:	58	328
187	HD 253214	8.917	B1.5:V:nn	8	220
188	HD 253215	10.444	...	...	298
189	HD 60848	7.071	O9.5IVe	67	305
<b>190</b>	HD 252904	9.089	B9V	11	w
191	HD 165854	7.903	B9e	59	274
<b>192</b>	HD 166291	8.303	B3II	45	272
193	SS 339	10.713	B8e:	33	250
<b>194</b>	HD 313062	9.676	...	...	327
195	HD 179343	6.613	B8III	68	266
196	HD 277241	10.836	B8	13	w
197	HD 166055	9.662	(B9)	62	221
<b>198</b>	HD 165894	8.183	B3IV/V	45	158
<b>199</b>	TYC 6262-371-1	9.301	...	...	164
<b>200</b>	Lan 671	9.976	...	...	280
<b>201</b>	BD-16 4888p	9.825	...	...	138
<b>202</b>	TYC 6266-143-1	10.487	...	...	w
A01	MWC 5	8.025	B0.5IV	7	122
A02	HD 2789	7.519	B3:Vne	23	320
A03	MWC 80	7.165	B1Vnnpe	8	as
A04	HD 35347	7.948	B2:nne	38	268
A05	HD 38191	8.380	B1:V:ne:	8	246
A06	HD 39018	7.898	(B9)	39	w
A07	HD 43703	7.475	B1IV:p?	8	w
A08	HD 46264	7.522	B5Vne	31	409
A09	HD 259597	7.779	B1Vnne	28	289
A10	HD 50424	8.971	B8e	35	178
A11	HD 50891	7.880	B0.5Ve	68	215
A12	HD 51193	8.039	B1.5IVe	68	358
A13	HD 51354	7.183	B3Vn	40	257
A14	HD 54786	9.051	B1.5Ib:	45	256
A15	HD 55606	8.704	B0.5Vnnep	69	237
A16	HD 345122	8.963	B3Ve	46	231
A17	HD 190150	8.186	B6IV-Ve	40	240
A18	HD 201522	8.022	B0V	16	...
A19	MWC 640	7.206	B1.5V:nnep	8	205
A20	HD 204722	7.643	B1.5IV:np	25	358
A21	MWC 649	8.701	B3e	1	109
A22	AS 483	9.631	B1.5V:nne:	8	362
A23	MWC 922	7.396	unclB[e]	55	sp
A24	HD 34302	7.534	(B8)	39	163
A25	HD 280999	9.582	(B3)	52	214
A26	HD 35345	7.851	B1Vep	7	sp
A27	EM* CDS 496	8.669	OB	24	w?
A28	HD 250028	8.083	B2:V:nep	32	288
A29	HD 39340	7.579	B3Ve	59	197
A30	HD 248753	7.361	B2:Vnne	23	279
A31	HD 39478	7.691	B2Ve	59	242
A32	IGR J06074+2205	10.189	B0.5Ve	71	380
A33	EM* LkHA 208	9.834	A7e	65	sp?

Table 1: continued.

ABe ID	Star Name	2MASS mag	Lit. Spec. Type	Ref.	$\Delta v_{\text{pBr11}}$ $\text{km s}^{-1}$
A34	HD 251726	7.644	B1V:e	8	159
A35	MWC 137	7.840	sgB[e]	56	57
A36	HD 253659	8.327	B0.5:V:nne	8	312
Q01	HD 229239	7.093	B0.2III	66	...
Q02	HD 228932	9.386	B	35	...
Q03	BD+36 4032	7.566	O8.5V	66	...
Q04	Hen 3-1885	10.855	A0V	30	...
Q05	HD 291946	9.321	B9	2	...
Q06	HD 315177	10.022	...	...	...
Q07	HD 350989	10.534	B7III <sub>n</sub>	50	...
Q08	HD 345475	9.484	B0	4	...
Q09	EM* CDS 1459	7.471	O6.5(f)(n)p	72	...
Q10	EM* CDS 53	10.369	OB-e:	14	...
Q11	HD 232208	9.519	B3:e	3	...
Q12	HD 2083	7.041	O9.5III	34	...
Q13	EM* CDS 144	10.499	OB-e:	14	...
Q14	HD 276414	10.148	(B8)	52	...
Q15	HD 29332	8.246	B3ne	1	...
Q16	HD 32961	8.970	B2	13	...
Q17	HD 280006	7.747	A0Ibe:	33	...
Q18	HD 288805	9.611	B5	2	...
Q19	HD 52159	9.793	B3Vne	69	...
Q20	HD 34656	6.634	O7.5(f)II	73	...
Q21	HD 57539	6.834	B3IV	58	...
Q22	HR 2231	6.336	B6Ve	69	...

- [1] Merrill et al. (1942); [2] Cannon & Mayall (1949); [3] Merrill & Burwell (1949); [4] Popper (1950); [5] Miller & Merrill (1951); [6] Nassau & Harris (1952); [7] Morgan et al. (1953); [8] Morgan et al. (1955); [9] Heckmann et al. (1956); [10] Hiltner (1956); [11] Duflot et al. (1958); [12] Alknis (1958); [13] McCuskey (1959); [14] Hardorp et al. (1959); [15] Bouigue et al. (1961); [16] Fehrenbach et al. (1962); [17] Roslund (1963); [18] Feast & Thackeray (1963); [19] McCuskey (1967); [20] Schmidt-Kaler (1967); [21] Racine (1968); [22] Lesh (1968); [23] Guetter (1968); [24] Wackerling (1970); [25] Walborn (1971); [26] Cowley (1972); [27] Lesh & Aizenman (1973); [28] Turner (1976); [29] Henize (1976); [30] Voroshilov et al. (1976); [31] Davis (1977); [32] Christy (1977); [33] Stephenson & Sanduleak (1977b); [34] Hill & Lynas-Gray (1977); [35] Stephenson & Sanduleak (1977a); [36] Roman (1978); [37] Bartaya (1979); [38] Clausen & Jensen (1979); [39] Ochsenbein (1980); [40] Jaschek & Jaschek (1993); [41] Houk (1982); [42] Voroshilov et al. (1985); [43] Bopp (1988); [44] Bidelman (1988); [45] Houk & Smith-Moore (1988); [46] Radoslavova (1989); [47] Sato & Kuji (1990); [48] Turner et al. (1992); [49] Grillo et al. (1992); [50] Turner (1993); [51] Garrison & Gray (1994); [52] Nesterov et al. (1995); [53] Abt & Morrell (1995); [54] Kohoutek & Wehmeyer (1997); [55] Lamers et al. (1998); [56] Esteban & Fernandez (1998); [57] Grenier et al. (1999); [58] Houk & Swift (1999); [59] Yudin (2001); [60] Chauville et al. (2001); [61] Kharchenko (2001); [62] Fabricius et al. (2002); [63] Abt et al. (2002); [64] Miroshnichenko et al. (2003); [65] Hernández et al. (2004); [66] Negueruela (2004); [67] Negueruela et al. (2004); [68] Frémat et al. (2006); [69] Levenhagen & Leister (2006); [70] Uzpen et al. (2007); [71] Reig et al. (2010); [72] Walborn et al. (2010); [73] Sota et al. (2011); [74] Mathew & Subramaniam (2011); [75] Sebastian et al. (2012); [76] Chargeishvili et al. (2013); [77] Eikenberry et al. (2014)



TABLE 2  
OBSERVED EMISSION LINES AND SUMMARY OF  $\Delta v_p$  MEASUREMENTS

(1)	(2)	(3)	(4)	(5)	(6)	(7)	(8)	(9)	(10)	(11)	(12)
Atom	$\lambda_{\text{vac}}$	$\lambda_{\text{vac}}$	Diff.				N	$\Delta v_p$	$\Delta v_p$	$\Delta v_p$	Other
or	lab	obs <sup>a</sup>	lab-obs	$E_i$	$E_k$	$\log(gf)$	detections	N	range	mean	possible
ion	[Å]	[Å]	[Å]	[eV]	[eV]		yes (maybe)	stars	[km s <sup>-1</sup> ]	[km s <sup>-1</sup> ]	contribution
H I (Br20)	15195.996	15195.932	0.064	12.749	13.564	-1.487	...	48	68–566	314	...
H I (Br19)	15264.708	...	...	12.749	13.561	-1.414	...	...	...	...	DIB 15271
Fe I	15298.740	15298.528	0.212	5.309	6.119	0.650	6	3	188–283	228	...
H I (Br18)	15345.982	15345.987	-0.005	12.749	13.556	-1.337	...	57	67–533	276	...
H I (Br17)	15443.139	15443.187	-0.048	12.749	13.551	-1.255	...	73	66–537	266	...
H I (Br16)	15560.699	15560.697	0.002	12.749	13.545	-1.166	...	47	65–436	266	...
N I	15586.545	15586.591	-0.046	12.126	12.922	-0.023	1	1	52–52	52	...
H I (Br15)	15704.952	15705.015	-0.063	12.749	13.538	-1.071	...	76	65–552	282	...
Mg I	15753.291	blend	...	5.932	6.719	0.140	7	...	...	...	Mg I 15745
$\lambda 15760$	...	15760.161	...	...	...	...	36 (13)	11	27–304	161	Mg I
Mg I	15770.149	15770.943	-0.794	5.933	6.719	0.411	9 (1)	2	338–375	356	$\lambda 15760$
H I (Br14)	15884.880	15884.875	0.005	12.749	13.529	-0.967	...	91	61–522	259	...
Si I	15892.771	blend	...	5.082	5.862	-0.007	6	...	...	...	...
Si I	15964.422	15963.229	1.193	5.984	6.761	0.198	7 (1)	3	321–383	345	...
C I	16009.270	blend	...	9.631	10.406	0.234	7 (3)	...	...	...	...
C I	16026.080	blend	...	9.631	10.405	0.222	5 (5)	...	...	...	...
H I (Br13)	16113.714	16113.766	-0.052	12.749	13.518	-0.852	...	96	61–517	249	...
H I (Br12)	16411.674	16411.763	-0.089	12.749	13.504	-0.725	...	95	59–524	252	...
Ca II	16565.590	16565.973	-0.383	9.235	9.983	0.368	6	3	208–333	291	C I 16564
Ca II	16654.430	blend	...	9.240	9.984	0.626	1 (2)	...	...	...	...
Si I	16685.341	blend	...	5.984	6.727	-0.117	1 (2)	...	...	...	...
Mg II	16764.800	16764.922	-0.122	12.083	12.822	0.481	2 (2)	1	34–34	34	...
$\lambda 16781$	...	16781.115	...	...	...	...	36 (13)	13	28–309	157	...
Fe II	16791.762	16791.953	-0.191	5.484	6.222	-2.325	8 (6)	1	48–48	48	...
Mg II	16804.520	blend	...	12.085	12.822	0.737	2 (2)	...	...	...	Mg II 16804
H I (Br11)	16811.111	...	...	12.749	13.486	-0.582	...	194	57–1153	282	...
Fe II	16877.808	16877.822	-0.014	5.484	6.219	-1.256	76 (33)	26	24–232	82	...
C I	16895.031	16894.898	0.133	9.003	9.736	0.534	43 (19)	14	31–539	243	...
Si II	16911.430	16911.646	-0.216	12.147	12.880	0.350	1 (1)	1	41–41	41	...

<sup>1</sup>The emission peak midpoint corrected by the emission peak midpoint of Br11.

TABLE 3  
LINE-EMITTING DISK RADIUS ESTIMATES

ABE ID	Lit. $v \sin i$ [km s <sup>-1</sup> ]	Ref.	Atom or Ion	# spectra	Mean $\Delta v_p$ [km s <sup>-1</sup> ]	Mean $r_d$ [ $R_*$ ]
001 <sup>a</sup>	266	9	Br11	4	208	6.56
			$\lambda 15760$	4	246	4.67
			$\lambda 16781$	4	261	4.16
003	225	5	Br11	10	305	2.18
006	231	7	Br11	3	294	2.47
014	230	3	Br11	7	326	1.99
016 <sup>a</sup>	250	4	Br11	1	238	4.43
			Fe II 16878	1	111	20.41
026 <sup>b</sup>	230	3	Br11	12	324	2.02
028	242	4	Br11	12	297	2.66
036 <sup>b</sup>	307	4	Br11	3	456	1.81
046 <sup>b</sup>	235	2	Br11	1	294	2.56
049	120	2	Br11	23	197	1.48
			Fe II 16878	7	67	12.73
067	120	5	Br11	8	133	3.24
			Fe II 16878	8	41	34.32
085	182	8	Br11	4	321	1.29
098	166	11	Br11	1	301	1.21
133 <sup>b</sup>	286	4	Br11	3	285	4.02
138	243	7	Br11	2	365	1.77
140	328	4	Br11	4	382	2.95
165	274	4	Br11	3	397	1.91
167	160	7	Br11	3	300	1.14
170	130	5	Br11	6	153	2.90
			Fe II 16878	6	64	16.76
			C I 16895	2	169	2.36
189	256	6	Br11	5	305	2.81
191	242	4	Br11	1	274	3.11
195 <sup>b</sup>	148	7	Br11	3	266	1.24
A08	343	11	Br11	3	409	2.82
A11	220	7	Br11	3	215	4.19
A12	215	7	Br11	1	358	1.44
A13 <sup>b</sup>	306	4	Br11	6	257	5.68
			$\lambda 15760$	4	248	6.07
			$\lambda 16781$	4	250	6.00
A15 <sup>a</sup>	350	7	Br11	3	237	8.76
			Fe II 16878	3	232	9.07
			C I 16895	3	345	4.12
			$\lambda 15760$	3	233	9.05
			$\lambda 16781$	3	233	9.04
A17 <sup>b</sup>	300	1	Br11	3	241	6.19
			Fe II 16878	3	102	34.32
A20	210	4	Br11	3	358	1.37
A29 <sup>a</sup>	222	4	Br11	3	197	5.09
			Fe II 16878	3	121	13.42
			$\lambda 15760$	3	144	9.55
			$\lambda 16781$	3	144	9.52
A32	260	10	Br11	3	380	1.87

<sup>1</sup>Asymmetric emission peak intensities.

<sup>2</sup>Shell stars.

References. — [1] Uesugi & Fukuda (1970); [2] Uesugi & Fukuda (1982); [3] Halbedel (1996); [4] Yudin (2001); [5] Abt et al. (2002); [6] Frémat et al. (2005); [7] Frémat et al. (2006); [8] Huang & Gies (2006); [9] Bhavya et al. (2007); [10] Reig et al. (2010); [11] Huang et al. (2010)

## Supplemental data table

An expanded version of Table 1 is provided below, including ABE identifier, 2MASS designation, HD number, an alternate identifier,  $V$  magnitudes from SIMBAD,  $H$  magnitudes from 2MASS, the spectral type and reference, and finally, line detection or  $\Delta v_p$  measures for Br11 and the stronger metallic lines. If a  $\Delta v_p$  measurement could not be made in any of the available spectra despite evidence of emission or shell absorption in a line, one of the following abbreviations is provided in place of a  $\Delta v_p$  value: “w” detection but lack of visible emission peaks, “w?” weak or ambiguous detection, “sp” single-peaked emission, “sh” shell absorption without resolved adjacent emission peaks, “as” highly asymmetric emission peaks such that only one is visible (ABE-056 and ABE-A03), “bl” V peak of Br11 is severely blended with Fe II 16792 (ABE-013), “tc” spectra are heavily contaminated by telluric features (ABE-058).

Table 4: List of ABE stars

	ABe	2MASS ID	HD	Other	V	H	Spec Type	Ref.	$\Delta v_p$							
									Br11	$\lambda 15760$	$\lambda 16781$	Fe II 16792	Fe II 16878	C I 16895		
									mag	mag	km s <sup>-1</sup>	km s <sup>-1</sup>	km s <sup>-1</sup>	km s <sup>-1</sup>		km s <sup>-1</sup>
001	20212485 + 3722482		...	VES 203		12.09	9.108	B0.5Ve	74	208		246	261	-	w	-
002	20151525 + 3654562		228576	AS 394		11.41	9.888	Ae	29	152		w	86	-	85	-
003	20162816 + 3703229		192987	HR 7757		6.46	6.548	B6IIIe	22	305		-	-	-	w?	w
004	20234596 + 3830033		229221	MWC 344		9.22	6.734	B0.2IIIe	66	115		131	105	-	w?	191
005	20184170 + 3759106		...	Hen 3-1876		11.37	9.699	OB	6	271		w	w	-	-	-
006	19124025 - 0627316		179405	MWC 615		9.12	8.084	B2Ve	68	294		-	-	-	-	-
007 <sup>new</sup>	19104149 - 0542581		178920	BD-05 4897		10.38	9.236	B8II/III	58	181		-	-	-	w	w?
008 <sup>new</sup>	18000176 - 2323071		...	...		12.20	10.699	...	...	233		-	-	-	w	w?
009 <sup>new</sup>	20461437 + 5039005		...	TYC 3586-282-1		9.99	9.192	(B8)	CSSC	175		-	-	-	-	-
010	20450869 + 5033004		...	BD+50 3188		10.48	9.311	(B)	CSSC	138		-	-	-	-	-
011 <sup>new</sup>	20535693 + 5005293		...	TYC 3583-670-1		10.83	9.698	...	...	252		w	w	-	w?	w
012 <sup>new</sup>	20554731 + 5040274		...	...		11.00	10.766	...	...	115		-	-	-	-	-
013	18574179 - 0419113		...	EM* CDS 1038		11.77	10.428	OB	24	bl		w	w	w	98	-
014	21300088 + 4529390		204860	V2163 Cyg		6.94	6.931	B5.5Ve	60	326		-	-	-	-	-
015	18123846 - 2708292		166629	MWC 911		9.31	9.155	B5nne	41	70		w	w	w	w	112
016	18185069 - 1227145		168135	MWC 289		7.92	7.406	B8Ve	59	238		w?	w?	-	111	-
017	18122758 - 1546123		...	BD-15 4863		10.21	9.695	Be	24	376		-	-	-	-	-
018 <sup>new</sup>	18194798 - 1724130		...	...		14.60	10.976	...	...	sp		-	-	-	-	-
019 <sup>new</sup>	23533653 + 5649116		223924	BD+56 3106		8.20	8.177	B1.5:III:n	25	296		w	w	-	-	-
020	18432516 - 0339100		...	SS 412		12.30	10.528	OB:e	33	217		-	-	-	-	w
021 <sup>new</sup>	04220085 + 5430434		232940	BD+54 764		9.45	8.625	(B9)	CSSC	291		-	-	-	-	-
022 <sup>new</sup>	04254177 + 5615294		...	TYC 3727-1849-1		10.40	9.438	...	...	495		-	-	-	-	-
023 <sup>new</sup>	03282223 + 4507560		...	BD+44 709s		11.09	10.546	OB	14	386		-	-	-	-	-
024 <sup>new</sup>	05113282 + 2408029		...	TYC 1846-17-1		10.30	9.596	(A3)	CSSC	158		-	-	-	w	w
025 <sup>new</sup>	05452088 + 2909281		247042	BD+29 981		9.51	9.165	O9.5:	15	346		-	-	-	-	-
026	05485364 + 2908100		38708	V438 Aur		8.05	8.015	B3:e:psh	8	324		-	-	-	-	-
027 <sup>new</sup>	05453713 + 3007253		...	TYC 2405-1358-1		10.15	9.825	...	...	489		-	-	-	-	-
028	06123985 + 3258216		42529	MWC 794		8.23	8.090	B9V	57	297		w?	w?	-	w	w
029 <sup>new</sup>	06165595 + 3414299		254168	BD+34 1307		9.57	9.169	...	...	301		-	-	-	-	-
030 <sup>new</sup>	06185921 + 3413502		43681	BD+34 1318		9.20	8.806	(A2)	39	333		-	-	-	w	w?
031	06273614 + 1815476		257473	MWC 807		9.57	9.378	B5e	5	133		-	-	-	101	193
032	22252246 + 5642384		...	SS 453		10.81	10.200	Be:	33	508		-	-	-	-	-
033 <sup>new</sup>	23181131 + 5550356		240249	BD+55 2936		9.78	9.250	(B8)	CSSC	205		-	-	-	-	-
034	23521212 + 6710073		...	MWC 1085		9.97	8.787	B3Ve	54	551		-	-	-	-	-
035	06334350 - 3202486		...	Hen 3-14		9.55	9.650	B	24	241		w	w	-	97	-



Table 4: continued.

	ABe	2MASS ID	HD	Other	V	H	Spec Type	Ref.	$\Delta v_p$						
									Br11	$\lambda 15760$	$\lambda 16781$	Fe II 16792	Fe II 16878	C I 16895	
									mag	mag	$\text{km s}^{-1}$	$\text{km s}^{-1}$	$\text{km s}^{-1}$	$\text{km s}^{-1}$	$\text{km s}^{-1}$
036	06283925 − 3222165		45871	HR 2364		5.74	6.113	B3Ve	69	456	-	-	-	-	-
037 <sup>new</sup>	05590290 + 3101488		40254	BD+31 1154		9.48	9.210	(B8)	39	234	-	-	-	-	-
038 <sup>new</sup>	20032620 + 2242411		345589	BD+22 3902		11.19	10.595	A3	52	224	-	-	-	-	-
039	18000839 − 2356576		...	SS 338		11.41	9.647	B8e:	33	259	-	-	-	-	-
040	17375482 − 2457569		159845	MWC 883		8.66	6.773	B3IIIe	45	99	w?	w?	w	39	164
041 <sup>new</sup>	18382765 − 1014211		...	...		12.50	10.640	...	...	141	-	-	-	w	w
042	18464650 − 1021523		...	BD-10 4799		10.57	10.094	(B)	CSSC	181	-	-	-	89	-
043	17441414 − 2727284		161004	MWC 952		8.79	7.880	B9IVe	41	290	-	-	-	w	w?
044	17432344 − 2715411		316179	AS 238		9.69	7.673	Be:	35	247	-	-	-	-	-
045 <sup>new</sup>	01542524 + 5651061		...	TYC 3692-1234-1		10.99	10.321	...	...	344	-	-	-	w?	-
046 <sup>new</sup>	02135183 + 5354525		13544	V353 Per		8.88	9.055	B0.5IIIIn	27	294	-	-	-	-	-
047 <sup>new</sup>	05390426 + 3758359		37266	BD+37 1271		7.50	7.309	B8V	57	250	-	-	-	w	-
048 <sup>new</sup>	21375002 + 4258309		...	BD+42 4162		9.30	8.916	(A0)	39	333	-	-	-	w?	w
049	21103095 + 4741321		201836	HR 8107		6.49	6.360	B6IV	22	197	-	-	-	67	w
050	19584848 + 2305215		345439	ALS 10681		11.12	10.629	B2Vpe	77	1153	-	-	-	-	-
051 <sup>new</sup>	19571220 + 2158541		345339	BD+21 3985		10.47	9.869	A0	52	373	-	-	-	-	-
052 <sup>new</sup>	18052711 − 2921573		...	TYC 6854-2016-1		10.13	10.009	B8	61	405	-	-	-	-	-
053 <sup>new</sup>	18023404 − 3027418		317026	TYC 7391-2481-1		10.24	9.467	B9	52	216	-	-	-	-	-
054 <sup>new</sup>	05064093 + 2230389		32811	BD+22 825		7.14	6.523	B8.5V	57	315	-	-	-	w?	w
055 <sup>new</sup>	06591343 + 0427179		51893	BD+04 1529		9.00	9.077	B9V	58	344	-	-	-	w?	w?
056 <sup>new</sup>	00302445 + 6010093		...	HIP 2382		10.70	9.710	B6III	48	as(sh)	w?	w?	-	w	-
057 <sup>new</sup>	02534457 + 6443068		...	TYC 4056-415-1		9.95	9.293	B5	61	sh	-	-	-	-	-
058	18072725 − 2506165		165517	MWC 907		8.47	6.967	B0Iae	45	tc	-	-	-	-	-
059 <sup>new</sup>	18144388 − 2137597		167113	BD-21 4920		9.74	9.030	B9IV:	61	415	-	-	-	-	w?
060 <sup>new</sup>	07134058 + 3806302		55200	BD+38 1712		8.34	8.297	(A0)	39	sh	-	-	-	w	w?
061	04361726 + 5230217		28942	BD+52 856		8.67	8.159	Ash	44	sh	-	-	-	w	w?
062 <sup>new</sup>	03030934 + 6654223		...	TYC 4060-96-1		10.08	8.398	...	...	456	-	-	-	-	-
063 <sup>new</sup>	06351041 + 0634180		260153	TYC 158-270-1		9.63	9.417	B8III	42	w	-	-	-	-	-
064 <sup>new</sup>	18451050 − 0545120		...	TYC 5126-2325-1		11.93	10.733	...	...	291	-	-	-	w	-
065 <sup>new</sup>	18434859 − 0608188		173075	BD-06 4858		9.93	9.358	B9IV	58	235	-	-	-	w	-
066 <sup>new</sup>	18402120 − 0455127		...	TYC 5121-940-1		11.39	10.299	...	...	187	-	-	-	-	-
067	03292627 + 4656162		21455	HR 1047		6.23	5.902	B7Vne	51	133	w	w	-	41	-
068 <sup>new</sup>	17224642 − 2533273		157174	HIP 85034		9.10	8.488	A0IV	45	208	-	-	-	w?	-
069 <sup>new</sup>	18274975 − 1104312		...	...		11.80	10.165	...	...	238	-	-	-	-	-
070	18251991 − 0918163		...	BD-09 4724		10.67	9.550	(A0IV)	CSSC	w	-	-	-	-	-
071	18424368 − 1000273		...	TYC 5696-503-1		11.76	10.454	Be	33	138	-	-	-	w?	-
072	18043735 + 0155085		165174	V986 Oph		6.15	6.224	B0IIIIn	22	w	-	-	-	-	-
073 <sup>new</sup>	22583631 + 5528116		...	BD+54 2887		9.87	9.538	A0	61	193	-	-	-	-	-
074 <sup>new</sup>	19233702 + 3859363		182550	BD+38 3568		8.94	8.818	B8V	47	66	-	-	-	-	-
075	03464087 + 3217247		23478	BD+31 649		6.69	6.486	B3IVe	10	913	-	-	-	-	-
076	04432066 + 4754385		...	VES 828		11.60	10.896	...	...	301	-	-	-	w	-
077 <sup>new</sup>	04423114 + 3830469		...	...		11.40	10.455	...	...	162	-	-	-	w?	w?
078 <sup>new</sup>	21351726 + 5647589		...	TYC 3975-1585-1		12.21	10.101	B8	12	400	-	-	-	-	-
079 <sup>new</sup>	07081479 − 2325541		54551	HIP 34429		8.61	8.775	B1.5II	45	524	-	-	-	-	-
080 <sup>new</sup>	20282074 + 4526025		...	BD+44 3475		9.70	9.451	...	...	sh	-	-	-	-	-
081 <sup>new</sup>	00104514 + 5801058		628	BD+57 21		7.84	7.521	(B9)	39	205	-	-	-	w?	w?
082 <sup>new</sup>	05540108 + 1241033		...	BD+12 938		10.35	10.172	...	...	250	-	-	-	-	w
083 <sup>new</sup>	05453721 + 1311210		247299	BD+13 976		10.61	9.987	A0	62	119	-	-	-	-	-
084	01042742 + 5756263		236611	MWC 683		9.22	8.978	(A)	CSSC	265	-	-	-	w?	336

Table 4: continued.

	ABe	2MASS ID	HD	Other	V	H	Spec Type	Ref.	$\Delta v_p$						
									Br11	$\lambda 15760$	$\lambda 16781$	Fe II 16792	Fe II 16878	C I 16895	
									mag	mag	km s <sup>-1</sup>	km s <sup>-1</sup>	km s <sup>-1</sup>	km s <sup>-1</sup>	
085	01183306 + 5822304		236689	NGC 457 198		9.47	8.853	B1.5V:epsh	8	321	-	-	-	-	-
086 <sup>new</sup>	01355734 + 5809128		...	TYC 3683-1262-1		10.18	9.840	...	...	209	-	-	-	w	-
087	07331124 - 1136421		60260	MWC 564		9.04	9.232	B3Ve	58	129	-	-	-	-	-
088	01055296 + 6558158		6343	MWC 10		7.26	6.843	B5Vn:e	20	115	-	-	-	42	w
089 <sup>new</sup>	00573323 + 6709339		...	TYC 4029-428-1		10.58	9.595	...	...	342	-	-	-	-	-
090 <sup>new</sup>	00501808 + 6710377		...	BD+66 64		9.59	8.588	(B9)	CSSC	sh	-	-	-	w	w?
091 <sup>new</sup>	05564423 + 1601018		39984	BD+15 989		9.20	9.140	(A2)	39	115	-	-	-	-	-
092 <sup>new</sup>	03250006 + 5029394		...	TYC 3320-1906-1		10.32	9.425	B7	9	417	-	-	-	w?	-
093 <sup>new</sup>	00080292 + 7332356		...	TYC 4306-1125-1		9.66	9.115	B8V	37	337	-	-	-	w?	w?
094	00331160 + 5140069		232214	MWC 671		9.26	8.855	(B8)	CSSC	92	w	w	w	42	w?
095 <sup>new</sup>	06272285 + 0824429		45396	BD+08 1343		8.98	8.907	(A2)	39	w	-	-	-	-	-
096 <sup>new</sup>	06300018 + 0817453		45828	BD+08 1366		8.76	8.506	(B8?)	CSSC	w	-	-	-	-	-
097	05164674 + 3022455		34193	MWC 488		8.74	8.498	(A0e)	39	203	w	w	-	w	-
098 <sup>new</sup>	23152849 + 6416002		219523	BD+63 1955		7.17	7.218	B5V	36	301	-	-	-	-	-
099	06073989 + 2751354		41639	BD+27 991		8.46	8.599	B6Vne:	38	578	-	-	-	-	-
100 <sup>new</sup>	05341240 + 4516410		36467	TYC 3359-985-1		8.65	8.167	B9III	37	300	-	-	-	w	-
101 <sup>new</sup>	05124298 + 4754272		...	BD+47 1108		9.87	9.581	(A0)	39	326	-	-	-	-	-
102 <sup>new</sup>	05003547 + 3552170		...	TYC 2400-1784-1		11.62	10.396	...	...	273	w	w	-	w	w
103 <sup>new</sup>	17494627 - 2249517		...	...		13.80	10.473	...	...	<61	-	-	-	-	-
104 <sup>new</sup>	18411366 - 0247380		...	BD-02 4698		10.52	8.853	(B)	CSSC	sh?	-	-	-	-	-
105 <sup>new</sup>	20451060 + 5112379		235350	BD+50 3189		9.31	8.652	B0.5IV	8	502	-	-	-	-	-
106 <sup>new</sup>	02250591 + 5515032		...	TYC 3690-1236-1		10.80	10.581	...	...	480	-	-	-	-	-
107 <sup>new</sup>	21563126 + 5041249		...	TYC 3617-2074-1		10.49	10.112	...	...	233	-	-	-	-	-
108 <sup>new</sup>	06185755 + 2323286		254842	BD+23 1295		8.93	8.631	...	...	185	w?	w?	-	45	-
109 <sup>new</sup>	06231994 + 2506057		256137	BD+25 1244		9.97	9.734	(A2)	39	106	-	-	-	w?	-
110	04365908 + 5217135		29035	BD+51 956		8.78	7.930	B9.5Ve	64	w	-	-	-	w?	-
111	18581515 - 0528567		...	AS 332		10.48	9.639	Be	43	w	-	-	-	w	-
112 <sup>new</sup>	04321707 + 4816572		28543	BD+47 1002		8.62	7.725	(A0)	39	w	-	-	-	w?	-
113 <sup>new</sup>	04363913 + 4104368		29096	BD+40 999		7.96	7.323	B8IV	57	333	-	-	-	-	-
114 <sup>new</sup>	04460607 + 4705516		...	TYC 3347-1615-1		11.56	10.713	...	...	sh?	-	-	-	-	-
115 <sup>new</sup>	20185676 + 3745319		...	...		13.30	11.326	...	...	139	-	-	-	-	-
116 <sup>new</sup>	17331509 - 1922379		159032	BD-19 4652		9.56	8.725	B9IV	45	387	-	-	-	w?	-
117 <sup>new</sup>	17515926 - 3029411		162345	TYC 7378-989-1		9.12	8.291	(B8)	39	128	-	-	-	-	-
118 <sup>new</sup>	17534729 - 2945087		316573	TYC 6853-1108-1		11.07	9.850	B9	52	115	-	-	-	39	w
119	17531191 - 2857284		...	AS 251		11.00	9.961	B	24	259	-	-	-	w?	w
120 <sup>new</sup>	17521395 - 2744257		316475	TYC 6849-617-1		9.64	9.225	(B9)	39	282	-	-	-	w	w?
121 <sup>new</sup>	17525570 - 2218434		...	TYC 6262-3203-1		10.74	9.292	...	...	166	-	-	-	-	-
122	18194176 - 1058093		...	TYC 5681-507-1		12.39	10.027	A5	62	179	-	-	-	-	-
123 <sup>new</sup>	18220126 - 1048042		...	TYC 5681-151-1		12.28	10.614	...	...	177	-	-	-	w	w
124 <sup>new</sup>	18161427 - 2906365		167401	TYC 6855-539-1		9.23	9.322	B4II/III	41	627	-	-	-	-	-
125 <sup>new</sup>	18221389 - 1307360		...	TYC 5689-54-1		11.27	10.273	...	...	<60	-	-	-	w	-
126 <sup>new</sup>	18245968 - 1406408		169418	BD-14 5035		9.90	8.995	B9.5III	45	326	-	-	-	-	-
127 <sup>new</sup>	18205460 - 1243598		168566	BD-12 5014		9.62	8.710	B9III	45	114	-	-	-	-	-
128	18404465 - 0758241		...	HIP 91591		10.17	8.825	B8Ve	49	276	w?	w?	-	132	-
129 <sup>new</sup>	18385819 - 0827466		...	GSC 05692-00540		11.77	10.451	B7	17	267	-	-	-	w?	w
130 <sup>new</sup>	18405017 - 0741018		...	GSC 05692-00399		11.96	10.508	B7	17	423	-	-	-	w?	w?
131	18395898 - 0733138		...	BD-07 4647		10.95	9.642	B5	17	143	-	-	-	w?	-
132 <sup>new</sup>	18355878 - 0744307		...	BD-07 4630		10.76	8.963	B9	17	w	-	-	-	-	-
133	17500331 + 4823391		162732	88 Her		6.89	6.913	B6IIInpsh	53	285	w?	w?	-	w	-

Table 4: continued.

	ABe	2MASS ID	HD	Other	V	H	Spec Type	Ref.	$\Delta v_p$							
									Br11	$\lambda 15760$	$\lambda 16781$	Fe II 16792	Fe II 16878	C I 16895		
									mag	mag	$\text{km s}^{-1}$	$\text{km s}^{-1}$	$\text{km s}^{-1}$	$\text{km s}^{-1}$		
134 <sup>new</sup>	18295996 – 0908375		...	...			12.70	10.761	...	...	198	-	-	-	-	-
135	18432970 – 0919127	173010	MWC 952				9.22	7.179	O9.7Ia	73	sh?	-	-	-	-	-
136 <sup>new</sup>	18064578 – 2821496	165365	HIP 88720				7.11	7.024	B7.5III	41	232	-	-	-	w?	-
137 <sup>new</sup>	18042703 – 2228572	...	NGC 6531 F195				15.08	11.130	...	...	<25	w?	w?	w	w	31
138	19150144 + 0948272	180126	V1448 Aql				7.99	7.565	B2IV	68	365	-	-	-	-	-
139	19164642 + 1058468	180587	BD+10 3849				8.25	7.578	Apsh	18	sh	-	-	-	-	-
140	20234436 + 3728351	194335	HR 7807				5.86	6.228	B2Vne	63	382	-	-	-	-	-
141 <sup>new</sup>	21061887 + 2824477	201036	BD+27 3970				8.99	8.996	B6/8Vn	38	247	-	-	-	w?	w
142 <sup>new</sup>	19270008 + 1632172	183035	BD+16 3853				8.07	7.844	A0V	70	320	-	-	-	-	-
143 <sup>new</sup>	20040584 + 3009117	333378	TYC 2670-3437-1				10.50	10.150	A0	52	313	-	-	-	w?	-
144 <sup>new</sup>	20005874 + 3113497	189847	BD+30 3853				6.92	7.122	B7V	16	260	w?	w?	-	w	w?
145 <sup>new</sup>	17530194 – 2219531	...	TYC 6262-1413-1				11.78	9.926	...	...	sh?	-	-	-	-	-
146 <sup>new</sup>	06072002 + 2640558	41600	BD+26 1082				7.07	7.132	B9IV	57	w	-	-	-	w?	-
147 <sup>new</sup>	19424993 + 4239003	186485	BD+42 3425				8.52	8.484	B9V	34	123	-	-	-	-	-
148 <sup>new</sup>	20002133 + 2135515	345506	BD+21 4007				10.54	9.683	B8	52	sh?	-	-	-	-	-
149 <sup>new</sup>	03434449 + 3143092	...	IRAS F03406+3133				18.14	10.780	...	...	sp	-	-	-	w	w
150 <sup>new</sup>	18412551 – 0534033	...	...				12.90	10.902	...	...	388	-	-	-	-	-
151 <sup>new</sup>	18404500 – 0740458	...	TYC 5692-1370-1				11.47	10.799	B7	17	137	-	-	-	-	-
152	07290132 – 0832539	...	SS 120				10.64	10.733	B8e:	35	461	-	-	-	-	-
153 <sup>new</sup>	17221970 – 2833450	...	...				12.31	10.940	...	...	sh	-	-	-	-	-
154 <sup>new</sup>	05394249 + 2215279	...	TYC 1310-2084-1				12.31	9.969	B8	61	360	-	-	-	-	-
155	01590196 + 5725521	...	TYC 3692-1671-1				10.98	10.611	...	...	819	-	-	-	-	-
156 <sup>new</sup>	23380341 + 5556420	222185	BD+55 2992				8.82	8.343	(A2)	39	w	-	-	-	-	-
157	19450599 + 1617091	186637	BD+15 3925				8.82	7.937	(B9e)	39	359	-	-	-	w	w
158	21520306 + 5853123	...	AS 478				9.50	9.792	...	...	87	w	w	-	w	-
159	22275192 + 6300090	...	MWC 1062				9.34	8.804	B5:e	3	265	w?	w?	-	98	-
160	21365704 + 6811073	206135	V433 Cep				8.27	7.811	B3V	21	316	-	-	-	-	w?
161 <sup>new</sup>	21551055 + 5326166	...	TYC 3968-1354-1				11.15	10.574	OB-	14	422	-	-	-	-	-
162 <sup>new</sup>	06063872 + 2754038	...	BD+27 981				10.10	9.960	B8	62	219	-	-	-	-	-
163 <sup>new</sup>	22465987 + 5345241	215837	BD+52 3293				8.27	8.104	(A0)	39	357	-	-	-	-	-
164	22202269 + 5151395	212044	MWC 386				6.98	7.702	B1:V:nnep	8	191	-	-	-	-	-
165	22245295 + 5207583	212666	MWC 1059				8.49	8.681	B5.5e	59	397	-	-	-	-	-
166 <sup>new</sup>	06460565 – 0558109	...	TYC 4812-2496-1				10.20	9.971	...	...	308	-	-	-	w?	w
167	06495552 – 0530472	49787	MWC 153				7.54	7.836	B1Ve	68	300	-	-	-	-	-
168	06570947 – 0832309	51477	V747 Mon				8.10	8.223	B3Ve	58	628	-	-	-	-	-
169 <sup>new</sup>	06024105 + 2202482	40897	BD+22 1147				8.03	8.000	(B9)	39	255	-	-	-	w	w?
170 <sup>new</sup>	06014161 + 2224036	40724	HR 2116				6.39	6.400	B8V	26	153	-	-	-	64	169
171 <sup>new</sup>	06081219 + 2156586	...	TYC 1326-1188-1				10.39	10.257	A2	62	362	-	-	-	-	-
172 <sup>new</sup>	05212545 + 1601440	34906	BD+15 793				9.20	8.641	B9V	61	142	-	-	-	w	-
173 <sup>new</sup>	05175643 + 1519211	...	TYC 1283-1360-1				11.52	10.617	...	...	sh	-	-	-	-	-
174 <sup>new</sup>	05240938 + 1633455	35269	BD+16 767				7.88	7.552	A0V	76	448	-	-	-	w?	-
175 <sup>new</sup>	05214456 + 1709194	...	TYC 1300-652-1				11.94	10.731	...	...	w	-	-	-	-	-
176 <sup>new</sup>	05133229 + 3806348	33656	BD+37 1093				9.40	9.215	B5	2	551	-	-	-	-	-
177 <sup>new</sup>	05194374 + 3820304	280849	BD+38 1116				9.87	9.654	B3	52	522	-	-	-	w?	-
178 <sup>new</sup>	06450343 – 0034140	...	CoRoT 102762536				13.97	11.651	B1V	75	sp	-	-	-	-	-
179	06450928 – 0115205	...	EM* RJHA 51				13.13	10.563	B5Ib	75	243	w	w	-	w	-
180	06422978 + 0053582	...	EM* RJHA 40				13.17	10.613	B3Ib	75	183	181	183	-	w?	-
181	05355408 – 0537423	37115	MWC 114				7.16	7.204	B7.5V	58	238	w	w	w	102	-
182 <sup>new</sup>	06123495 + 4145095	...	TYC 2934-118-1				10.53	10.240	...	...	376	-	-	-	-	539

Table 4: continued.

	ABe	2MASS ID	HD	Other	V	H	Spec Type	Ref.	$\Delta v_p$							
									Br11	$\lambda 15760$	$\lambda 16781$	Fe II 16792	Fe II 16878	C I 16895		
									mag	mag	km s <sup>-1</sup>	km s <sup>-1</sup>	km s <sup>-1</sup>	km s <sup>-1</sup>	km s <sup>-1</sup>	
183 <sup>new</sup>	07364229 – 1303499		60993	BD-12 2050			8.76	9.131	B2II	45	348	-	-	-	-	-
184 <sup>new</sup>	05361555 + 3257145		245174	BD+32 1046			10.07	9.790	B3	62	268	-	-	-	-	-
185 <sup>new</sup>	05580029 + 2437017		40132	BD+24 1043			7.88	7.564	B9	19	85	-	-	-	w	97
186 <sup>new</sup>	07075533 + 0143105		54167	BD+01 1699			9.67	9.672	B5/7Ib:	58	328	-	-	-	-	-
187	06121659 + 2005097		253214	MWC 134			9.54	8.917	B1.5:V:nn	8	220	w	w	-	w?	436
188	06121386 + 2000034		253215	MWC 795			10.76	10.444	...	...	298	-	-	-	-	388
189	07370572 + 1654153		60848	MWC 184			6.87	7.071	O9.5IVe	67	305	-	-	-	-	-
190 <sup>new</sup>	06110671 + 1810591		252904	BD+18 1115			8.89	9.089	B9V	11	w	w?	w?	-	w	-
191	18084894 – 1858344		165854	Hen 3-1600			8.27	7.903	B9e	59	274	-	-	-	w	-
192 <sup>new</sup>	18103823 – 1910006		166291	BD-19 4882			9.06	8.303	B3II	45	272	-	-	-	-	-
193	18011841 – 2721498		...	SS 339			11.39	10.713	B8e:	33	250	-	-	-	-	w
194 <sup>new</sup>	18173492 – 1842282		313062	GSC 06269-02665			10.26	9.676	...	...	327	-	-	-	-	w
195	19120326 + 0237212		179343	MWC 978			6.92	6.613	B8III	68	266	-	-	-	w	w
196	05010612 + 4134002		277241	VES 860			11.26	10.836	B8	13	w	-	-	-	w	-
197	18095327 – 2302251		166055	Hen 3-1606			10.09	9.662	B9	62	221	-	-	-	w?	-
198 <sup>new</sup>	18091443 – 2246378		165894	BD-22 4583			8.71	8.183	B3IV/V	45	158	-	-	-	-	-
199 <sup>new</sup>	17554711 – 2142367		...	TYC 6262-371-1			10.96	9.301	...	...	164	-	-	-	w	w
200 <sup>new</sup>	18235550 – 1547477		...	Lan 671			10.92	9.976	...	...	280	-	-	-	-	-
201 <sup>new</sup>	18282453 – 1642195		...	BD-16 4888p			9.83	9.825	...	...	138	-	-	-	-	w
202 <sup>new</sup>	18283909 – 1512088		...	TYC 6266-143-1			11.00	10.487	...	...	w	-	-	-	w?	-
A01	00201742 + 6227498		...	MWC 5			8.85	8.025	B0.5IV	7	122	-	-	-	-	-
A02	00320285 + 6709401		2789	MWC 6			8.36	7.519	B3:Vne	23	320	-	-	-	-	-
A03	04042164 + 5319447		...	MWC 80			8.18	7.165	B1Vnnpe	8	as	w	w	w?	w	-
A04	05251782 + 2936535		35347	MWC 494			8.93	7.948	B2:nne	38	268	w?	w?	-	-	-
A05	05445623 + 2127384		38191	MWC 125			8.60	8.380	B1:V:ne:	8	246	w	w	-	-	-
A06	05503228 + 1801349		39018	MWC 779			7.72	7.898	(B9)	39	w	-	-	-	w	-
A07	06183944 + 2300285		43703	MWC 799			8.65	7.475	B1IV:p?	8	w	-	-	-	-	-
A08	06330559 + 1656553		46264	QQ Gem			7.64	7.522	B5Vne	31	409	-	-	-	-	-
A09	06333223 + 0820080		259597	MWC 149			8.59	7.779	B1Vnne	28	289	w	w	-	-	-
A10	06525305 – 1000270		50424	MWC 825			8.90	8.971	B8e	35	178	w	w	-	97	w?
A11	06545882 – 0342013		50891	MWC 828			8.88	7.880	B0.5Ve	68	215	-	-	-	-	-
A12	06561908 – 0348254		51193	MWC 541			8.06	8.039	B1.5IVe	68	358	-	-	-	-	-
A13	06574289 + 1754071		51354	MWC 160			7.15	7.183	B3Vn	40	257	248	250	-	w	-
A14	07093697 – 1605467		54786	MWC 837			9.01	9.051	B1.5Ib:	45	256	-	-	-	-	-
A15	07133410 – 0204390		55606	MWC 549			9.04	8.704	B0.5Vnnep	69	237	233	233	w?	232	345
A16	19525141 + 2214226		345122	AS 367			9.79	8.963	B3Ve	46	231	w?	w?	-	-	-
A17	20024644 + 2151160		190150	MWC 998			8.28	8.186	B6IV-Ve	40	240	w	w	-	104	-
A18	21082962 + 4715254		201522	MWC 362			7.90	8.022	B0V	16	...	-	-	-	-	-
A19	21250244 + 4427063		...	MWC 640			8.91	7.206	B1.5V:nnep	8	205	w	191	-	w	w
A20	21291483 + 4420173		204722	MWC 370			7.63	7.643	B1.5IV:np	25	358	-	-	-	-	-
A21	22013820 + 5010046		...	MWC 649			9.31	8.701	B3e	1	109	47	49	-	50	-
A22	22060834 + 4954088		...	AS 483			9.69	9.631	B1.5V:nne:	8	362	-	-	-	-	-
A23	18211606 – 1301256		...	MWC 922			13.90	7.396	unclB[e]	55	sp	w	w	w	w	w
A24	05181018 + 3739003		34302	MWC 752			7.88	7.534	(B8)	39	163	-	-	w?	61	216
A25	05231490 + 3742536		280999	MWC 753			9.93	9.582	B3	52	214	w	w	-	102	-
A26	05254477 + 3538499		35345	MWC 109			8.43	7.851	B1Vep	7	sp	27	28	w?	24	w
A27	05280968 + 3516540		...	EM* CDS 496			9.81	8.669	OB	24	w?	-	-	-	-	-
A28	05595354 + 2505190		250028	MWC 786			9.14	8.083	B2:V:nep	32	288	304	309	-	w	-
A29	05530609 + 2626435		39340	MWC 127			8.13	7.579	B3Ve	59	197	144	144	w?	121	-



Table 4: continued.

	ABe	2MASS ID	HD	Other	V	H	Spec Type	Ref.	$\Delta v_p$							
									Br11	$\lambda 15760$	$\lambda 16781$	Fe II 16792	Fe II 16878	C I 16895		
									mag	mag	km s <sup>-1</sup>	km s <sup>-1</sup>	km s <sup>-1</sup>	km s <sup>-1</sup>	km s <sup>-1</sup>	
A30	05533110 + 2544321		248753	MWC 128		8.48	7.361		B2:Vnne	23	279	w	w	w?	w	-
A31	05535984 + 2625212		39478	MWC 129		8.25	7.691		B2Ve	59	242	w	w	-	w	-
A32	06072661 + 2205477		...	IGR J06074+2205		12.10	10.189		B0.5Ve	71	380	-	-	-	-	-
A33	06074953 + 1839264		...	EM* LkHA 208		11.30	9.834		A7e	65	sp?	-	-	-	w	-
A34	06065436 + 1902040		251726	AS 118		9.34	7.644		B1V:e	8	159	155	153	-	w	w
A35	06184553 + 1516522		...	MWC 137		11.95	7.840		sgB[e]	56	57	55	50	48	52	183
A36	06135416 + 1631049		253659	MWC 796		9.56	8.327		B0.5:V:nne	8	312	-	-	-	-	-
Q01	20240654 + 3829332		229239	MWC 1016		9.05	7.093		B0.2III	66	...	-	-	-	-	-
Q02	20194162 + 3811060		228932	Hen 3-1880		10.04	9.386		B	35	...	-	-	-	-	-
Q03	20213867 + 3725151		...	BD+36 4032		10.46	7.566		O8.5V	66	...	-	-	-	-	-
Q04	20213589 + 3721395		...	Hen 3-1885		11.13	10.855		A0V	30	...	-	-	-	-	-
Q05	06382991 + 0042351		291946	BD+00 1516		9.27	9.321		B9	2	...	-	-	-	-	-
Q06	18071193 - 2516305		315177	TYC 6846-654-1		10.50	10.022		...	...	...	-	-	-	-	-
Q07	19582996 + 2033006		350989	VES 95		10.92	10.534		B7IIIn	50	...	-	-	-	-	-
Q08	20012170 + 2217258		345475	EM* CDS 1118		10.42	9.484		B0	4	...	-	-	-	-	-
Q09	23204452 + 6111404		...	EM* CDS 1459		8.71	7.471		O6.5(f)(n)p	72	...	-	-	-	-	-
Q10	00350607 + 6258585		...	EM* CDS 53		10.60	10.369		OB-e:	14	...	-	-	-	-	-
Q11	00310135 + 5539101		232208	MWC 670		9.77	9.519		B3:e	3	...	-	-	-	-	-
Q12	00255124 + 7148258		2083	BD+21 16		6.91	7.041		O9.5III	34	...	-	-	-	-	-
Q13	01243585 + 5812454		...	EM* CDS 144		11.07	10.499		OB-e:	14	...	-	-	-	-	-
Q14	04310304 + 4146289		276414	EM* CDS 427		10.75	10.148		B8	52	...	-	-	-	-	-
Q15	04390489 + 4115001		29332	MWC 475		8.71	8.246		B3ne	1	...	-	-	-	-	-
Q16	05085056 + 4144262		32961	EM* CDS 468		8.93	8.970		B2	13	...	-	-	-	-	-
Q17	04360336 + 3640031		280006	SS 20		9.31	7.747		A0Ibe:	33	...	-	-	-	-	-
Q18	06321639 + 0110289		288805	AS 128		9.82	9.611		B5	2	...	-	-	-	-	-
Q19	06594264 - 1109265		52159	EM* CDS 648		9.63	9.793		B3Vne	69	...	-	-	-	-	-
Q20	05204307 + 3726192		34656	EM* CDS 487		6.80	6.634		O7.5(f)II	73	...	-	-	-	-	-
Q21	07213463 - 0553498		57539	V757 Mon		6.58	6.834		B3IV	58	...	-	-	-	-	-
Q22	06154017 + 0603582		43285	HR 2231		6.07	6.336		B6Ve	69	...	-	-	-	-	-

[1] Merrill et al. (1942); [2] Cannon & Mayall (1949); [3] Merrill & Burwell (1949); [4] Popper (1950); [5] Miller & Merrill (1951); [6] Nassau & Harris (1952); [7] Morgan et al. (1953); [8] Morgan et al. (1955); [9] Heckmann et al. (1956); [10] Hiltner (1956); [11] Dufloc et al. (1958); [12] Alknis (1958); [13] McCuskey (1959); [14] Hardorp et al. (1959); [15] Bouigue et al. (1961); [16] Fehrenbach et al. (1962); [17] Roslund (1963); [18] Feast & Thackeray (1963); [19] McCuskey (1967); [20] Schmidt-Kaler (1967); [21] Racine (1968); [22] Lesh (1968); [23] Guetter (1968); [24] Wackerling (1970); [25] Walborn (1971); [26] Cowley (1972); [27] Lesh & Aizenman (1973); [28] Turner (1976); [29] Henize (1976); [30] Voroshilov et al. (1976); [31] Davis (1977); [32] Christy (1977); [33] Stephenson & Sanduleak (1977b); [34] Hill & Lynas-Gray (1977); [35] Stephenson & Sanduleak (1977a); [36] Roman (1978); [37] Bartaya (1979); [38] Clausen & Jensen (1979); [39] Ochsenbein (1980); [40] Jaschek & Jaschek (1993); [41] Houk (1982); [42] Voroshilov et al. (1985); [43] Bopp (1988); [44] Bidelman (1988); [45] Houk & Smith-Moore (1988); [46] Radoslavova (1989); [47] Sato & Kuji (1990); [48] Turner et al. (1992); [49] Grillo et al. (1992); [50] Turner (1993); [51] Garrison & Gray (1994); [52] Nesterov et al. (1995); [53] Abt & Morrell (1995); [54] Kohoutek & Wehmeyer (1997); [55] Lamers et al. (1998); [56] Esteban & Fernandez (1998); [57] Grenier et al. (1999); [58] Houk & Swift (1999); [59] Yudin (2001); [60] Chauville et al. (2001); [61] Kharchenko (2001); [62] Fabricius et al. (2002); [63] Abt et al. (2002); [64] Miroshnichenko et al. (2003); [65] Hernández et al. (2004); [66] Negueruela (2004); [67] Negueruela et al. (2004); [68] Frémat et al. (2006); [69] Levenhagen & Leister (2006); [70] Uzpen et al. (2007); [71] Reig et al. (2010); [72] Walborn et al. (2010); [73] Sota et al. (2011); [74] Mathew & Subramaniam (2011); [75] Sebastian et al. (2012); [76] Chargeishvili et al. (2013); [77] Eikenberry et al. (2014)

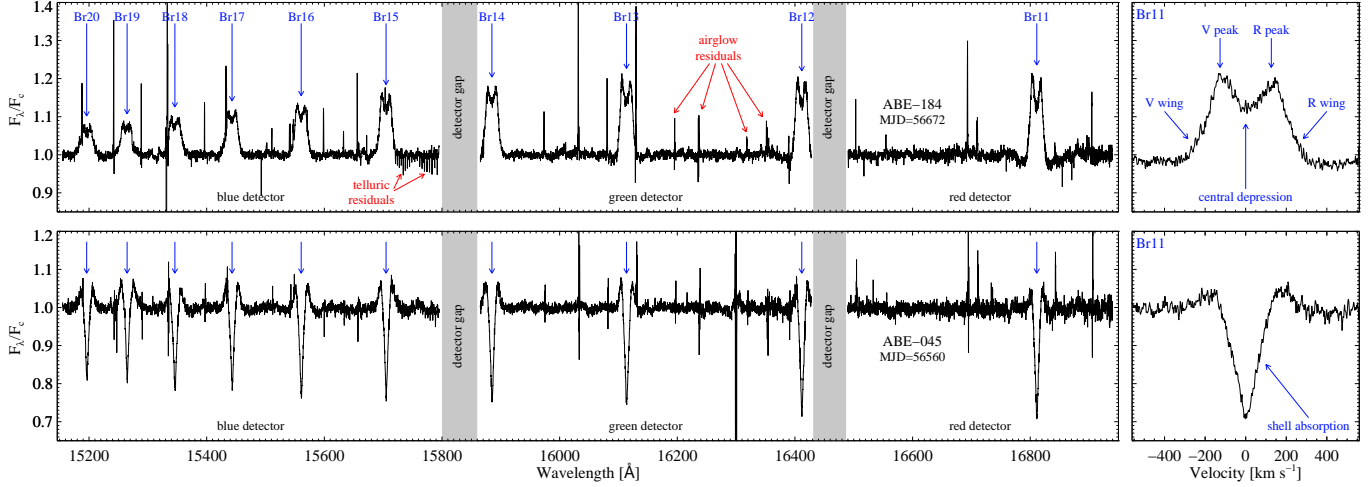


FIG. 1.— Two examples of APOGEE spectra of Be stars. The ‘red’, ‘green’, and ‘blue’ detectors and the gaps between detectors are labeled in the left panels and examples of residuals from the airglow and telluric removal process airglow residuals are labeled in the upper left panel (red arrows and text). The APOGEE Be star designations (ABE-184 and ABE-045) are shown along with the modified Julian date (MJD) of observation, and the Brackett series lines are labeled (blue arrows and text). Right-hand panels show the Br11 profiles on a velocity scale: ABE-184 exhibits a typical Be star line profile, where the central depression is a consequence of the disk geometry (e.g. Huang 1972), while the Brackett lines for ABE-045 are dominated by shell absorption resulting from occultation of the star by the disk in a nearly or exactly edge-on system (e.g. Rivinius et al. 2006). A color version of this figure is available online.

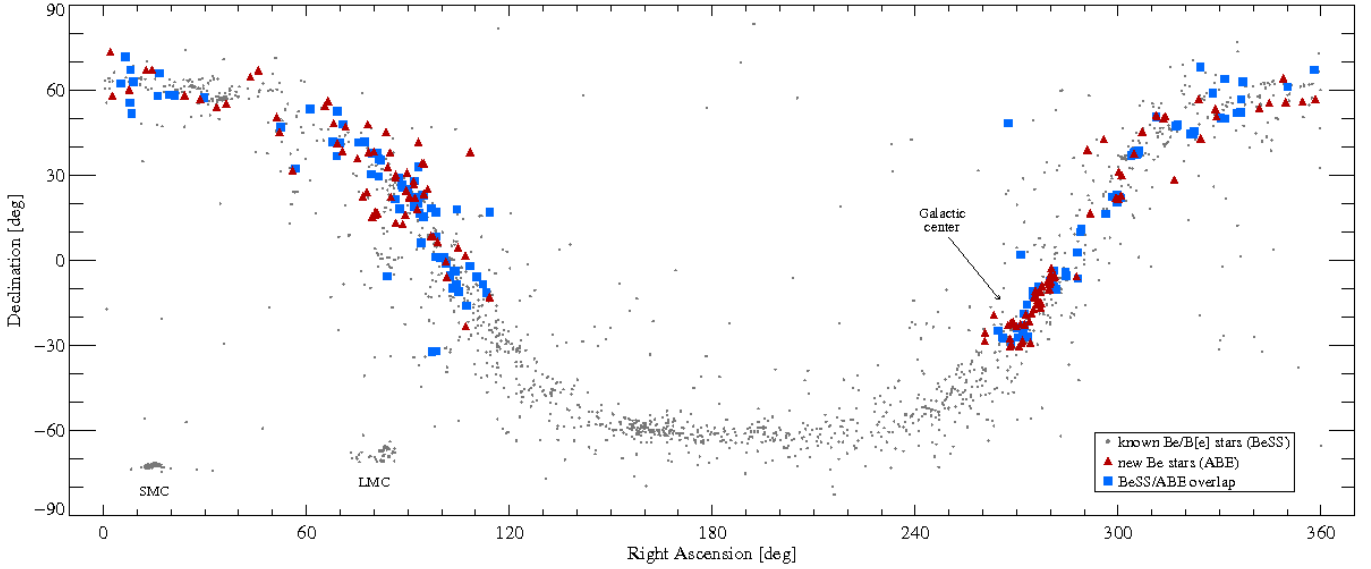


FIG. 2.— This adaptation of Neiner et al. (2011) Figure 1 shows the RA and Dec positions of all the BeSS entries as black dots, known Be stars observed by APOGEE as squares (blue), and new Be stars discovered in the APOGEE survey as triangles (red). The Galactic Center and Magellanic Clouds are labeled. A color version of this figure is available online.

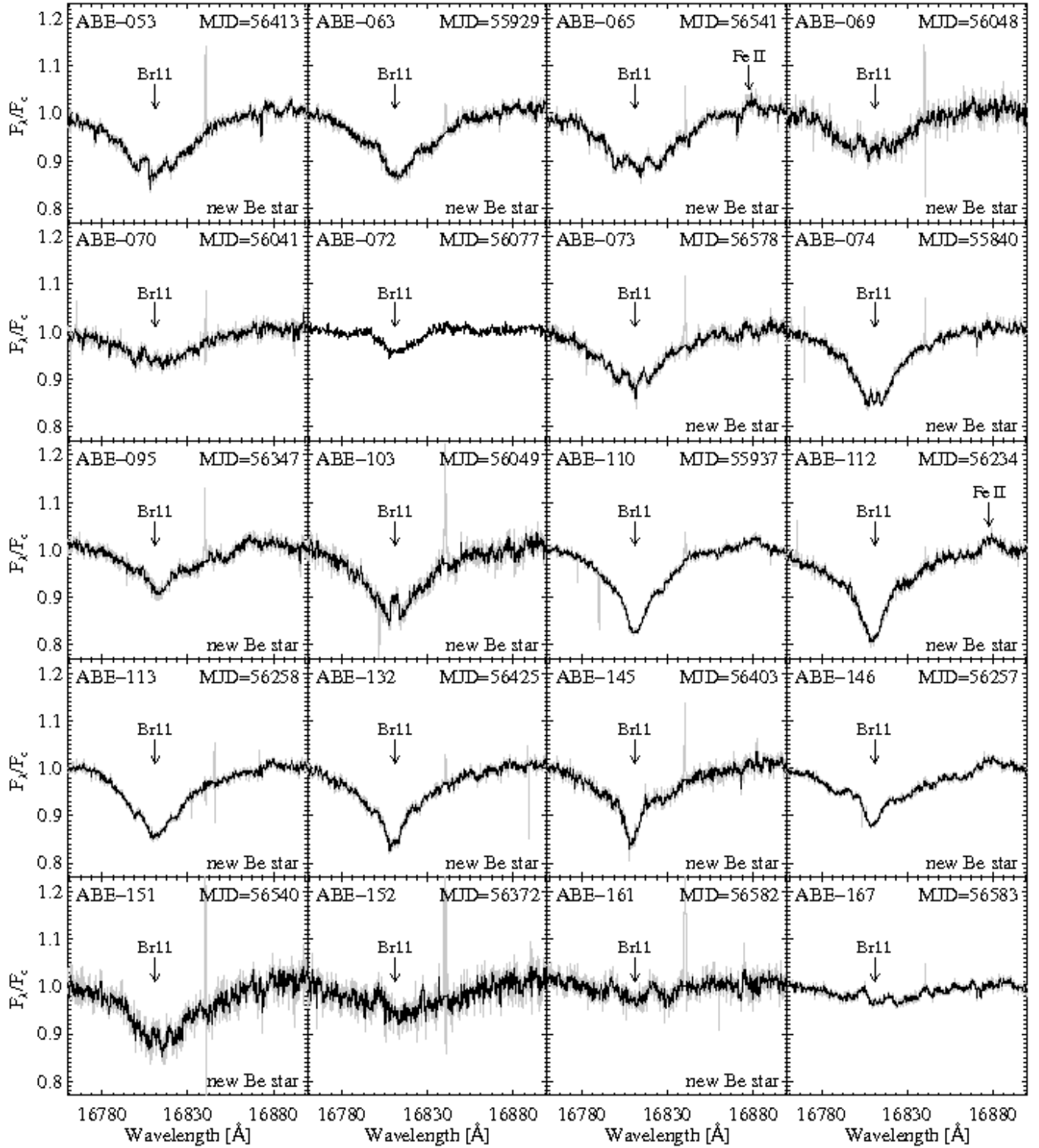


FIG. 3.— The Br11 region for some new and previously-known Be stars showing very weak evidence of circumstellar emission.

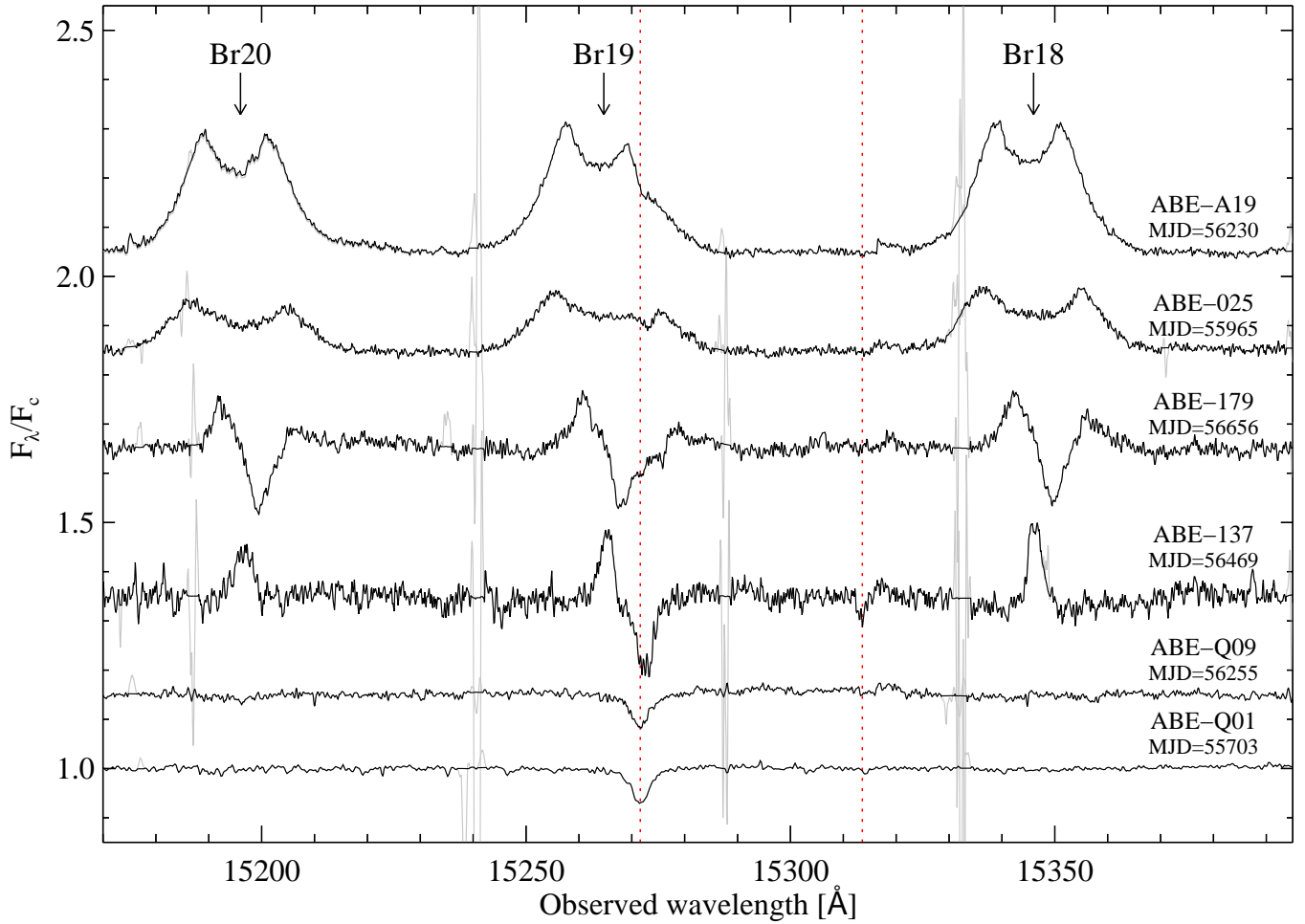


FIG. 4.— Spectra for six stars with visible DIB 15271 absorption around or on the Br19 line. No correction for radial velocity has been applied to the spectra. The dotted lines (red) mark DIB 15271 and another likely DIB at  $\sim 15314$  that appears in numerous APOGEE spectra. A color version of this figure is available online.

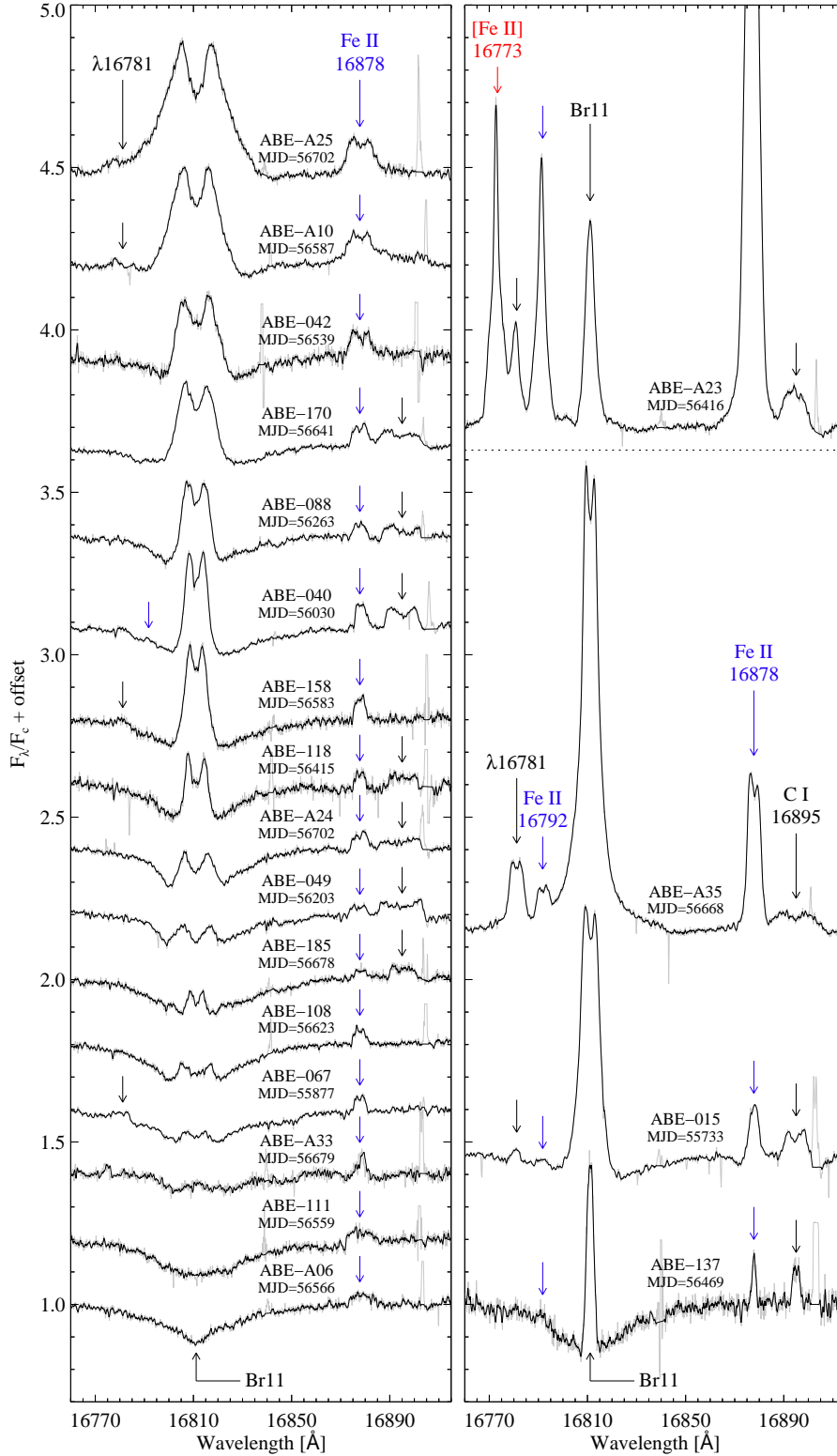


FIG. 5.— Be star spectra with combinations of emission from  $\lambda 16781$ , Fe II 16792 and 16878 (blue), and C I 16895 over a spectrum of Brackett series emission strength. The left and right panels show the same wavelength and intensity ranges. A dotted line separates the unclassified B[e] star ABE-A23 (MWC 922) from the other stars; ABE-A23 is unique among this sample (see Section 3.5) in being the only source to show forbidden line emission (mostly [Fe II]). A color version of this figure is available online.



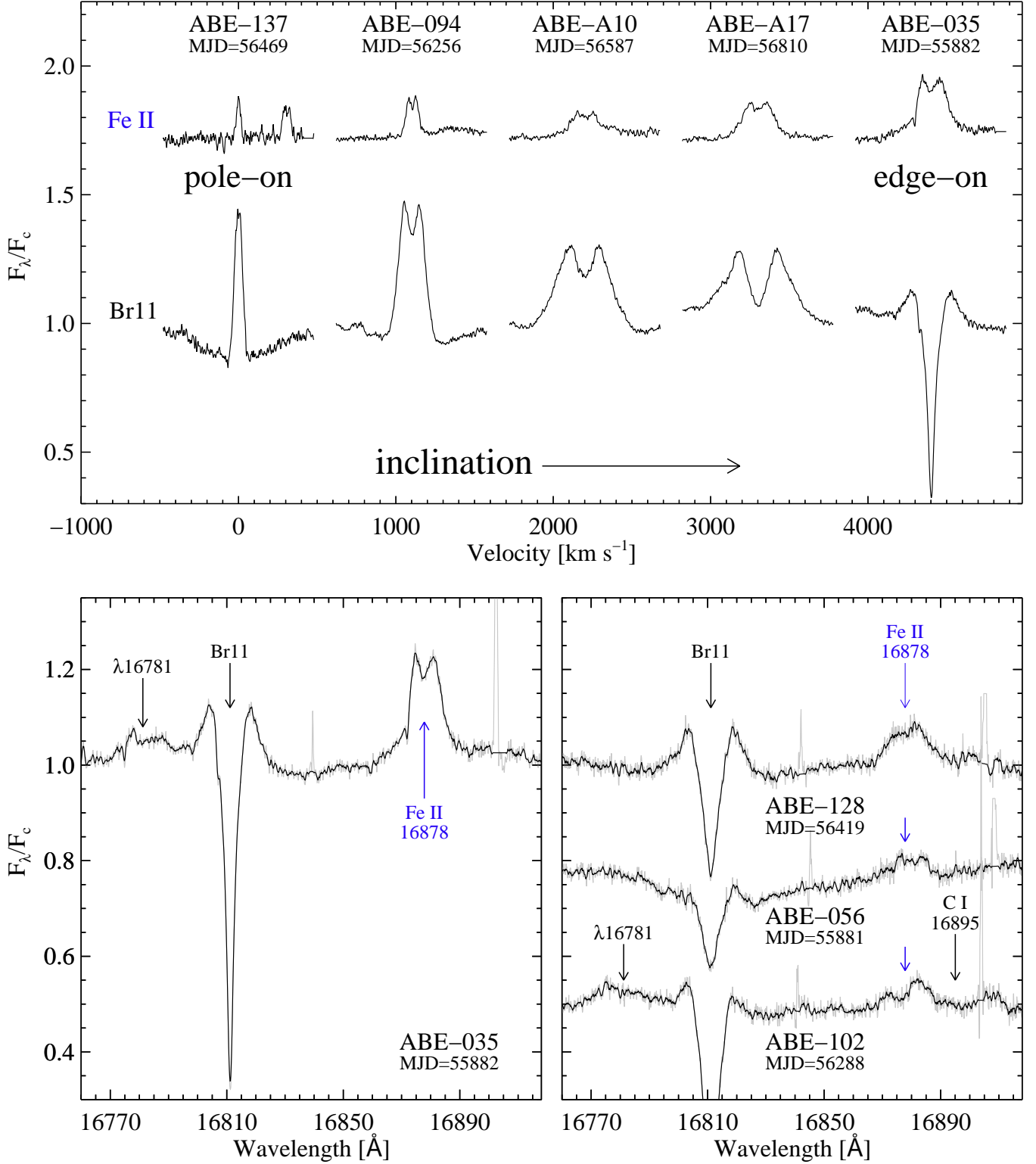


FIG. 6.— (Top panel) An assortment of observed spectra, showing the variety of metallic and hydrogen line profiles observed in the sample as a function of inclination angle. (Left, bottom) A portion of a spectrum for ABE-035, highlighting the immunity of metallic emission lines to shell absorption, a fact that is observed in all shell absorption sources (examples shown on right, bottom). A color version of this figure is available online.

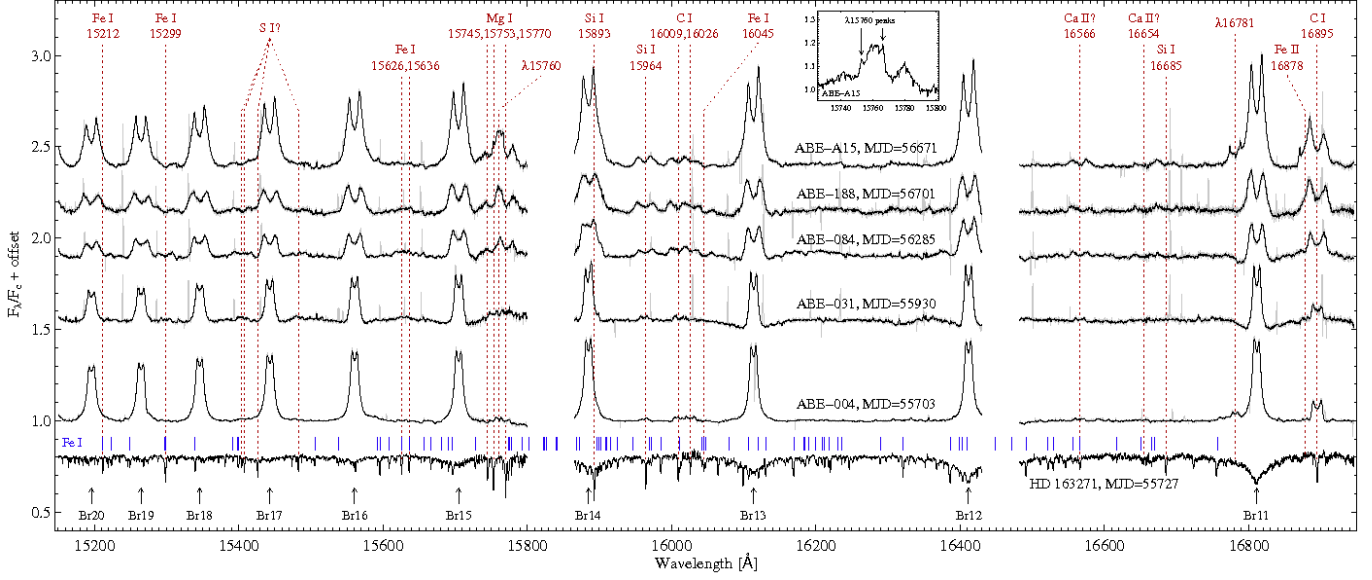


FIG. 7.— Spectra of five Be stars (ABE-A15, ABE-188, ABE-084, ABE-031, ABE-004) with strong C I 16895 emission and many weak, double-peaked metallic emission features. The spectrum of a strong-metal-lined A star (HD 163271) is included to demonstrate that the additional emission lines for these four Be stars correspond to absorption lines for cooler stars. The small lines (blue) above the A star spectrum mark the positions of numerous Fe I lines with  $\log(g_i f_{ik}) > -3$ . A color version of this figure is available online.

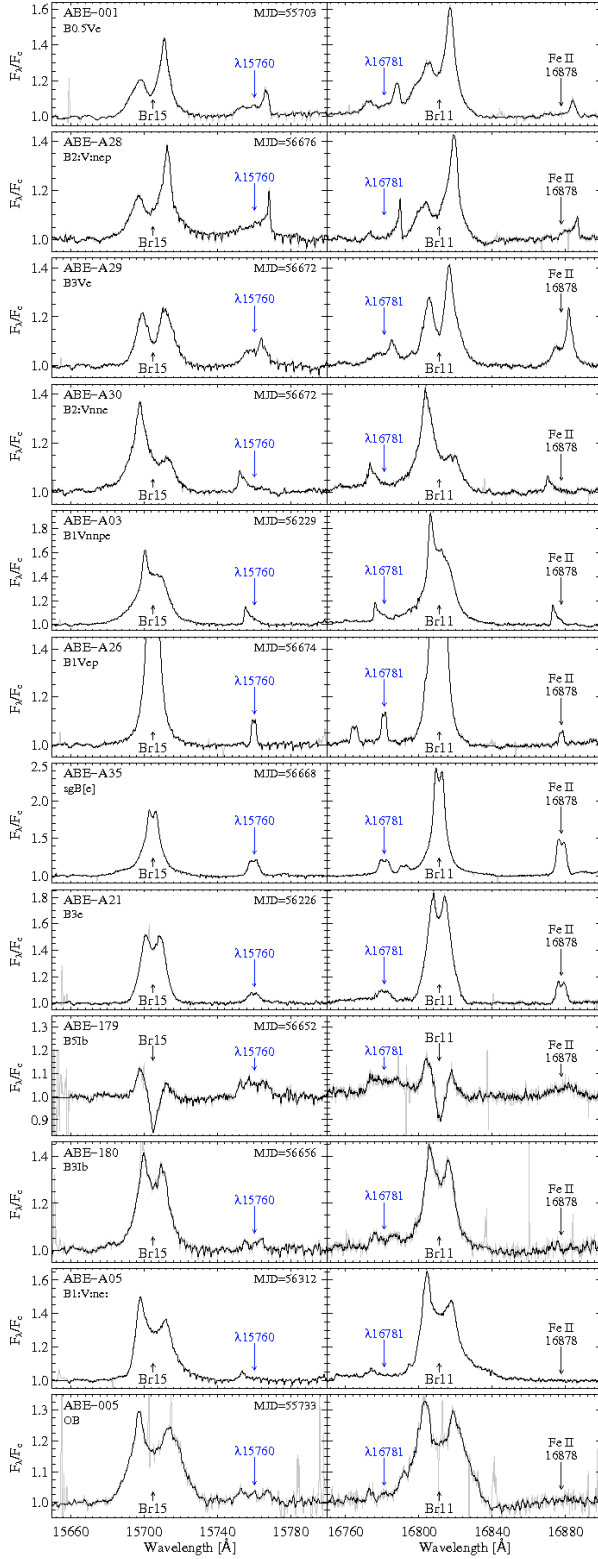


FIG. 8.— The identifications of  $\lambda 15760$  and  $\lambda 16781$  are uncertain; however, these lines are never detected separately and in most cases Fe II 16878 emission is also present. The three lines always share a common V/R orientation, but the Fe II intensity varies with respect to  $\lambda 15760$  and  $\lambda 16781$ . Small absorptions around the  $\lambda 15760$  line are telluric correction artifacts. A color version of this figure is available online.

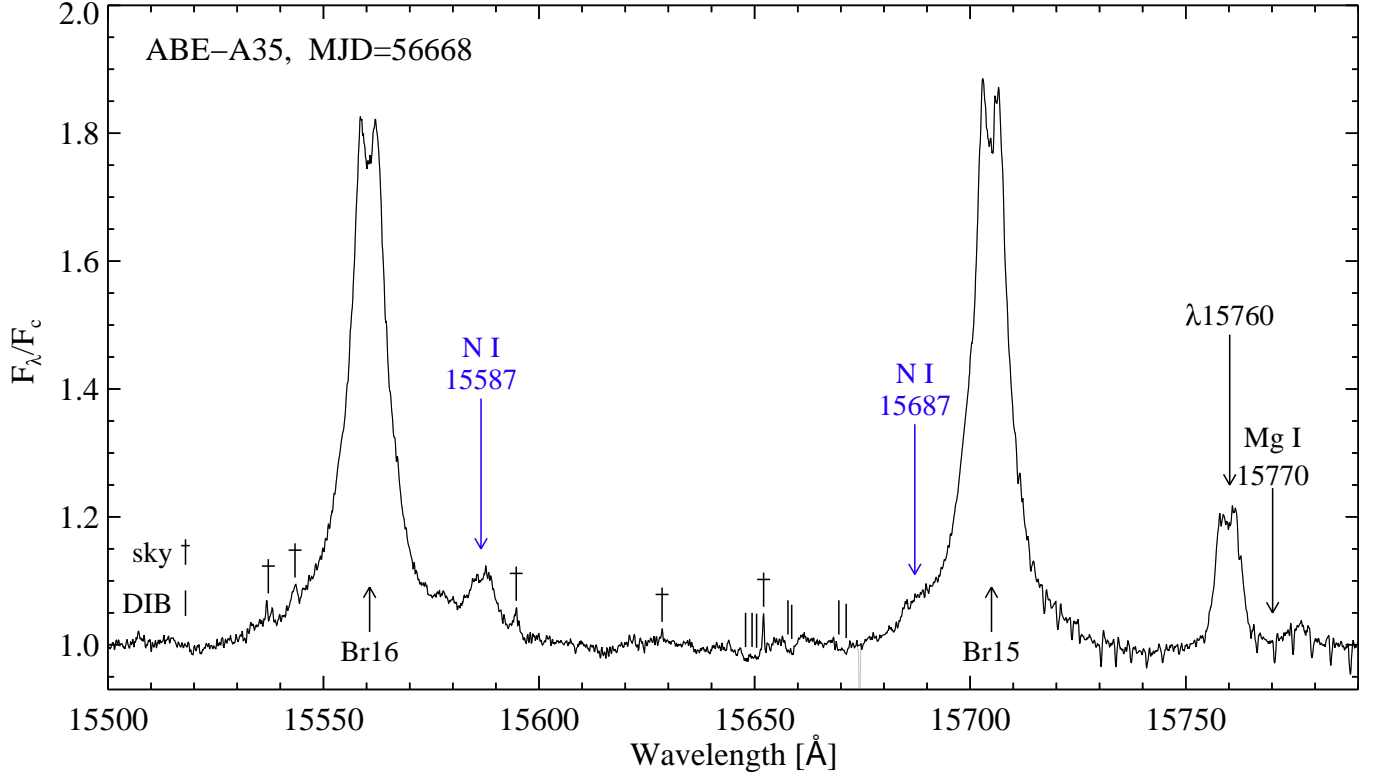


FIG. 9.— Emission from N I is seen only for ABE-A35, a supergiant B[e] star (Esteban & Fernandez 1998; Oksala et al. 2013). Both lines, N I 15587 and N I 15687, are partially blended with H I emission wings. A color version of this figure is available online.

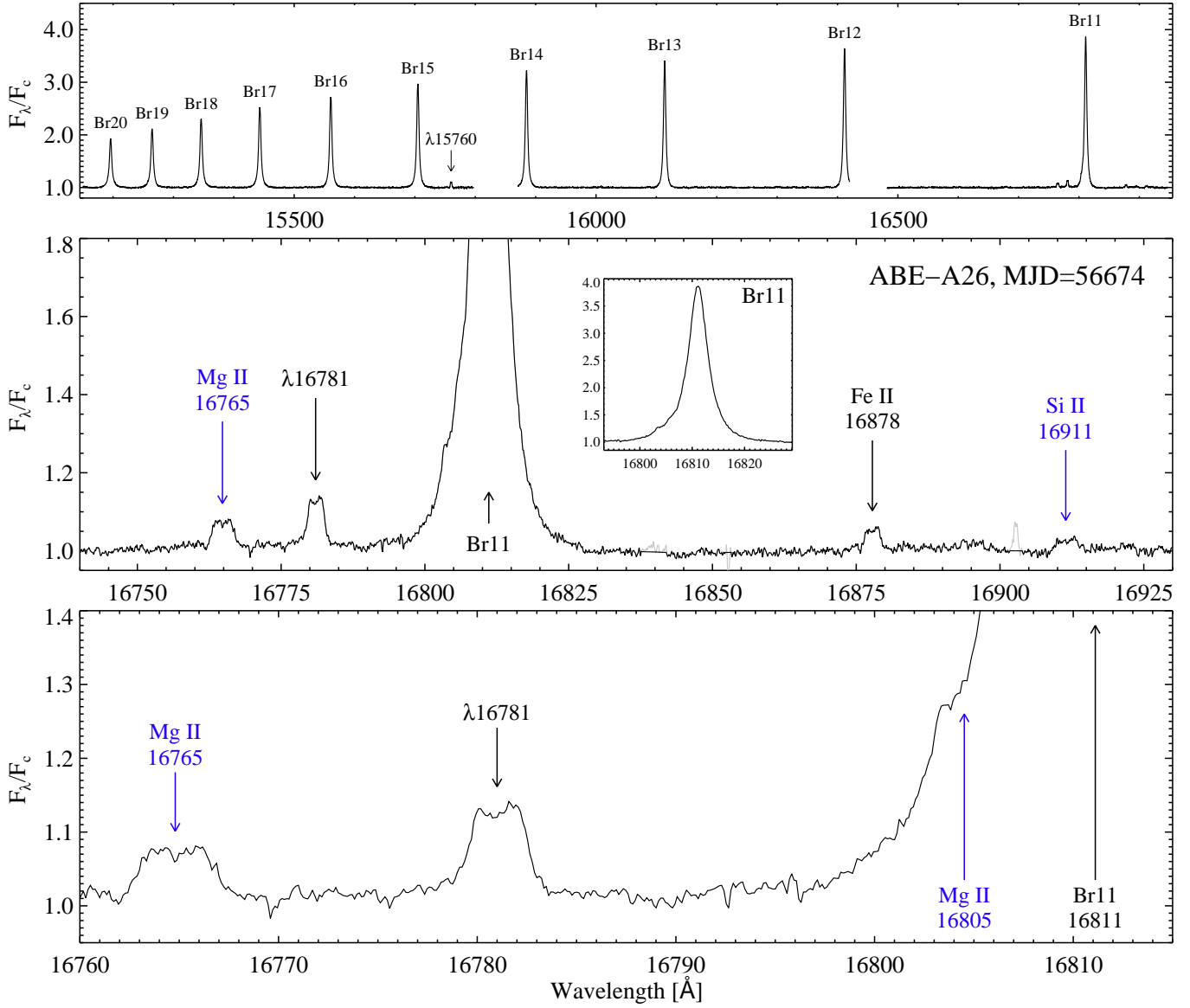


FIG. 10.— Mg II and Si II emission lines in a spectrum of ABE-A26, the only star for which these lines are detected. While the full spectrum is presented in the upper panel, the lower two panels highlight the Br11 region and the weak metallic lines therein. The single-peaked Br11 line profile is displayed in the inset panel of the larger middle panel for comparison to the double-peaked profiles of the metallic lines. As expected from the detection of Mg II 16765, the stronger line of this multiplet, Mg II 16804, appears blended with Br11 in the lowermost panel. A color version of this figure is available online.



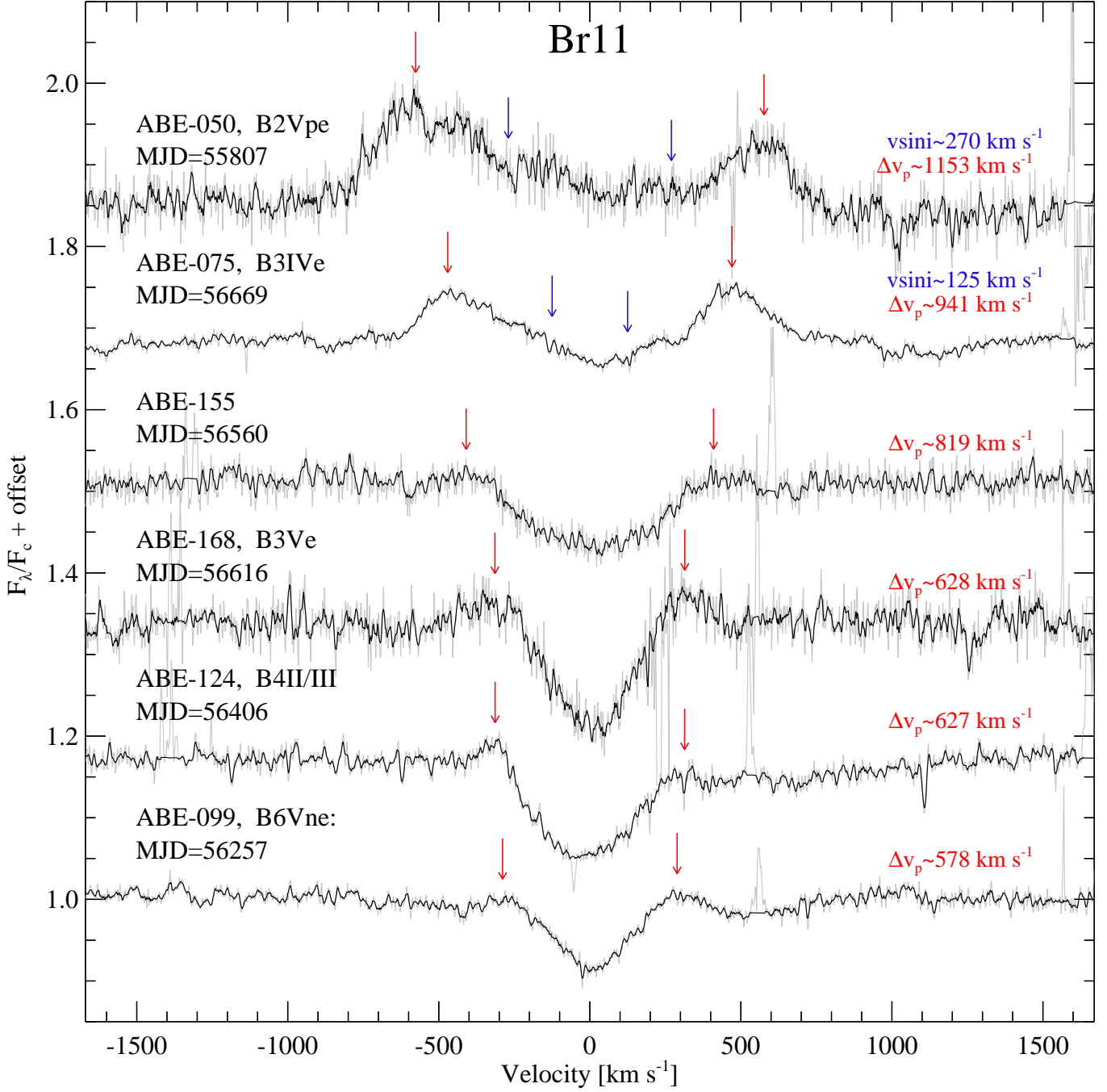


FIG. 11.— Br11 line profiles for the ABE stars with the largest peak separations are shown. The  $\Delta v_p$  is listed and marked with arrows (red) for each source, while the  $v \sin i$  measurements for ABE-050 and ABE-075 are given and indicated with arrows (blue) interior to the  $\Delta v_p$  arrows. Whereas ABE-050 and ABE-075 are confirmed  $\sigma$  Orionis E type stars, the other four stars remain to be investigated further. A color version of this figure is available online.

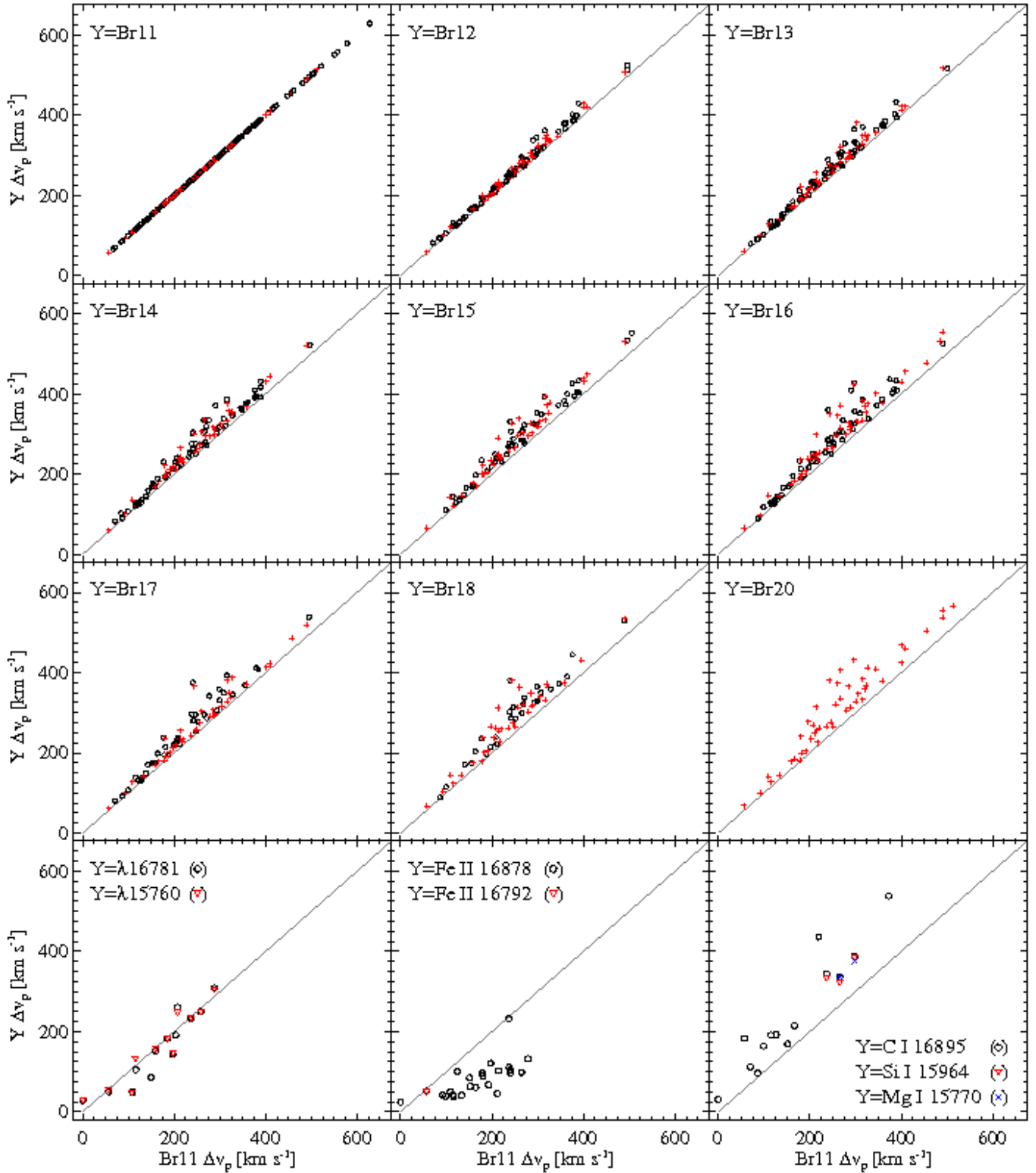


FIG. 12.— The peak separation of Br11 is compared to the peak separations for the other Brackett series lines as well as the most routinely detected metallic emission lines. Symbol meanings are described in Section 5.2. A color version of this figure is available online.

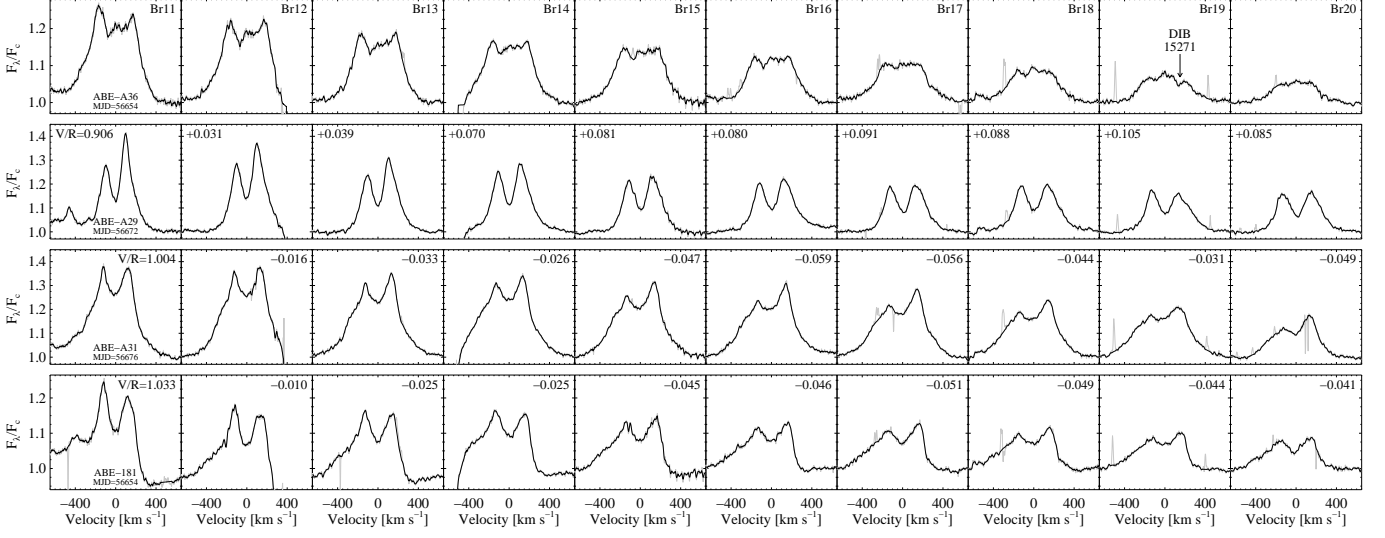


FIG. 13.— Four examples of variation in V/R phase across the Brackett series lines. The Br11 profile for ABE-A36 has a quasi-triple-peaked morphology which gradually becomes a single-peaked morphology at Br20. For ABE-A29, ABE-A31, and ABE-181, the V/R ratio of Br11 is provided in the leftmost panels and subsequent panels provide the difference between the Br12–Br20 V/R ratios and the Br11 V/R ratio. Gradual changes in V/R orientation are seen among Brackett series lines for these stars: blue text for the differences means increasing V/R ratio from Br11 to Br20 (ABE-A29) while red text means decreasing V/R ratio from Br11 to Br20. DIB 15271 absorption is evident on the Br19 line for all four stars.

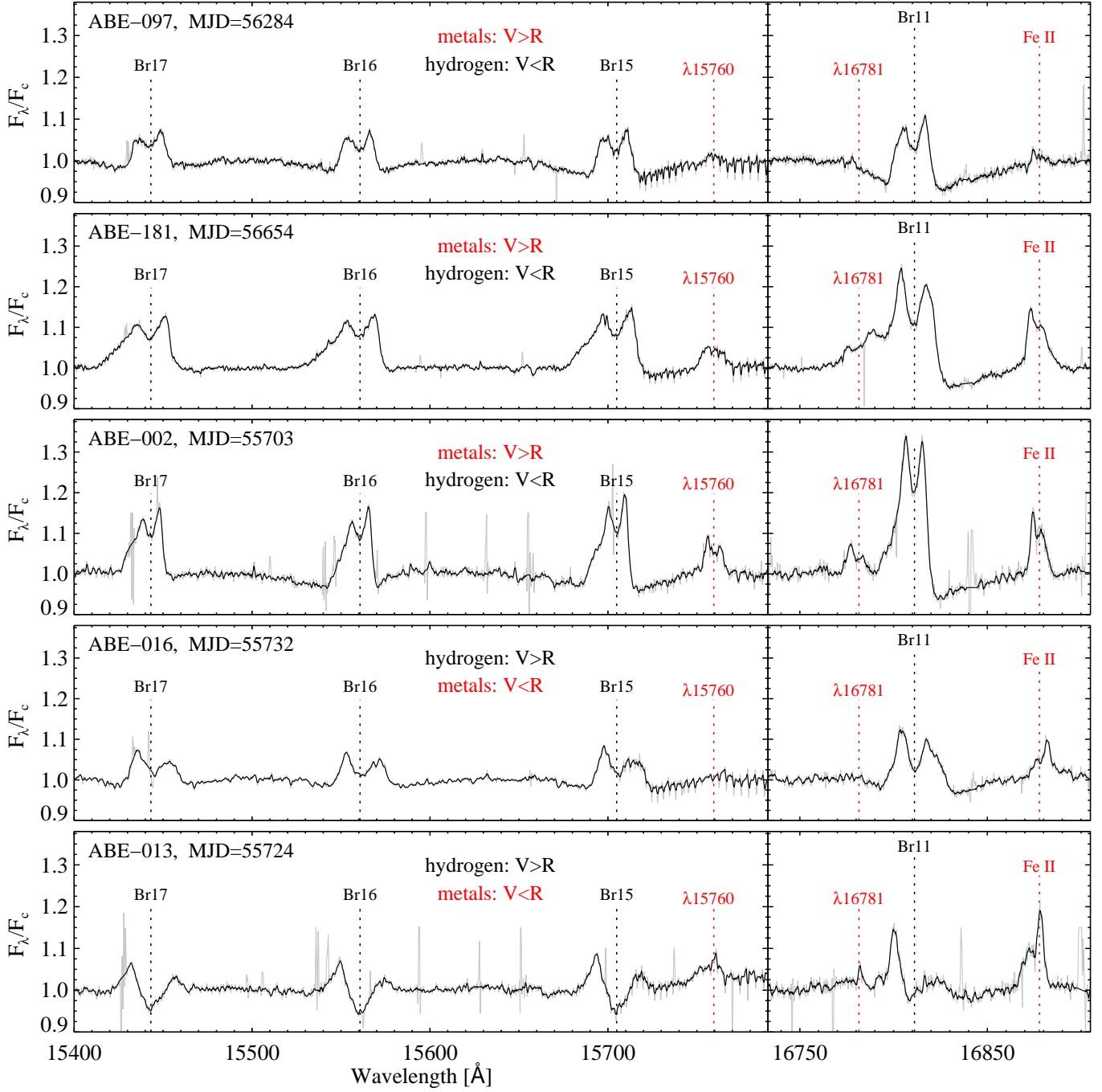


FIG. 14.— H I versus metallic V/R orientation mismatches are evident in the APOGEE spectra of ABE-097, ABE-181, ABE-002, ABE-016, and ABE-013. The emission wings for ABE-181 and ABE-002 are also clearly extended in the direction of the weaker emission peak for each line, and the metallic emission profiles for ABE-013 appear to be offset in radial velocity from the Brackett lines. A color version of this figure is available online.

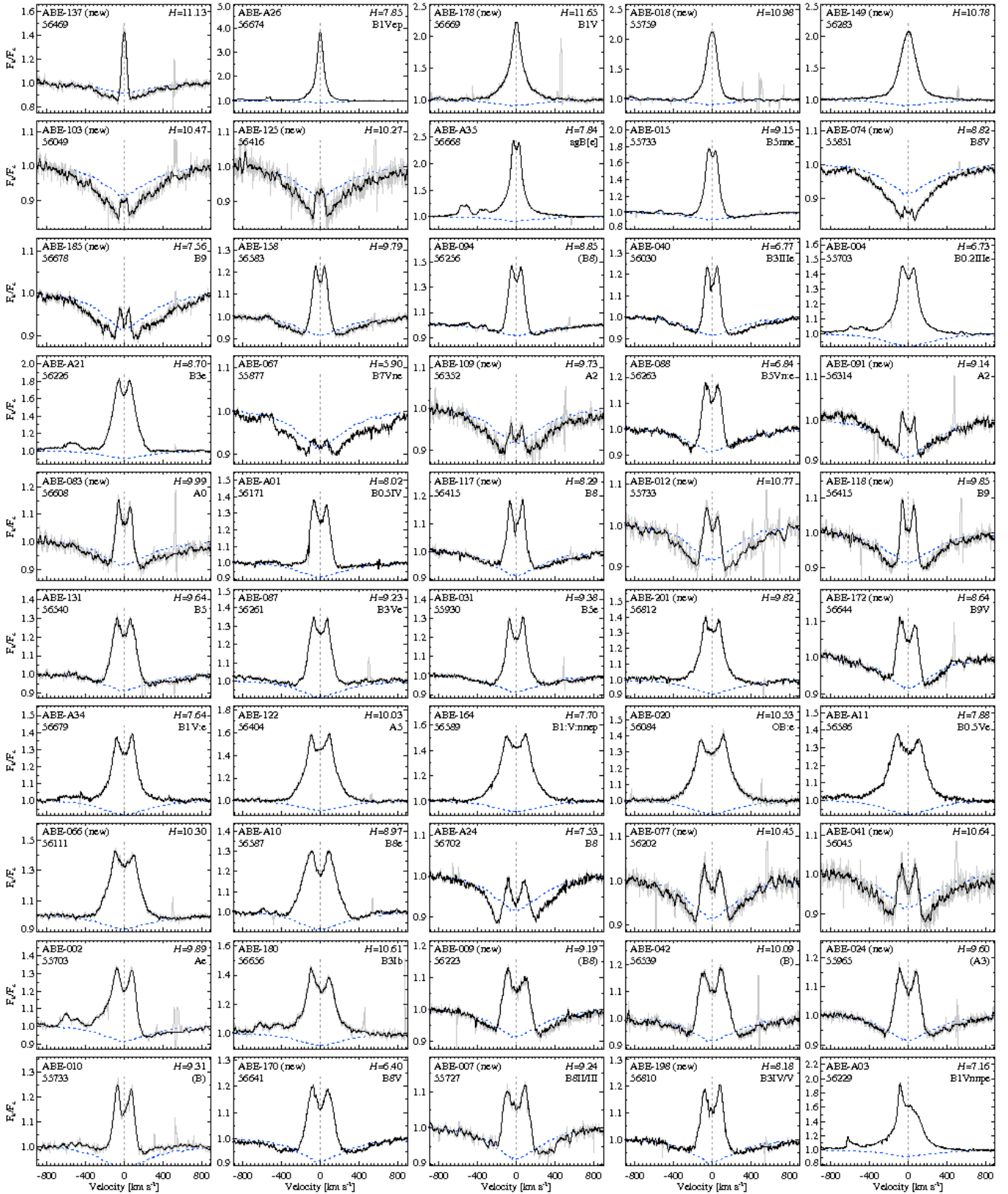


FIG. 15.— Br11 line profiles sorted approximately according to inclination angle, from pole-on to edge-on. ABE identifiers, observation MJDs, 2MASS  $H$  magnitudes, and literature spectral types (where available) are printed in each panel. The average Br11 profile of the quiescent Be stars (ABE-Q01-ABE-Q23) is displayed as a dotted line (blue), and vertical dotted lines (grey) indicate emission peak midpoints or estimated line centers if emission peaks are not present. Color versions of this figure as well as Figures 16–20 are available online.



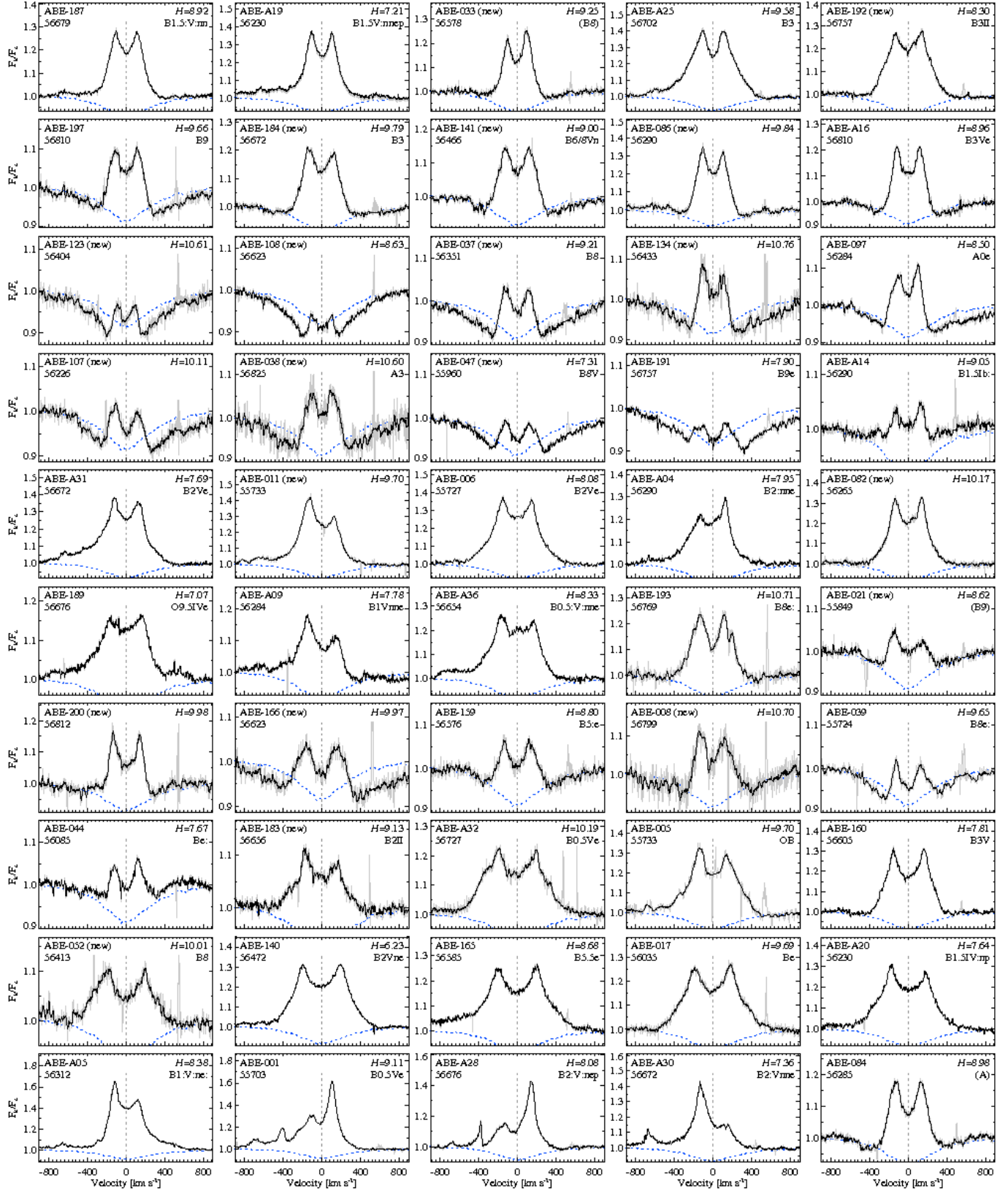


FIG. 16.— Br11 line profiles sorted by inclination angle, going from pole-on to edge-on. Meanings are the same as in Figure 15.

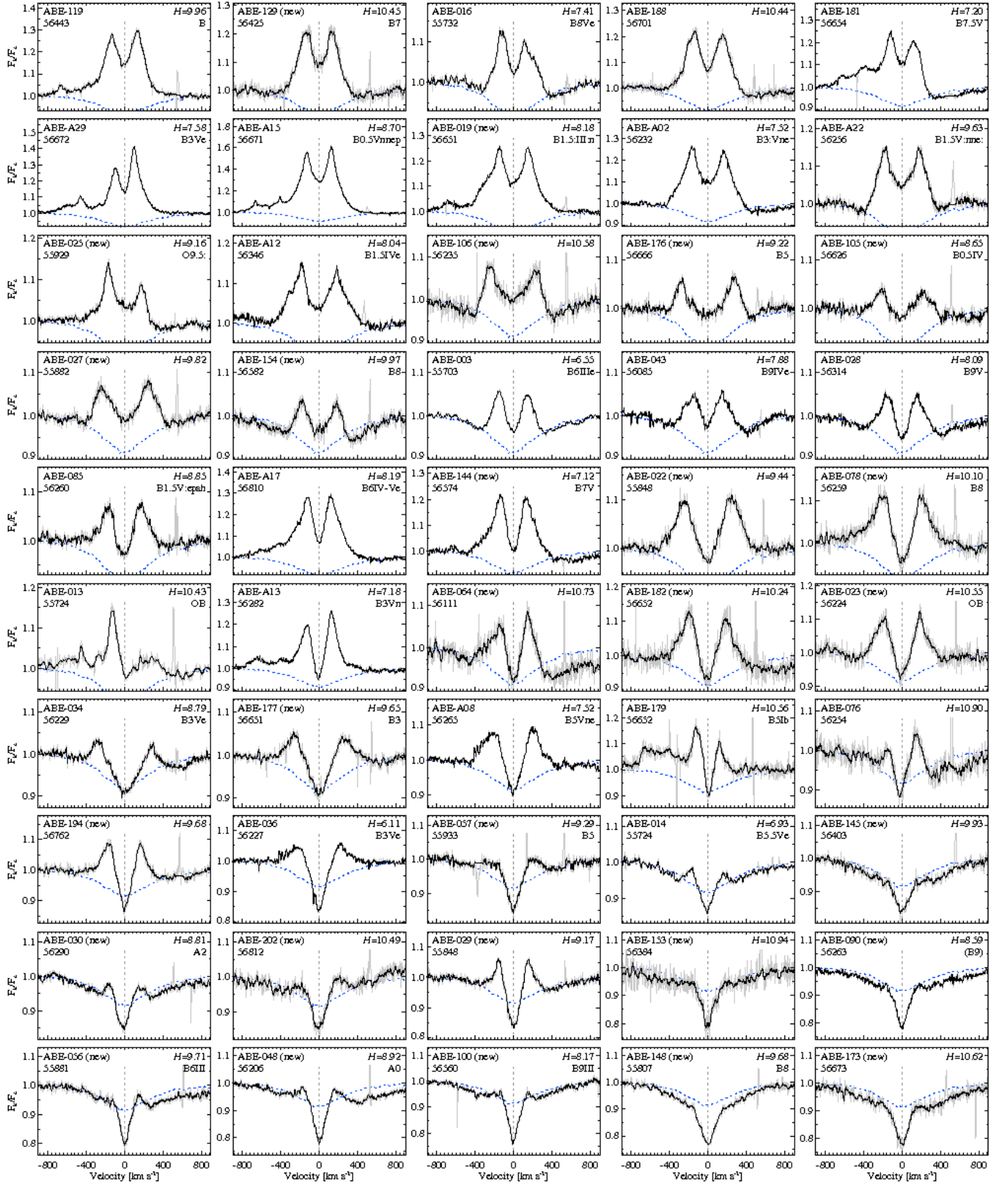


FIG. 17.— Br11 line profiles sorted by inclination angle, going from pole-on to edge-on. Meanings are the same as in Figure 15.

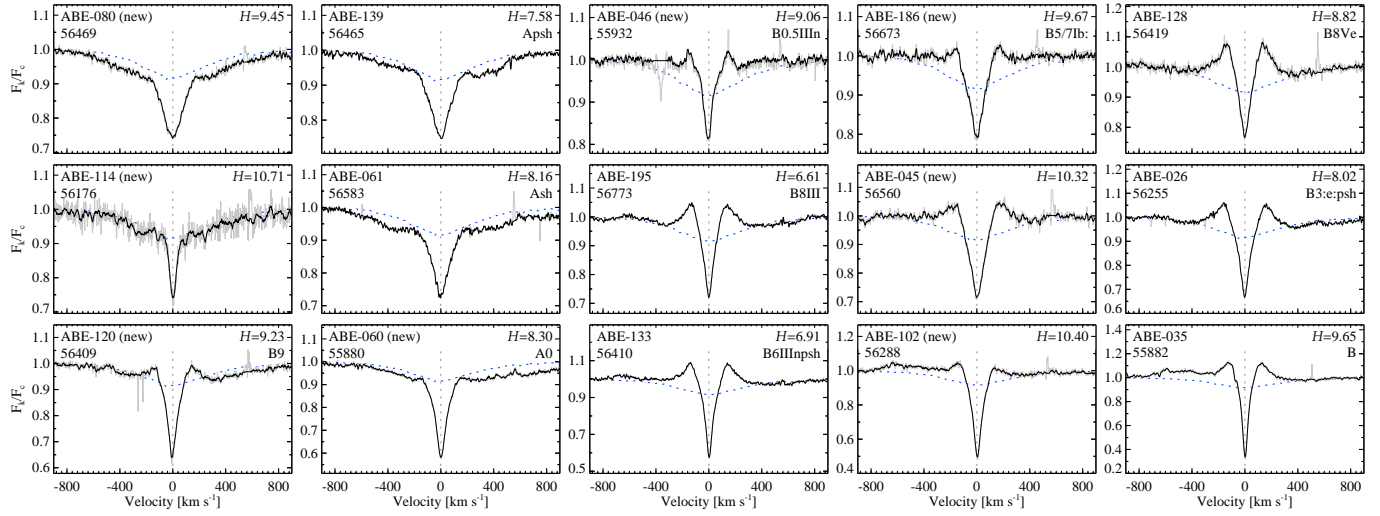


FIG. 18.— Br11 line profiles sorted by inclination angle, going from pole-on to edge-on. Meanings are the same as in Figure 15.

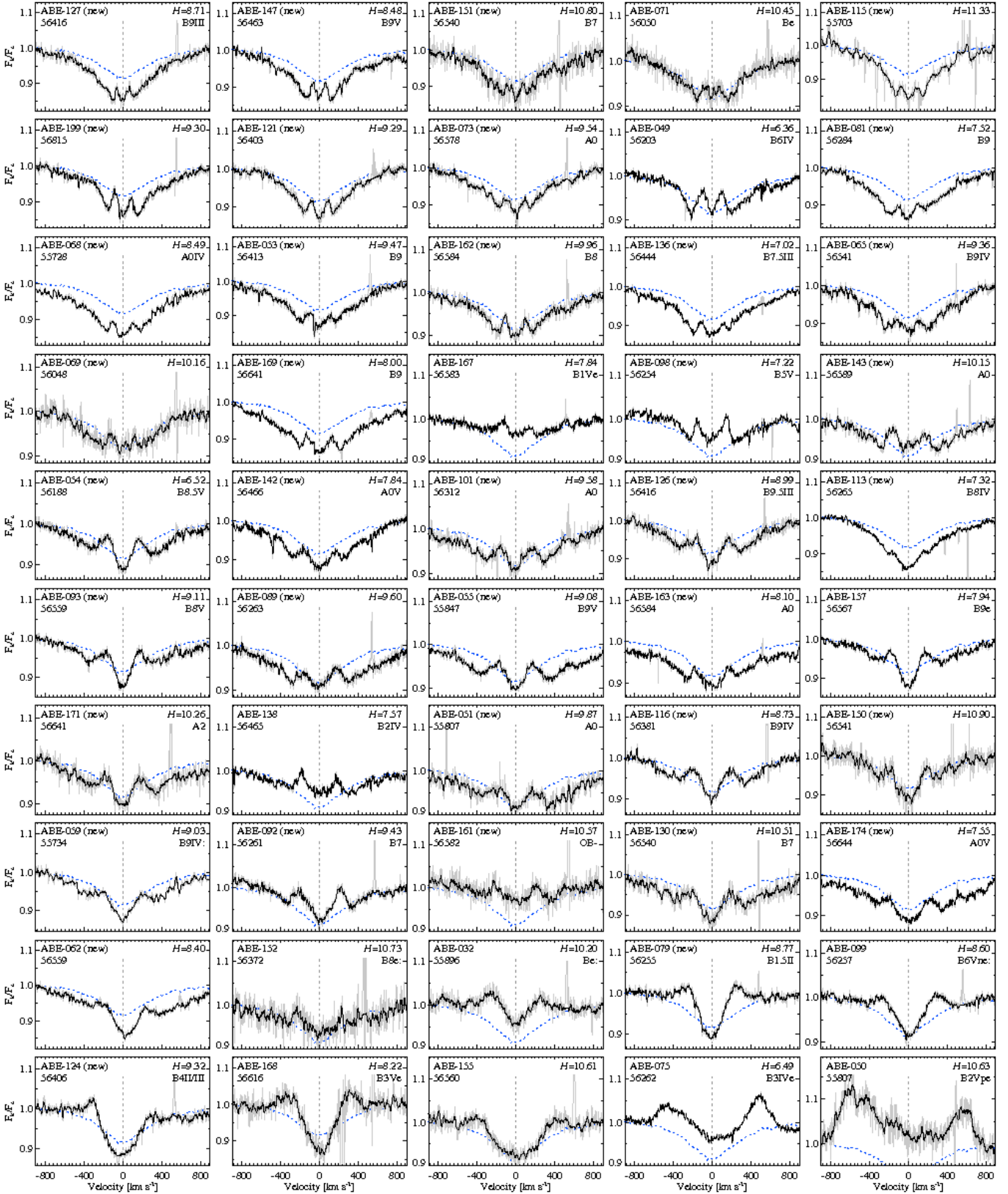


FIG. 19.— Br11 line profiles for stars with weak or ambiguous emission profile type, as well as for the  $\sigma$  Ori E type stars ABE-075 and ABE-050. The panels are sorted by Br11 peak separation. Meanings are otherwise the same as in Figure 15.

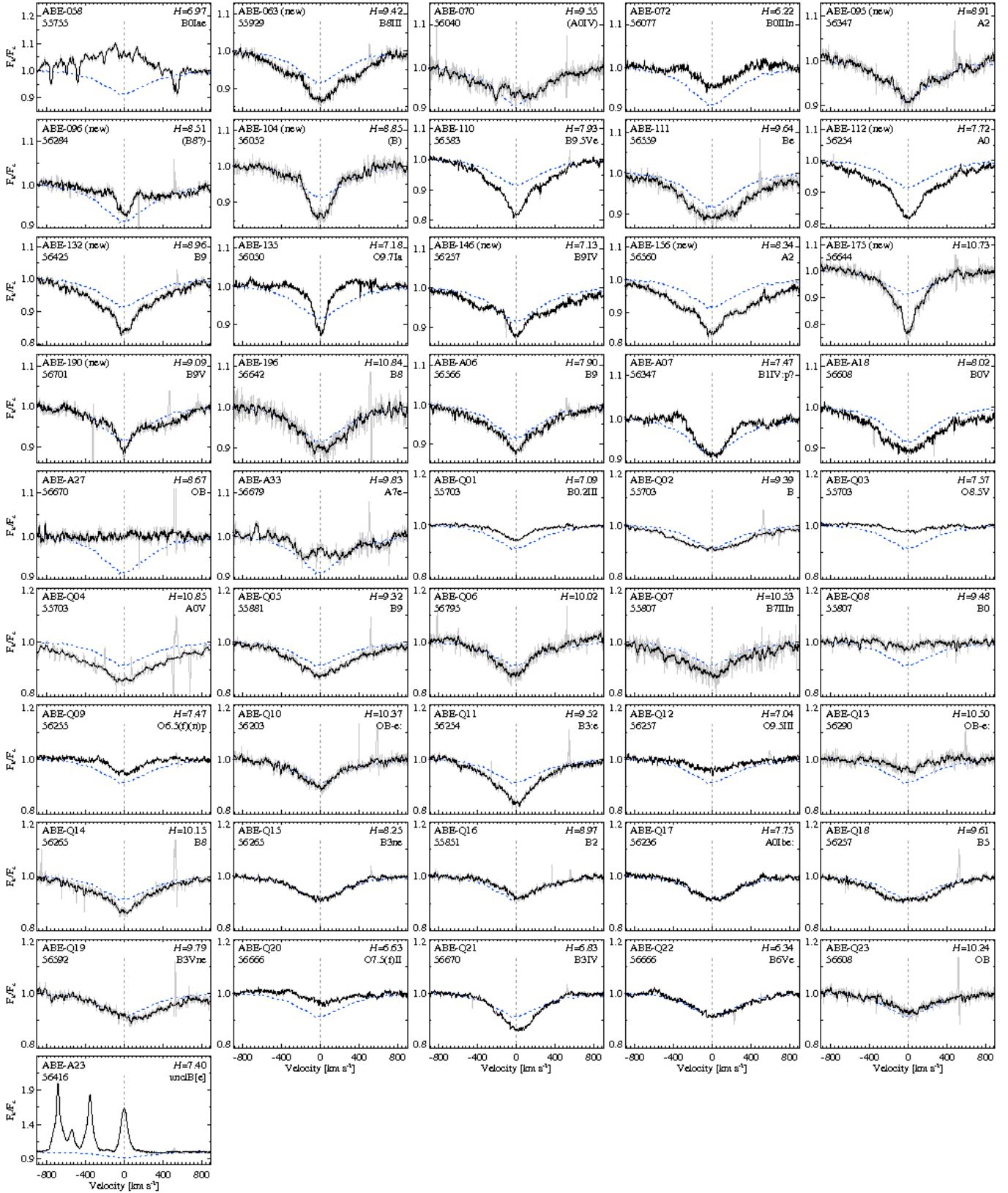


FIG. 20.— Br11 line profiles for stars with weak or ambiguous emission profile type and lack of discernible emission peaks, followed by the sample of previously-known emission stars that produced little or no emission in the APOGEE spectra. The panels are mostly sorted by ABE identifier (followed by ABE-A23). Note that the telluric correction is problematic for the plug-plate on which ABE-058 was observed; Br11 is clearly in emission, but the profile is badly contaminated by telluric absorption features. Means are otherwise the same as in Figure 15.



## APPENDIX

## Supplemental figures

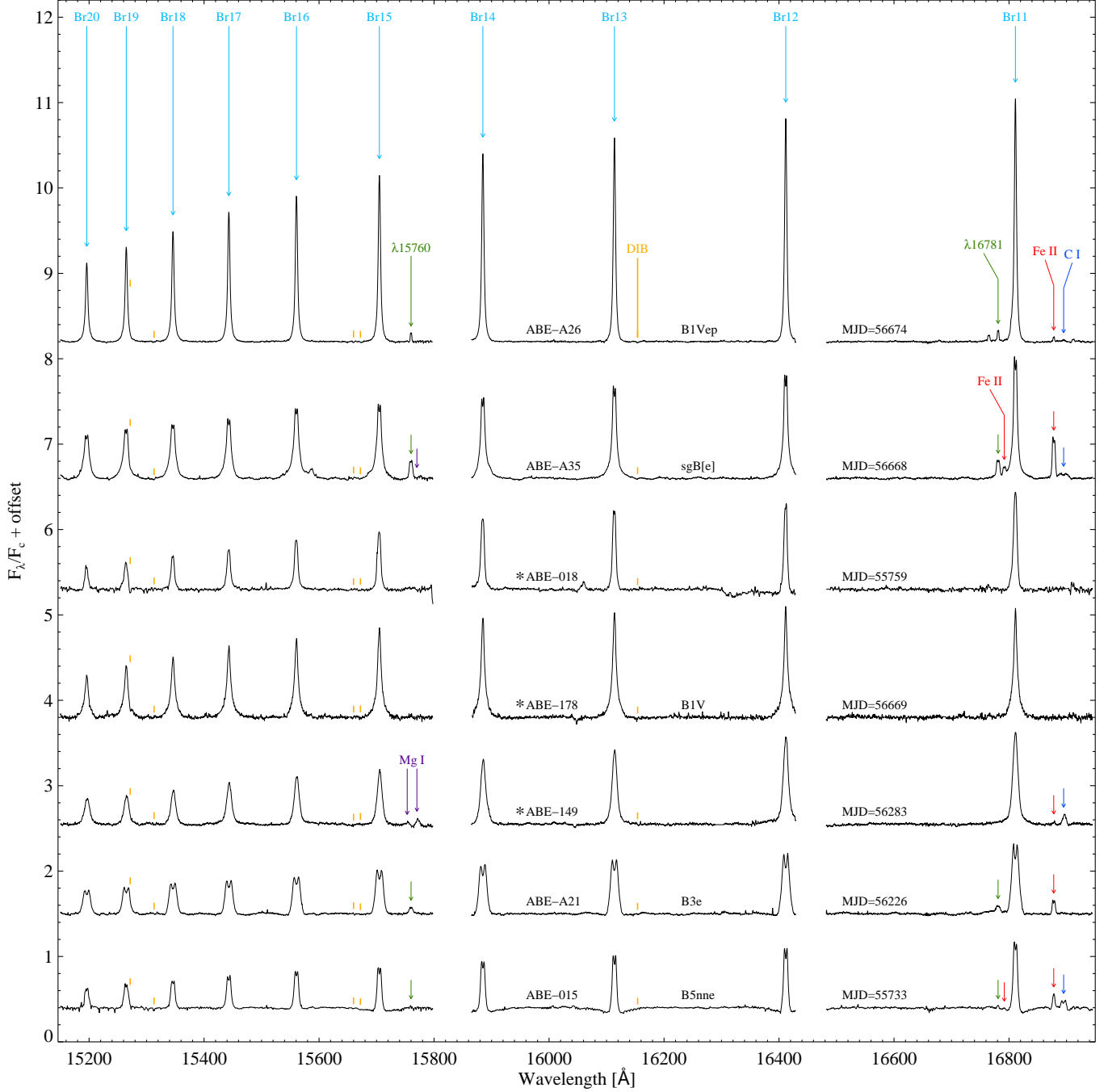


FIG. A21.— Full APOGEE spectra for Be stars with strong Brackett series emission. The emission lines for ABE-A35, ABE-A21, and ABE-015 are double-peaked, whereas the other stars have single-peaked emission. ABE identifiers, observation MJDs and literature spectral types for each star are provided, and newly-identified-via-APOGEE Be stars are indicated with a large asterisk preceding the ABE identifier. Small line segments mark the positions of the most prominent DIBs appearing for these stars, and arrows mark the positions of the most frequently-detected metallic emission features.

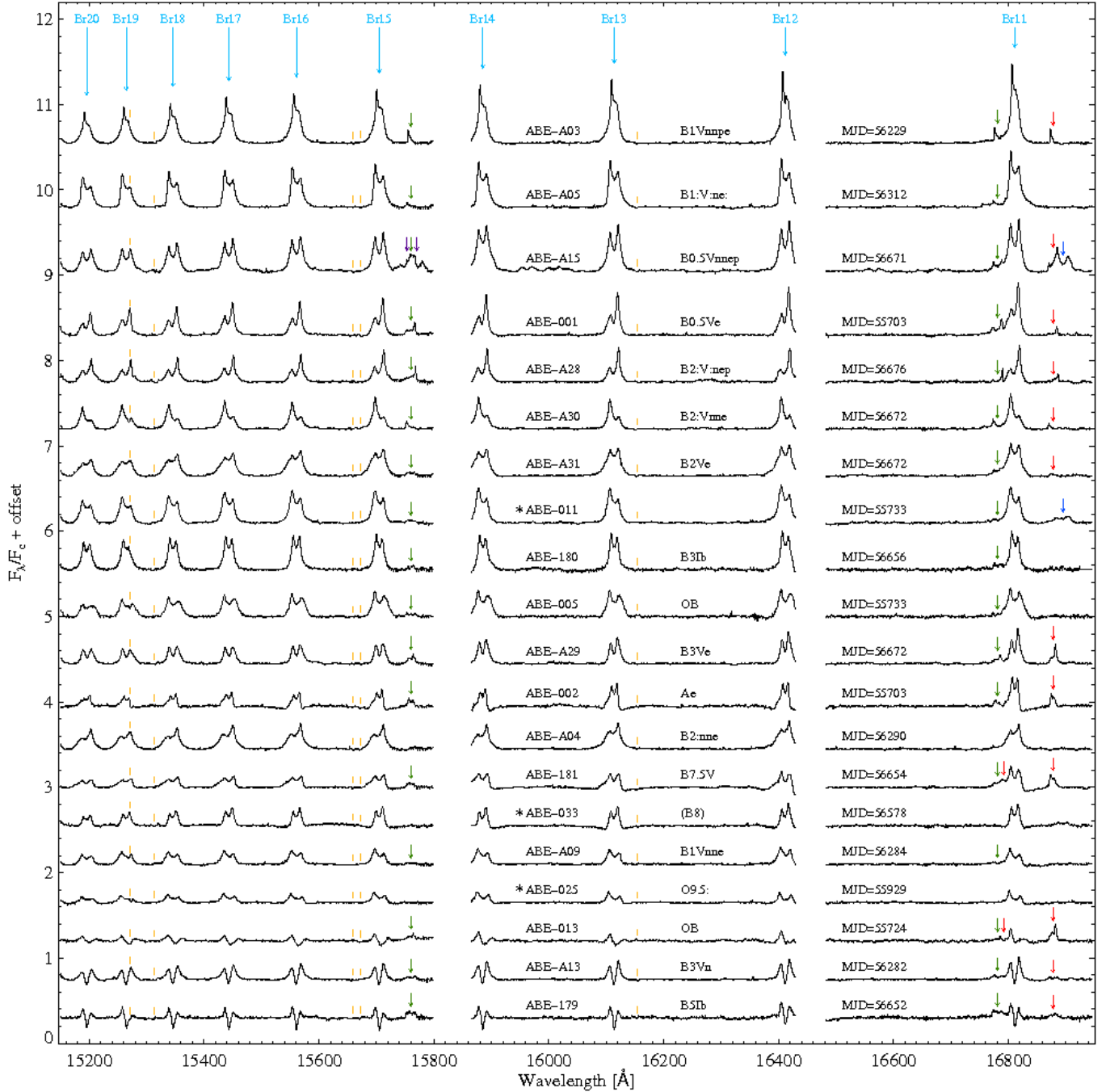


FIG. A22.— Full APOGEE spectra for a selection of 20 Be stars with asymmetric Brackett series emission. Note the striking similarity between the spectra of ABE-001, ABE-A28, and ABE-A30 (the latter a V/R reflection of the former two). Meanings are the same as in Figure A21.

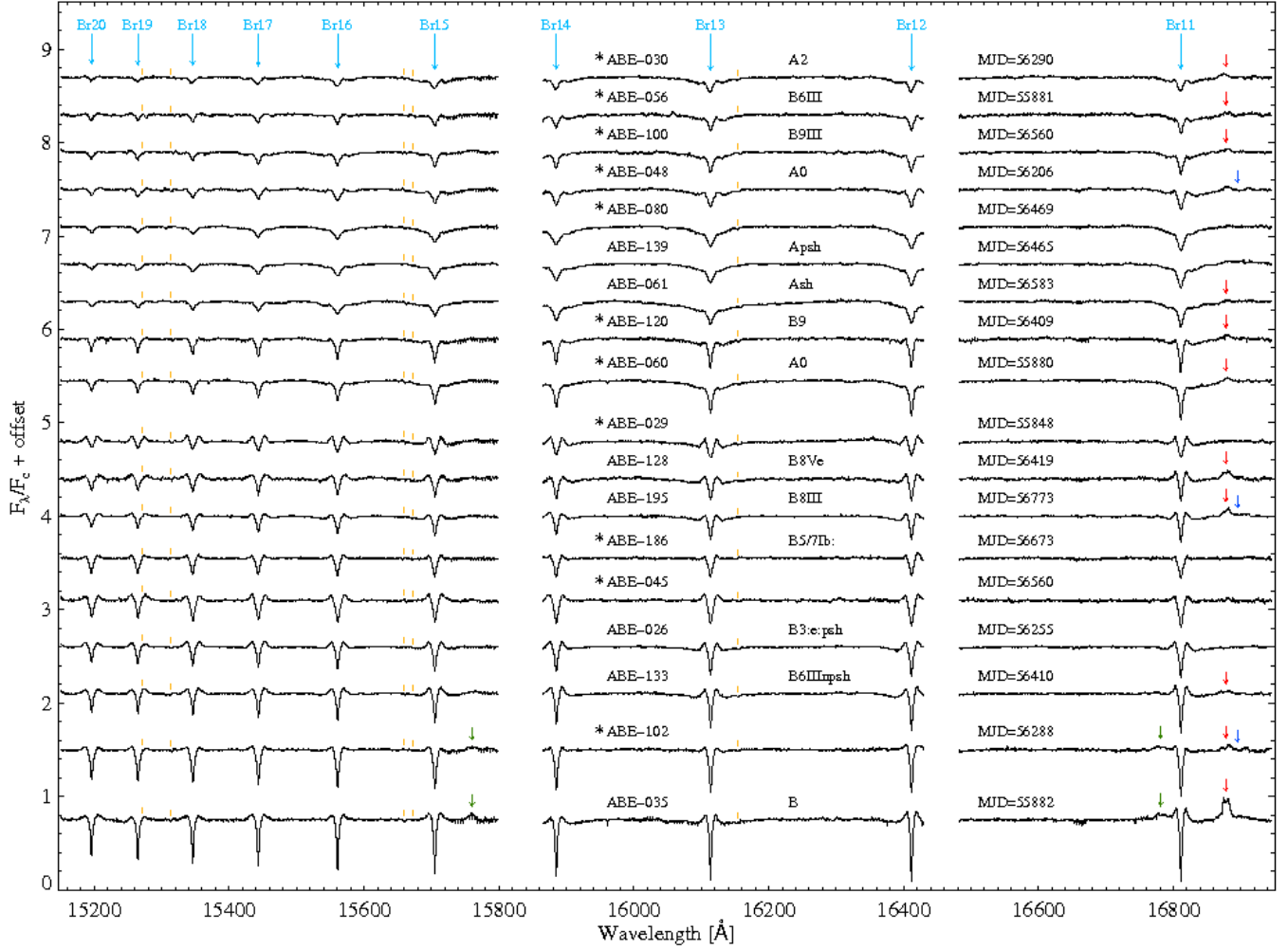


FIG. A23.— Full APOGEE spectra for a selection of 18 Be-shell stars. Broad photospheric absorption wings are clearly evident in the Brackett lines for the upper 9 stars, while the lower 9 stars exhibit mostly smooth continua and shell features with adjacent emission. Meanings are the same as in Figure A21.